UNIVERSITA' DEGLI STUDI DEL MOLISE

Department of Agriculture, Environmental and Food Technology

PhD Course in:
AGRICULTURE TECHNOLOGY AND BIOTECHNOLOGY
(Curriculum: Food science, Technology and Biotechnology)

CYCLE (XXXII)

Related Disciplinary Scientific Sector: CHIM/02 (Physical Chemistry)

PhD Thesis

ALGINATE-BASED NANODISPERSIONS TO ASSEMBLE EDIBLE COATINGS AND FILMS FOR FOOD APPLICATIONS

Coordinator of the PhD course: Prof. Giuseppe Maiorano
Supervisor: Prof. Francesco Lopez
co-Supervisor: Dr. Francesca Cuomo

PhD Student: Martina Cofelice
158077

Academic Year 2018/2019

Contents

Summary

Nowadays, issues of environmental interest aimed at reducing pollution due to anthropization, together with changing lifestyles, are modifying the choices of consumers in the food field and, consequently, the actions of the food industries. Therefore, intending to respect the environment, the use of alternative technologies for the production and preservation of food is becoming increasingly popular [1]. In particular, the ever-growing request of *ready-to-eat* foods, such as fresh-cut fruits, and the need to preserve them as long as possible while maintaining their quality, has led to a total revolution in the food packaging sector to replace the traditional petroleum-based packaging. For these reasons, taking advantage of the features of biopolymers such as hydrocolloids and lipids, an alternative way to accomplish the mentioned task could be the use of such polymers to formulate biodegradable packaging. Generally, the required preservation systems, when made up of edible components, are called edible films and coatings i.e. thin layers of material that can be directly applied to the food product (coating) or preformed (film) and used for enrobing the food product or to separate food components [2]. Edible coatings and films, defined as primary packaging, can be made up of a single constituent or by the combination multiple elements. Such kind of materials should have good mechanical and barrier properties to prevent deterioration of commodities on which they are applied. Colloidal systems such as nanoemulsions, for example, are optimal devices that can be used for the production of edible coatings and films, which are gaining increasing attention thanks to their interesting properties [3]. These systems, that are made by colloidal dispersions of oil droplets stabilized by surfactant in a continuous aqueous phase, can combine the positive aspects of proteins and polysaccharides (good mechanical and structural properties) to the one of lipids (good water vapour barrier). Furthermore, nanoemulsions enable improving physical stability and performance of active ingredients within an edible coating, bringing out the possibility of enhancing quality and/or nutritional value of food products combined with the extension of their shelf-life [4]. Alginate is one of the hydrocolloids that can be hosted in the continuous phase of nanoemulsions. It is the most abundant marine biopolymer and it is characterized by favourable structural properties, that make it suitable for a broad range of applications. To date, the importance of this polymer has been highlighted thanks to its involvement in food nanoformulation [5]. Beside alginate, essential oil, a mixture of aromatic compounds obtained from plant parts, can be employed as lipid phase and its use in nanoformulations for food application is well accepted by consumers because it is perceived as a natural antimicrobial and antioxidant compound [6]. Alginate/essential oil in nanoemulsions allow to overcome the strong impact that essential oil would have on organoleptic properties of food. An important step in the design of edible films and coatings is the optimization of the starting nanodispersion formulations that can be carried out through several physico-chemical analyses. In particular, rheological analysis plays a crucial role in the design of formulations for edible coatings and films [7]. As a whole, edible coatings and films represent suitable and mild approaches that can ensure food protection dwindling the food waste, so it appears necessary refining the research in this field to obtain optimal and enhanced systems using biodegradable and environmental-friendly ingredients.
Based on these considerations, the general objective of the following doctoral thesis is the development and production of alginate-based nanodispersions, encapsulating essential oil as antimicrobial and antioxidant compound, for the production of edible films and coatings to be used as active packaging. To achieve this goal, specific objectives were examined: the assessment of the

rheological behaviour of alginate influenced by the presence of essential oil (EO) stabilized by Tween 80; the antifungal activity of the obtained systems; the interaction between the polymer and cross-linking agent (calcium ions) in colloidal systems based on alginate and EO to obtain hydrogels and edible films; the efficacy of the same nanodispersions as edible coating formulation applied on perishable foods, like fresh-cut apples, to increase their shelf-life.

1 Dissertation outlines

This doctoral thesis is structured in two main sections; the first one is composed of three chapters where general lines concerning the production of edible packaging are presented, together with the principal notions on colloidal systems, since these can be used for the production of edible packaging, together with experimental techniques; in the second sections the main results concerning the specific issues of the present study are presented and discussed. The results and discussion part is structured with chapters referring to the different specific topics covered in this thesis, all of them treated with a suitable description of the results, discussion and followed by final concluding remarks. Briefly, **Chapter 1** introduces the topic of food packaging and lists the different technologies that can be used to obtain edible packaging (coatings and films). These systems can be made of a single ingredient or a combination thereof, obtaining the so-called composite films. Considering the properties of the ingredients of edible coatings and films, mainly their hydrophobicity and hydrophilicity, it is possible to overcome some problems, through the use of colloidal systems like emulsions and nanoemulsions. In **Chapter 2** colloidal systems are described, considering their main properties and characteristics. **Chapter 3** reports the principal experimental techniques used in this thesis work. The experimental section is organized as represented in Fig. 1.

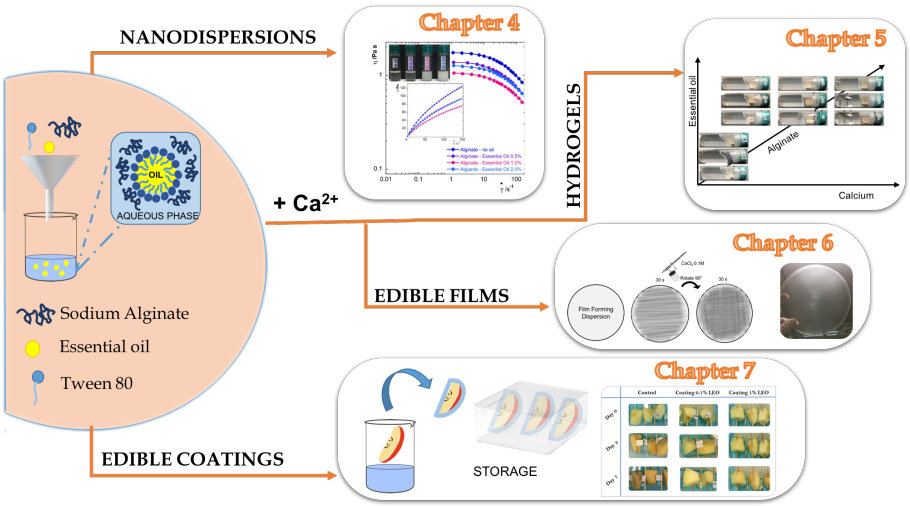

Figure 1: *Schematization of the chapters of the thesis.*

Thus, bearing in mind the characteristics of colloidal systems, **Chapter 4** is based on the production of nanodispersions at different concentrations of alginate (continuous phase) and essential oil (dispersed phase), stabilized by Tween 80. The nanodispersions have been prepared and characterized through rheology, conductivity and for their antifungal activity. **Chapter 5** reports the study conducted on nanodispersions obtained with the same ingredients, in this case treated with calcium solution through the inner gelation method. The homogeneous gels formed have been studied for their rheological properties influenced by the different amounts of

calcium added. Taking into account the reaction between alginate and Ca^{2+}, in **Chapter 6** the features of the edible films obtained from alginate-based nanodispersions, treated or not with calcium solution, are reported. The obtained films have been characterized, starting from their microstructure to their mechanical and other physicochemical properties. Finally, **Chapter 7** illustrates the features of the application of a coating layer, based on the alginate/essential oil nanodispersions, on fresh-cut apples. Quality parameters of fruits as well as the extension of the shelf-life, have been assessed after the characterization of the nanodispersions taken into consideration.

References

1. González-Aguilar, G.; Ruiz-Cruz, S.; Cruz-Valenzuela, R.; Ayala-Zavala, J.; De La Rosa, L.; Alvarez-Parrilla, E. New technologies to preserve quality of fresh-cut produce. In *Food Engineering: Integrated Approaches*, Springer: **2008**; pp. 105-115.
2. Embuscado, M.E.; Huber, K.C. *Edible films and coatings for food applications*; Springer: **2009**; Vol. 9.
3. Norde, W. *Colloids and interfaces in life sciences*; CRC Press: **2003**.
4. Acevedo-Fani, A.; Soliva-Fortuny, R.; Martín-Belloso, O. Nanoemulsions as edible coatings. *Current Opinion in Food Science* **2017**, 15, 43-49.
5. Narsaiah, K.; Sharma, M.; Sridhar, K.; Dikkala, P. Garlic Oil Nanoemulsions Hybridized in Calcium Alginate Microcapsules for Functional Bread. *Agricultural Research* **2019**, 8, 356-363.
6. Burt, S. Essential oils: their antibacterial properties and potential applications in foods—a review. *International journal of food microbiology* **2004**, 94, 223-253.
7. Peressini, D.; Bravin, B.; Lapasin, R.; Rizzotti, C.; Sensidoni, A. Starch–methylcellulose based edible films: rheological properties of film-forming dispersions. *Journal of Food Engineering* **2003**, 59, 25-32.

1 Food Packaging: State of Art

«You must be the change you wish to see in the World»
M.Gandhi

1.1 Bio-Packaging: Edible Films and Coatings

Packaging in product distribution has multiple roles. Apart from protecting products from the external environment, it also represents a marketing tool that communicates to the consumer and aims at maximizing sales. As a consequence, the packaging is a mean of communication and containment to be optimized rather than a cost to be minimized [1]. Packaging should be considered as part of the product manufacturing and distribution processes, and the economics of the supply chain should take into account all the operations - including packaging - involved in the delivery of the product to the final user. For traditional packaging, it is possible to define some primary functions such as the identification of the product (presentation), protection and preservation, promotion and marketing (economy) and facilitation of the use of the product (convenience). One of the aims of industries is to achieve an optimal balance between performance, quality and costs of packaging. The main role of food packaging is to protect food products against physical, chemical and biological agents. To cope with this role food spoilage should be delayed by prolonging the beneficial effect of their processing and retaining the quality and safety of the commodities in order to extend the product shelf life [2]. Traditionally, food companies used polymeric films (polyethylene-PE, polypropylene - PP and polystyrene - PS) to package fresh fruits and vegetables because of their wide availability at relatively low costs and their good mechanical properties [3]. The extensive use of synthetic packaging films has led to serious ecological problems mainly related to their non-biodegradability. In response to this there is a growing demand for alternative packaging to replace the petrochemical-based packaging [4]. The traditional concept of inert and passive packaging is no longer sufficient, but it musts evolve in response to the different demand of the market. The development of active and intelligent packaging is attracting more and more interest so that new ways to design packaging are being defined. In this context, the development of edible coatings and films fits well to the new category of food packaging.

1.1.1 Edible Films and Coatings

Edible films (EF) and coatings (EC) have been used for centuries on foods, for many purposes: from the use of the wax applied to citrus fruits in the XII and XIII centuries to give a glossy appearance, to the coating of candies. Also, lipid coatings (larding) on meats and cheeses have been used since the Middle Ages for shrinkage prevention [5-6]. The reason why these systems were used in previous centuries is that they were the only solution to preserve food. Subsequently, with industrial development, this kind of food preservation has been replaced by petroleum-based plastic packaging. Nowadays, considering the environmental concerns, it is necessary to research in this field, making the natural raw materials or by-products the principal ingredients of the packaging sector. Edible coatings and films can be classified as primary packaging made from edible ingredients. Any kind of material used for enrobing (coating or wrapping) food and which can be consumed together with it with or without further removal is considered an edible film

or coating. For example, when applied on fruit EF and EC provide the replacement and/or fortification of natural layers to prevent moisture losses, while allowing selectively a controlled exchange of important gases, such as oxygen, carbon dioxide, and ethylene, which are involved in respiration processes. A film or coating can also provide surface sterility and prevent the loss of other important components. Generally, their thickness is less than 0.3 mm. Like classical packaging, EF and EC protect food from mechanical, physical, chemical and microbiological damage. In some cases, the terms film and coating are used interchangeably to indicate a thin layer of material covering the food surface. However, the term film identifies a stand-alone, pre-formed wrapping material, while the term coating is used for the layer of material adhering to the food surface and applied in the liquid form. The increase in the demand for EC and EF has been determined by modification in consumers' lifestyles and by the increased attention to healthy and nutritional food. To meet this request, the development of alternative preservation methods has been encouraged like the application of edible biopolymers from renewable sources, by-products and/or industrial waste. Even a few days of shelf-life extension could represent a significant economic advantage for food companies. Providing barrier to moisture, edible coatings and films are potential systems for improving the quality and shelf life of fresh produce [7]. Besides being a barrier against water loss, they can also have functional attributes, mechanical (flexibility, tension) and optical properties (brightness and opacity) and be a good barrier against the flow of gases. One major advantage of coatings is that they can be used for encapsulating natural or chemical antimicrobial agents, antioxidants, enzymes, probiotics or mineral and vitamins. When the packaging includes functional compounds able to enhance the quality of food it is called active packaging (AP). As defined in the European regulation (EC) n. 450/2009 [8] AP systems are designed to ´deliberately incorporate components that would release or absorb substances into or from the packaged food or the environment surrounding the food´. Active packaging materials are thereby ´intended to extend the shelf-life or to maintain or improve the condition of packaged food´[9]. However, this concept has been innovated by the use of antimicrobial compounds, so active packaging can reduce, inhibit or stop the growth of microorganisms on food surfaces [10]. So an AP is a system in which food, packaging and external environment interact to extend shelf life of food product and/or to reach certain characteristics that the product would not obtain on its own. To achieve this purpose, and therefore to incorporate certain compounds, an help is given by the production of edible films and coatings starting from emulsion or nanoemulsions systems. Nowadays, edible coatings and films have different applications and their use is expected to be expanded with the development of Active Coating Systems. This second generation of coating materials can use chemicals, enzymes or microorganisms that prevent, for example, microbial growth or lipid oxidation in coated food products. In this sense, essential oils, in combination with structural polymers, can be a promising source [11-13] for their antimicrobial and antioxidant properties, as it will be described later. Second-generation of coatings could be enriched with nutrients or other bioactive compounds that have a positive effect on health, especially due to the application of new microencapsulation or nano-encapsulation techniques [14-15].

1.2 Films and Coatings formation

The methods used for the formation of edible films or the conditions of coating application have an important impact on the physical properties of films [16]. Generally, in film formation inter and intra molecular interactions or cross-linking of polymer chains with other compounds are involved in order to form a rigid or semi-rigid three dimensional network in which the solvent is trapped or immobilized.

1.2.1 Edible Film production methods

The processes used to obtain film could be distinguished in *wet* and *dry* methods.
Casting method
This technique is the most used method for producing edible films and it is also known as *wet* process. Biopolymers and other ingredients are dissolved in solvent (water or in general an edible one) in order to obtain a uniform system. The suspensions are successively poured onto acrylic plates (or material that will not interact with the film ingredients) and left to dry at specific temperature and humidity. At laboratory scale it is possible to accurately control spreading thickness as well as drying conditions (rate and temperature) which will determine the final characteristics affecting film microstructure and properties. Once dried, films can be easily peeled from plates and left to equilibrate in desiccators to avoid moisture intake [17,18]. During drying of the solution, solubility of the polymer decrease as result of solvent evaporation, until polymer chains align themselves to form films [16].
Compression molding
This is a thermo-processing method based on thermoplastic properties of certain biopolymers, without or with low content of water, for this it is defined a *dry* method. Usually two main steps characterize the process: first film components are well mixed with other additives or plasticizers and subjected to high temperatures and pressures. Then the obtained paste or pellet is thermo-molded to form films. So ingredients need to have thermoplastic properties to be used in this process.

1.2.2 Edible Coating formation methods

Starting from the same composition of films, the coating is applied in a liquid form onto the food product. The choice of coating systems, as well as the equipment, depends mainly on size and shape of the product to be coated and on the desired thickness of the coating. The first step of the process is the deposition of coating formulation on the product surface. Coating integrity is a critical factor that depends on surface tension, adhesion to the food surface and flexibility of the coating. Once the coating is applied, the coating material adheres to the surface of the food. Then a film formation phase occurs, through coalescence of the coating on the product. Subsequently, the continuous coating layer is stabilized on its support or food product through coacervation by drying, cooling, heating or coagulation.
Depending on the viscosity, the coating could be applied through different methods (Fig. 1.1):

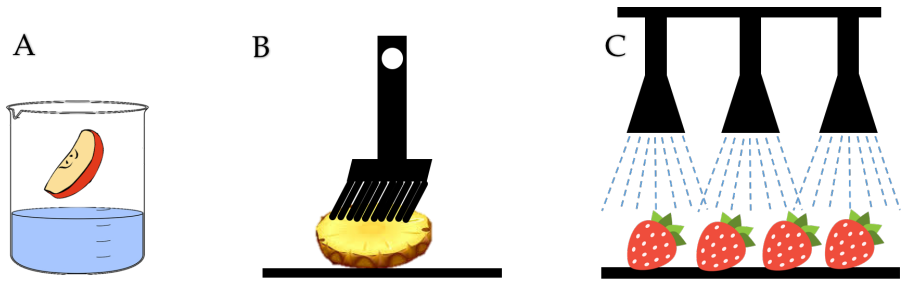

Figure 1.1: *Representation of different coating method: dipping (A), brushing (B) and spraying (C).*

Dipping
Among different coating formation methods, dipping is the simplest that does not requires particular equipment but coating solutions with a certain viscosity. Through dipping method a coating layer is formed with a thickness proportional to the viscosity of the solution [19] and also depending on other properties like the density and surface tension. In this method the food

product is dipped, for a given time, in a container with the aqueous medium of coating dispersion. The excess of coating is left to drip, and then the coated sample is stored at controlled temperature and humidity.

Spraying

When coating solution has low viscosity, the spraying method can be used alone or in combination with pan, drum screw or fluidized-bed coaters. The method allows to control the thickness of coating that is also influenced by the shape of the noozle positioned at the end of the sprayer, which regulates the flow. Temperature, pressure and viscosity will affect the flow rate so the size of droplets. This method requires a smaller amount of coating material to achieve good coverage due to high spraying pressure [20].

Spreading or Brushing

This method can be used with medium or highly viscous coating solutions that are spread onto the product. The application is made with the use of external tools such as brushes that will produce thin coating that forms a semipermeable membrane on the surface of food products.

1.3 Ingredients used in Edible Coatings and Films formulation

The optimization of edible films and coatings composition, therefore the choice of ingredients and their amount, is one of the most important steps since EC and EF must be formulated according to the properties of the foods on which they have to be applied. The compounds used, to ensure compliance with the edibility condition of coatings and films, must be food grade. Furthermore, all items and ingredients which are edible or in contact with food should be classified by qualified experts as the Food and Drug Administration (FDA) as safe under the conditions of intended use. Usually, ingredients that meet this requisite are defined as Generally Recognized As Safe (GRAS). Therefore, main components of our everyday foods (proteins, carbohydrates and lipids) can fulfil the requirements for preparation of supporting matrix for edible films and coatings. Depending on the final aim of the coating, each ingredient has a specific function; usually fats/oils are used to reduce water transmission, due to their hydrophobicity, polysaccharides are used to control oxygen and other gas transmission, while proteins with their good mechanical properties can give mechanical stability to films with excellent oxygen barrier. However, their hydrophilicity causes them to be less effective against moisture loss [7].

Addition of other ingredients, in small amount, can modify functional, organoleptic, nutritional and mechanical properties. Hydrocolloids (polysaccharides and proteins) are abundant in nature, commercially available, economical and totally biodegradable, thus they are attractive raw materials to be used for the development of completely degradable and edible coatings or films.

As shown in Fig. 1.2, coatings and films can be classified according to the main component of the matrix; when two or more components are used it is possible to have composite films that combine the benefits of lipids and hydrocolloids. Through the different techniques that considered the use of more than one polymer, emulsions or nanoemulsions systems seem to be the best choice for the production of efficient edible films and coatings that overcomes the disadvantage deriving from the use of only lipids or polysaccharides.

As will be described in Chapter 2, the preparation parameters of the nanoemulsions are important factors for obtaining homogeneous films and coatings because they will influence the final performances of the systems obtained. One of the positive features of the nanoemulsions is that they can be carrier of bioactive compounds [21]. Understanding the rheological behaviour of film or casting suspension is critical for process scale-up, to ensure that processing requirements and machinability issues can be properly addressed. Measurement of viscosity is important for choosing the application technique; spraying requires low viscosity, while immersion requires a

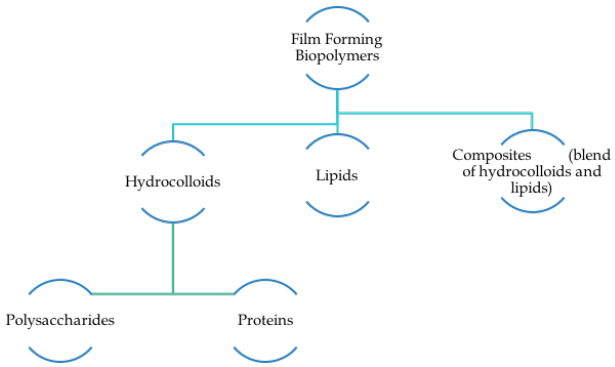

Figure 1.2: *Different film forming biopolymers.*

higher viscosity coating solution.

1.4 Polysaccharides

Polysaccharides are hydrocolloids characterized by high molecular weight. They dissolve in water and form intensive hydrogen bonds among the molecular chains. Thanks to their conformation and size, they have the ability to thicken aqueous solutions, as result of the friction of hydrogen bonds between polymer chains when subjected to shear. In solution, the polymer molecules can be arranged in ordered structures that can trap water, increasing the viscosity, or converted into gel in presence of cross-linking agents. Polysaccharides can present either a neutral, a negative or a positive charge due to the presence of various chemical groups attached to individual monosaccharide units. Based on the molecular weight, conformation, electrical charge, degree of branching they are classified into different types and all these features together contribute to their differences in solubility, synergy or incompatibility with other compounds, as well as to their thickening, gelling and emulsifying properties and, above all, their film formation properties [22].
Among polysaccharides, alginate, chitosan, starch and cellulose are the most commonly used due to their remarkable properties. The interest toward chitosan is mostly due to its physicochemical, antimicrobial and antifungal properties. For these reasons it has been widely used in edible films and coatings, alone or in combination with proteins or other active compounds [23,24].
Cellulose is the most abundant natural polymer and it can be identified as a linear polysaccharide of anhydroglucose units. Derivatives of cellulose show excellent film-forming properties even when combined with other substances to obtain composite films [25-27].
Starch is the storage polysaccharide of cereals, legumes and tubers like cassava or tapioca. It is used for the production of edible films and coating because it is a low cost material, abundant and biodegradable. It also shows thermo-plastic behaviour, and its properties can be improved by destructing the native conformation of starch and adding synthetic substances [28,29].
Sodium Alginate
Among the polysaccharides, in the present thesis, the interest has been turned on alginate. This linear anionic polymer is an appealing film-forming compound due to its non-toxicity, biodegradability, biocompatibility and low-price. Alginate shows functional properties that make it interesting for several applications. Alginic acid was first discovered at the end of XIX century by Stanford and began to be widely used around 1923 when, in United Kingdom, a briquette business based on alginate was established as binder for anthracite coal dust [30].

Alginate is extracted from cell walls of brown algae (*Laminaria hyperborean, Laminaria digitate, Ascophyllum nodosum, Sargassum* sp.), where alginic acid is present in form of salts of calcium, magnesium, and sodium. It is also synthetized by some microorganisms (*Azotobacter vinelandii, Pseudomonas aeruginosa*). When alginate is extracted from seaweed, these are crushed and stirred with a hot solution of alkali, such as sodium carbonate. The solution is diluted and filtered to eliminate the undissolved parts of seaweeds (mainly cellulose). After that, the alginate precipitates from the filtered solution, either as alginic acid or calcium alginate.
Pre-treatment, before the alkaline extraction, of the seaweed with acid leads to a more efficient extraction, a less coloured product and reduced loss of viscosity during extraction [30]. Structurally alginate is composed by monomeric units of β -D-mannuronic (M) and α-L-guluronic (G) acids residues, linked by 1-4 glycosidic bonds, that organize between them creating 3 kind of regions or blocks with different proportion and different distribution in the chain (Fig. 1.3). The G block is characterized only by guluronic acid, and it is responsible for the strength of

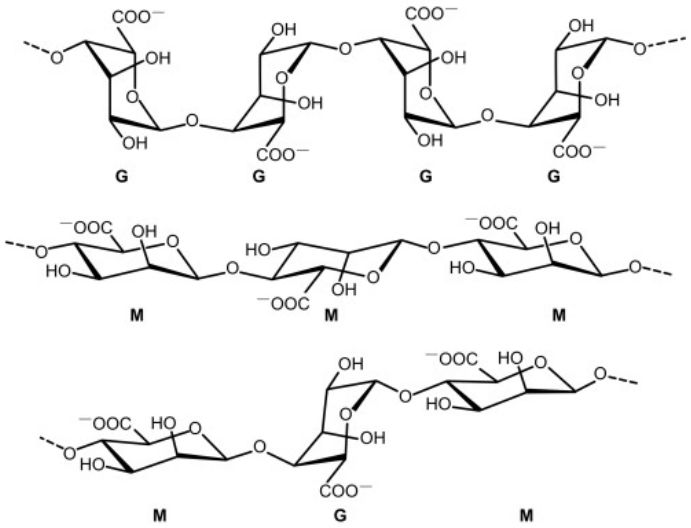

Figure 1.3: *Three blocks characterizing alginate: main monomers guluronic (G), mannuronic (M) acids.*

gel that can be formed. The M block is composed by mannuronic acid, and MG block consist of alternating units of mannuronic and guluronic acid, which determine the solubility of alginate in acid. The M and G blocks are defined as homopolymer regions, while MG with both polyuronic acids is heteropolymer. The relative proportion of the 3 blocks will influence the physical properties of alginates, and the preponderance of one block over another depends on the species, part and age of seaweeds from which the alginate is isolated. The same importance on the final properties is given by the biological source, growth and seasonal conditions [31].
The M/G ratio and the distribution of M and G blocks in the alginate chain affect the physical properties of the polymer. The FDA classifies food grade sodium alginate as GRAS substance and lists its usage as emulsifier, stabilizer, thickener and gelling agent [32].
Gelification of alginate
It is widely known that alginate is polyuronide, hence a natural ion exchanger [33]. The formation of strong gel can occur lowering the pH of the alginate solutions under the pK_a value of the guluronic residues (pK_a=3.65) [34], or in presence of divalent cations [35]. The different affinity that alginate shows towards divalent ions decrease in the following order $Pb^{2+} > Cu^{2+} > Cd^{2+} > Ba^{2+} > St^{2+} > Ca^{2+} > Co^{2+}$,$Ni^{2+}$,$Zn^{2+} > Mn^{2+}$ [36]. Based on the toxicity limits of some of them, ions that can be used for the production in food field are Ba^{2+}, St^{2+} and Ca^{2+}. Monovalent cations and Mg^{2+} ions do not form a gel [37].

The interest towards calcium-alginate gels is the wide use that can be made of them in various fields: from medical sector [38,39] to the food industries and others. Gelation is possible because the divalent ions, such as calcium, through diffusion into the alginate solution, provoke an ion exchange process in which the water soluble alginate (sodium or potassium) exchange its counter-ions with Ca^{2+} obtaining sol/gel transition. This ionic cross-linking will form a rapid cold setting and thermostable gel. When forming alginate gels, two contiguous, di-axially linked guluronic residues form a cavity that acts as a binding site for calcium ions. This arrangement is commonly represented as the egg-box model (Fig. 1.4).
As result, film characteristics like water and mechanical resistance, barrier properties, cohesiveness and rigidity can be improved. The calcium cations tend to chelate the carboxylate and hydroxyl groups of the alginate, with the formation of a sort of bridge between metal ion and two carboxylate moieties and one or more pairs of the hydroxyl groups. This occurs through partially ionic and partially coordinate bonds respectively.

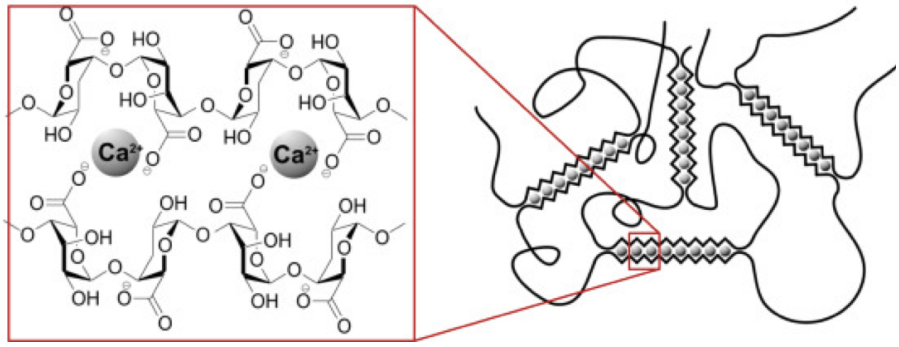

Figure 1.4: *Formation of egg-box structure after the cross-linking between Ca^{2+} and alginate.*

Therefore, a two-stage mechanism has been suggested to explain the phenomenon:

1. the formation of strongly linked dimer associations with important contributions of van der Waals and hydrogen bonding interactions in which the functional groups involved in chelation belong to the same chains;

2. the formation of weaker intermolecular dimer associations in which the carboxylate and hydroxyl functional groups are related to different chains that do not present particular specificity, and are mainly governed by electrostatic interactions.

The three blocks already described interact in a different way with the cations. The M blocks bind cations externally, close to their carboxylate groups, while G blocks integrate the cations, in a pocket-like structure formed by the G residues around. In MG blocks the cations prefer to locate in a concave structure formed by the pairs M and G [40]. To overcome the formation of irregular gels, due to the very rapid and irreversible formation of the junction between alginate and calcium, it is possible to use a method able to control the introduction of cross-linking agent, such as the internal setting method [36]. In the external gelation, the cross-linking agent diffuses from an outer reservoir into an alginate solution. In this method, Ca^{2+} will first cross-link the film surfaces drawing the polymer chains closer to form a less permeable surface to the diffusion of cations. Thus, the diffusion method yields gels having Ca^{2+} ion concentration gradient across the thickness [36].
In the internal method, also called *in situ* gelation, the calcium cations are incorporated as insoluble form, chelated to specific compounds (EDTA), and afterward the gelling ions are released by processes that lower the pH of the solution, for example the addition of organic

acids or slowly hydrolysing lactones [41]. The increase in the concentration of cations during the gelling of the alginate causes the formation of a more densely cross-linked structure. However, there is an optimal amount of cross-linker that can be used after which a further increase in Ca^{2+} does not exert significant changes in the gel´s properties [42]. Sodium alginate is attracting a lot of attention because it can produce water-soluble films, strong, glossy tasteless, odourless, flexible, low permeable to oxygen and oils. The phenomena related to the interaction between alginate and calcium have been well investigated in this thesis and, in particular, the effects on nanoemulsion systems are reported in Chapter 5.

1.4.1 Lipids

Lipids are used in edible packaging because they show good barrier properties linked to their hydrophobicity. They can form structures that reduce the passage of moisture from a phase to another of food system. Typically, they are used in combination with polysaccharides or protein based film to improve their barrier properties. Edible lipids include beeswax, candelilla wax, carnauba wax, triglycerides, acetylated monoglycerides, fatty acids, fatty alcohols and sucrose fatty acid esters. The waxes are the ones with the best barrier properties against water.
Lipids can be classified according to the presence of polar components, the length of the hydrocarbon chain, the number of unsaturation or acetylation. Increasing the hydrocarbon chain length can modify the barrier properties since molecular polarity decreases, and this does not favour water solubility of the film. This happen because the lateral packing of the acyl chain is less efficient, causing a reduction of the van der Waals' interaction and an increase in hydrocarbon chain mobility [43].
Essential Oils
With the purpose of satisfy consumers' request about the use of fewer chemicals in minimally processed fruits and vegetables, research into naturally occurring substances that can act as alternative antioxidants has become necessary. Among lipid compounds, essential oils (EOs) have attracted more and more interest because, in addition to their hydrophobic nature, they show antioxidant and antimicrobial properties. They can be defined as aromatic compounds, obtained from plant material (flowers, seeds, leaves, barks, herbs etc.) by physical means (Fig. 1.5). EOs consist in a complex mixture of natural volatile hydrophobic substances, such as terpenes, terpenoids, phenolic acids and other aromatic and aliphatic compounds, however the composition of EOs may vary depending on their origin and extraction method. Essential oils are considered antioxidant substances, defined by FDA as substances used to preserve food by retarding deterioration, rancidity or discoloration due to oxidation and are classified as Generally Recognized As Safe. Nanoemulsions contribute in an efficient way to support the use of EOs in food increasing their dispersibility. One of the main problem that limits the use of essential oil is their strong flavour, which can modify the organoleptic properties of systems incorporating EOs. This, together with their volatility, makes necessary the oil encapsulation in nanoemulsion. The antimicrobial properties [12,44,45], important feature of EOs, are also correlated to the composition of essential oil [46]. The mechanism of action is based on the reaction between the hydrophobic compounds of EO and the lipids of the cell membrane, which causes an increase in the permeability of the latter. Therefore, there is a modification of the original structure of the cells that involves the leakage of ions and cytoplasmic content. A main role is played by the formulation of the nanoemulsion. In fact, the average droplet size and surface charge influence the transport of EOs to the cell membrane, as well as their interaction with the multiple molecular sites on the microbial cell membrane. From *in vitro* studies it was determined that the antimicrobial action of essential oil is more efficient against Gram-positive (Gram +) due to the structure of the cell walls mainly composed by peptidoglycans, whereas the Gram-negative (Gram -) have a complex structure. Nanoemulsions, thanks to the size of

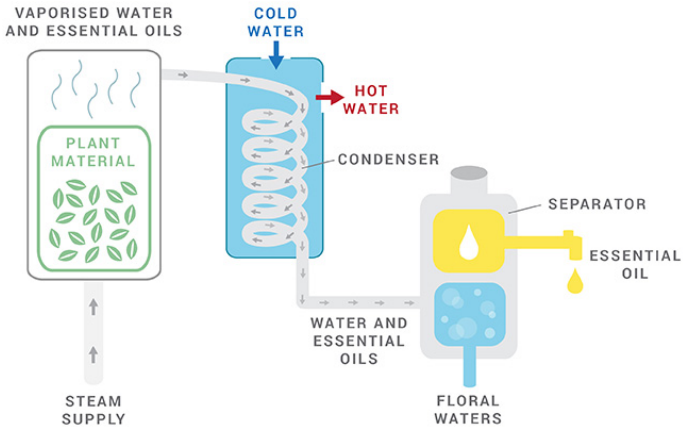

Figure 1.5: *Steam distillation method for the production of essential oils.*

their dispersed phase, can be efficiently transported through the porine proteins of the outer membrane of Gram- bacteria enabling an effective delivery of EOs also to the cell of them. Nanoemulsions encapsulating different essential oil demonstrate to be efficient against *Escherichia coli, Salmonella thyphimurium, Staphylococcus aureus, L. monocytogenes* and *L. innocua*. However, some study showed contradictory results; in some cases, the use of nanoemulsion seemed to lower the antimicrobial activity [47] if compared to the non-encapsulated compounds, while other studies highlighted the increase in antimicrobial activity of EO when nanoemulsions are used [48]. All this can be explained by the different mechanism of interaction of EOs with the cell membranes. It is necessary to bear in mind that to be accepted by consumers, the application of a certain essential oil to food products need to be equilibrated by selecting the EO according to the specific commodity, with a minor effect on sensory quality. The importance of antioxidants and antimicrobials is that they can prevent sensorial and nutritional quality loss and improve foods stability, prolonging their shelf-life [13,49,50].

1.4.2 Additives - Antibrowning agents

Surface browning of fruits and vegetables, especially after cutting or the removal of external protection represented by the peel, is a common phenomenon usually caused by a specific enzyme: polyphenol oxidase (PPO). This enzyme is present in all plants and, in presence of oxygen, converts the phenolic compound into dark colored pigments, but surface browning can be also due to non-enzymatic oxidation of phenolic compounds [51]. Color is a critical quality parameter, so the application of antioxidant treatments, combined with the use of edible coatings and films, is a common way to control browning of fresh-cut fruits. Ascorbic and citric acid and some sulfur-containing amino acids are the most extensively used to avoid enzymatic browning due to the reduction of the o-quinones, generated by the action of the PPO, back to phenolic substrate [52]. Furthermore, citric and other carboxylic acids, have also been suggested as an effective antioxidant agent in fresh-cut fruit [53,54]. Antibrowning agent can be used before or after the application of edible coating, or they can be included in the coating formulation [55,56].

1.5 Current uses of Edible Films and Coatings

Several are the studies that have addressed the use of edible films or coatings to extend the shelf life of different food products. Currently, edible films and coatings are used with several food products, mainly fruits, vegetables, candies, and some nuts [57]. Collagen films are used for

sausage casings, and some hydroxymethyl cellulose films as soluble pouches for dried food ingredients. Shellac and wax coatings on fruits and vegetables, zein coatings on candies, and sugar coatings on nuts are the most common commercial practices of edible coatings [58]. Concerning applications on fruits and vegetables, chitosan based coating containing lemon oil was successful applied to rucola leaves, prolonging the shelf-life up to 7 days [59], and when applied on fresh-cut broccoli, chitosan edible coating showed a bactericidal effect on *E.coli* [60]. The use of cellulose ethers (such as carboxymethyl cellulose, hydroxypropyl cellulose, and methylcellulose) as ingredients in coatings for fruits, vegetables, meats, fish, nuts, confectionery, bakery, grains and other agricultural products is increasing [61]. In particular, carboxymethyl cellulose-based coating was effective in maintaining the firmness and titratable acidity of plum fruits, proving to be a suitable method to enhance the shelf-life of this fruit [62]. Furthermore, for bakery products, methylcellulose coatings with cloves or oregano oil have been tested on sliced bread against spoilage microorganisms, with positive results and extension of bread shelf-life compared to the commercial antifungal product currently used in bakery [63]. Also, edible coatings based on corn starch, methylcellulose and soybeans oil applied to crackers, food with low water activity (a_w), become part of the product and allow to reduce the hydration kinetic in a high a_w environment [64]. The pharmaceutical industry uses sugar coatings on drug pills and gelatine films for soft capsules [65,66]. In general, this is a field in continuous development, with high interest in production on new formulations, in particular trying to evaluate raw materials that are ´thrown´ away in other processes.

1.6 Fresh-Cut Fruits

Fresh fruits are commodities that, after changes in lifestyle and eating habits of consumers, are getting more attention. They represent an important part of a healthy diet, contributing to the intake of vital nutrients (vitamins, minerals, dietary fibers) antioxidants and other substances, which promote a healthy lifestyle. Also, the consumption of fruits like apples (*Malus domestica*) has been associated with the reduced risk of degenerative diseases, such as cancer and cardiovascular diseases [67,68]. Therefore, it is necessary to use adequate postharvest technologies combined with edible coatings and films, to prolong the shelf life of these commodities in the most ´eco-friendly´ way. Fruits are generally characterized by the presence of natural barriers surrounding the entire surface; skin protects the fruits from water loss and pathogen invasion and provides partial barrier to gases. Mechanical operation like washing, peeling, cutting, slicing and other minimal processes, remove natural barriers and induce tissue lesions, causing quality losses (contamination, enzymatic browning, alteration in texture). Fruits that are minimally processed, as defined by the International Fresh-Cut Produce Association (IFPA), fall into the fresh-cut category. The fresh-cut sector is constantly evolving and innovating in order to enhance product quality and safety [69]. Fresh-cut products are considered wounded tissues as a consequence of the type of processing they are subjected to. As a consequence of wounding, since fruits consist of living tissue, there is an increase in the rate of respiration, transpiration and ethylene production, which may accelerate deterioration (non climateric) or ripening (climacteric) of fruits, compromising their quality. Understanding the processes that lead to changes in fresh-cut fruits is essential in order to develop better approaches to minimize them, thereby improving quality and shelf life of such commodities. Appearance and texture changes are two fundamental characters that determine the acceptability of fresh-cut fruits. In fact, at first instance, quality of fruit is judged by its appearance (colour) and afterwards, by parameter such as weight loss, titratable acidity, pH and phenol content. Matching these parameters, it is possible to obtain important information that consumers can use to recognize a more nutritional fruit [70]. Most fruits contain 65 to 85% of water when harvested and one of the main cause of postharvest deterioration is water loss, hence weight loss. It is not only in a direct quantitative

loss, but also in appearance and texture attributes, and therefore quality loss. The water loss of fresh-cut fruit is mainly due to the gradient of the vapour pressure and respiration, which causes wilting and shrivelling of produce. The rate of water loss is dependent primarily on the external vapour pressure deficiency. Of course, this loss is greater for fresh-cut products, due to the absence or disrupting of a cuticle and sub-epidermial layers causing the exposure of internal tissues [71]. A parameter that indicates the quality in terms of freshness of fruits is the titratable acidity (T.A.) which estimates the content of organic acids in fruit flesh. Organic acids tend to decrease their content during storage, while the amount of sugars increases. This reduction, common for the post-harvest of fruits, is basically attributed to the consumption of organic acids as respiration substrate [72]. T.A. is directly correlated to the pH of fruits, because organic acids donate hydrogen ions, which will lower the pH. Generally, the T.A. decrease with ripening and senescence, causes an increase of pH during storage [73]. Phenolic compounds are secondary metabolites present in plants and their ability to protect human body tissues against oxidative attacks makes them interesting. The concentration of phenolic compounds and the antioxidant activity in fruits, such as apples, seems to be different within cultivars, maturity stage, environmental conditions and part of the fruit [74]. During the ripening of fruits, the amount of phenols can decrease because they are used in some reactions. The main enzyme involved in the pathway of phenols is the Phenylalanina Ammonia Lyase (PAL), which increasing its activity (after cutting, as defense mechanisms) accumulates the phenolic compounds. The enzyme already described, called PPO as said before, oxidizes the phenolic compounds found in the tissue of fruits. This oxidation causes the phenolic compounds to condense into brown spots. The activity of PPO was found to be cultivar dependent in apples; *Red delicious* apples showed an enzymatic activity 10 times higher than the *Elstar* cultivar [75]. Although the cell structure remains intact, the enzyme and phenolic compounds are separated and so do not react each other. So, the enzymatic browning can begin with cellular disruption, causing the release of phenolic compounds stored within the vacuoles in cell wall compartments [52]. Then, PPO can catalyse in presence of oxygen through two different reactions: the hydroxylation of monophenols and the oxidation of o-quinones; a non-enzymatic polymerization of quinines occurs, leading to the formation of melanins, pigments of high molecular mass and dark in colour. [76-79]. This discoloration due to the interaction of phenols with PPO enzyme is an example of interaction between lipid components and enzymes, so to control this process it is important to avoid membrane lipid degradation. It is estimated that over 50% losses in fruit occur as a result of enzymatic browning. It is one of the most important color reactions that affects horticultural commodities, leading not only to tissue discoloration but also to the development of off-flavors. About 15% - 50% of fruits are lost after harvest, mainly due to microbiological spoilage [80]. Physiological and biochemical changes, together with physical injuries, can favour the development of pathogens. Fungi and bacteria can infect fruit tissue, and generally the growth of one or another is determined by the pH; when it is above 4.5 allows the growth of bacteria, while acidic values led to the sporulation of fungi. When fruit tissues are wounded, there is a high concentration of sugars and proteins, that together with the high surface moisture creates the ideal conditions for microbial growth [81] especially in case of minimally processed fruits. For the latter, the susceptibility is increased, due to the damage to the cellular structures, for a much wider range of microorganisms to invade and proliferate on the surface and subsurface of produce. Common species that can grow are *Pseudomonas, Flavobacterium, Enterobacter, Lactobacillus*, molds and yeasts. Due to the several problems facing fresh-cut fruits, natural preservative combined with new green technologies (edible films/coatings) should be explored to preserve these commodities. Some of the here explained quality attributes of fruits were analysed after the application of coating and results are discussed in Chapter 7.

References

1. Heather, P.; Paine, F. Handbook of food packaging. *Glasgow: Leonard Hill* **1983**.
2. Senturk Parreidt, T.; Müller, K.; Schmid, M. Alginate-based edible films and coatings for food packaging applications. *Foods* **2018**, 7, 170.
3. Siracusa, V.; Rocculi, P.; Romani, S.; Dalla Rosa, M. Biodegradable polymers for food packaging: a review. *Trends in Food Science & Technology* **2008**, 19, 634-643.
4. Galgano, F. Biodegradable packaging and edible coating for fresh-cut fruits and vegetables. *Italian Journal of Food Science* **2015**, 27, 1-20.
5. Debeaufort, F.; Quezada-Gallo, J.-A.; Voilley, A. Edible films and coatings: tomorrow's packagings: a review. *Critical Reviews in Food Science* **1998**, 38, 299-313.
6. Donhowe, I.G.; Fennema, O. Edible films and coatings: characteristics, formation, definitions, and testing methods. *Edible coatings and films to improve food quality* **1994**, 1-24.
7. Vargas, M.; Pastor, C.; Chiralt, A.; McClements, D.J.; Gonzalez-Martinez, C. Recent advances in edible coatings for fresh and minimally processed fruits. *Critical Reviews in Food Science and Nutrition* **2008**, 48, 496-511.
8. Commission, E. Commission Regulation (EC) No 450/2009 of 29 May 2009 on active and intelligent materials and articles intended to come into contact with food. *Official Journal of the European Union* **2009**, 135, 3-11.
9. Wilson, C.L. *Intelligent and active packaging for fruits and vegetables*; CRC press: **2007**.
10. Appendini, P.; Hotchkiss, J.H. Review of antimicrobial food packaging. *Innovative Food Science & Emerging Technologies* **2002**, 3, 113-126.
11. Atarés, L.; Bonilla, J.; Chiralt, A. Characterization of sodium caseinate-based edible films incorporated with cinnamon or ginger essential oils. *Journal of Food Engineering* **2010**, 100, 678-687.
12. Fernández-Pan, I.; Royo, M.; Ignacio Maté, J. Antimicrobial activity of whey protein isolate edible films with essential oils against food spoilers and foodborne pathogens. *Journal of food science* **2012**, 77, M383-M390.
13. Perdones, Á.; Vargas, M.; Atarés, L.; Chiralt, A. Physical, antioxidant and antimicrobial properties of chitosan–cinnamon leaf oil films as affected by oleic acid. *Food Hydrocolloids* **2014**, 36, 256-264.
14. Cuomo, F.; Lopez, F.; Ceglie, A.; Maiuro, L.; Miguel, M.G.; Lindman, B. pH-responsive liposome-templated polyelectrolyte nanocapsules. *Soft Matter* **2012**, 8, 4415-4420.
15. Cuomo, F.; Cofelice, M.; Venditti, F.; Ceglie, A.; Miguel, M.; Lindman, B.; Lopez, F. In-vitro digestion of curcumin loaded chitosan-coated liposomes. *Colloids and Surfaces B: Biointerfaces* **2018**, 168, 29-34.
16. Skurtys, O.; Acevedo, C.; Pedreschi, F.; Enronoe, J.; Osorio, F.; Aguilera, J.M. *Food hydrocolloid edible films and coatings*; Nova Science Publishers, Incorporated Hauppauge, New York, USA: **2014**.
17. Debeaufort, F.; Voilley, A. *Edible films and coatings for food applications*. Springer, New York: **2009**.
18. García, M.A.; Pinotti, A.; Martino, M.N.; Zaritzky, N.E. Characterization of starch and composite edible films and coatings. In *Edible films and coatings for food applications*, Springer: **2009**; pp. 169-209.
19. Dhanapal, A.; Sasikala, P.; Rajamani, L.; Kavitha, V.; Yazhini, G.; Banu, M.S. Edible films from polysaccharides. *Food science and quality management* **2012**, 3, 9.
20. Tharanathan, R. Biodegradable films and composite coatings: past, present and future. *Trends in food science & technology* **2003**, 14, 71-78.
21. Cuomo, F.; Perugini, L.; Marconi, E.; Messia, M.C.; Lopez, F. Enhanced Curcumin Bioavailability through Nonionic Surfactant/Caseinate Mixed Nanoemulsions. *Journal of food science* **2019**.
22. Nieto, M.B. Structure and function of polysaccharide gum-based edible films and coatings. In *Edible films and coatings for food applications*, Springer: **2009**; pp. 57-112.
23. Pereda, M.; Ponce, A.; Marcovich, N.; Ruseckaite, R.; Martucci, J. Chitosan-gelatin composites and bi-layer films with potential antimicrobial activity. *Food Hydrocolloids* **2011**, 25, 1372-1381.
24. Talón, E.; Trifkovic, K.T.; Nedovic, V.A.; Bugarski, B.M.; Vargas, M.; Chiralt, A.; González-Martínez, C. Antioxidant edible films based on chitosan and starch containing polyphenols from thyme

extracts. *Carbohydrate polymers* **2017**, 157, 1153-1161.
25. Park, H.J.; Weller, C.; Vergano, P.; Testin, R. Permeability and mechanical properties of cellulose-based edible films. *Journal of Food Science* **1993**, 58, 1361-1364.
26. Möller, H.; Grelier, S.; Pardon, P.; Coma, V. Antimicrobial and physicochemical properties of chitosan− hpmc-based films. *Journal of agricultural and food chemistry* **2004**, 52, 6585-6591.
27. Jiménez, A.; Fabra, M.; Talens, P.; Chiralt, A. Effect of lipid self-association on the microstructure and physical properties of hydroxypropyl-methylcellulose edible films containing fatty acids. *Carbohydrate Polymers* **2010**, 82, 585-593.
28. Parra, D.F.; Tadini, C.C.; Ponce, P.; Lugão, A.B. Mechanical properties and water vapor transmission in some blends of cassava starch edible films. *Carbohydrate polymers* **2004**, 58, 475-481.
29. Jiménez, A.; Fabra, M.J.; Talens, P.; Chiralt, A. Edible and biodegradable starch films: a review. *Food and Bioprocess Technology* **2012**, 5, 2058-2076.
30. McHugh, D.J. Production, properties and uses of alginates. *Production and Utilization of Products from Commercial Seaweeds. FAO. Fish. Tech. Pap* **1987**, 288, 58-115.
31. Zactiti, E.; Kieckbusch, T. Potassium sorbate permeability in biodegradable alginate films: Effect of the antimicrobial agent concentration and crosslinking degree. *Journal of Food Engineering* **2006**, 77, 462-467.
32. Petersen, K.; Nielsen, P.V.; Bertelsen, G.; Lawther, M.; Olsen, M.B.; Nilsson, N.H.; Mortensen, G. Potential of biobased materials for food packaging. *Trends in food science & technology* **1999**, 10, 52-68.
33. Kohn, R. Ion binding on polyuronates-alginate and pectin. *Pure and Applied Chemistry* **1975**, 42, 371-397.
34. Francis, N.L.; Hunger, P.M.; Donius, A.E.; Riblett, B.W.; Zavaliangos, A.; Wegst, U.G.; Wheatley, M.A. An ice-templated, linearly aligned chitosan-alginate scaffold for neural tissue engineering. *Journal of Biomedical Materials Research Part A: An Official Journal of The Society for Biomaterials, The Japanese Society for Biomaterials, and The Australian Society for Biomaterials and the Korean Society for Biomaterials* **2013**, 101, 3493-3503.
35. Cuomo, F.; Cofelice, M.; Lopez, F. Rheological characterization of hydrogels from alginate-based nanodispersion. *Polymers* **2019**, 11, 259.
36. Pawar, S.N.; Edgar, K.J. Alginate derivatization: a review of chemistry, properties and applications. *Biomaterials* **2012**, 33, 3279-3305.
37. Sutherland, I.W. Gel-forming polysaccharides. Google Patents: **1987**.
38. Slaughter, B.V.; Khurshid, S.S.; Fisher, O.Z.; Khademhosseini, A.; Peppas, N.A. Hydrogels in regenerative medicine. *Advanced materials* **2009**, 21, 3307-3329.
39. Leong, J.-Y.; Lam, W.-H.; Ho, K.-W.; Voo, W.-P.; Lee, M.F.-X.; Lim, H.-P.; Lim, S.-L.; Tey, B.-T.; Poncelet, D.; Chan, E.-S. Advances in fabricating spherical alginate hydrogels with controlled particle designs by ionotropic gelation as encapsulation systems. *Particuology* **2016**, 24, 44-60.
40. Emmerichs, N.; Wingender, J.; Flemming, H.-C.; Mayer, C. Interaction between alginates and manganese cations: identification of preferred cation binding sites. *International journal of biological macromolecules* **2004**, 34, 73-79.
41. Draget, K.I.; Østgaard, K.; Smidsrød, O. Homogeneous alginate gels: A technical approach. *Carbohydrate polymers* **1990**, 14, 159-178.
42. Chan, L.W.; Lee, H.Y.; Heng, P.W. Mechanisms of external and internal gelation and their impact on the functions of alginate as a coat and delivery system. *Carbohydrate Polymers* **2006**, 63, 176-187.
43. Bourlieu, C.; Guillard, V.; Vallès-Pamiès, B.; Gontard, N. Edible moisture barriers for food product stabilization. In *Food Materials Science*, Springer: **2008**; pp. 547-575.
44. Burt, S. Essential oils: their antibacterial properties and potential applications in foods—a review. *International journal of food microbiology* **2004**, 94, 223-253.
45. Tiwari, B.K.; Valdramidis, V.P.; O'Donnell, C.P.; Muthukumarappan, K.; Bourke, P.; Cullen, P. Application of natural antimicrobials for food preservation. *Journal of agricultural and food chemistry* **2009**, 57, 5987-6000.

46. Donsi, F.; Ferrari, G. Essential oil nanoemulsions as antimicrobial agents in food. *Journal of biotechnology* **2016**, 233, 106-120.
47. Shah, B.; Davidson, P.M.; Zhong, Q. Nanodispersed eugenol has improved antimicrobial activity against Escherichia coli O157: H7 and Listeria monocytogenes in bovine milk. *International journal of food microbiology* **2013**, 161, 53-59.
48. Xue, J.; Davidson, P.M.; Zhong, Q. Antimicrobial activity of thyme oil co-nanoemulsified with sodium caseinate and lecithin. *International journal of food microbiology* **2015**, 210, 1-8.
49. Ponce, A.G.; Roura, S.I.; del Valle, C.E.; Moreira, M.R. Antimicrobial and antioxidant activities of edible coatings enriched with natural plant extracts: in vitro and in vivo studies. *Postharvest biology and technology* **2008**, 49, 294-300.
50. Tongnuanchan, P.; Benjakul, S. Essential oils: extraction, bioactivities, and their uses for food preservation. *Journal of food science* **2014**, 79, R1231-R1249.
51. Rocha, A.M.C.N.; Morais, A.M.M.B. Polyphenoloxidase activity and total phenolic content as related to browning of minimally processed 'Jonagored'apple. *Journal of the Science of Food and Agriculture* **2002**, 82, 120-126.
52. Pareek, S. Fresh-cut fruits and vegetables: technology, physiology, and safety. *Science* **2004**, 71, S615-S620.
53. Pizzocaro, F.; Torreggiani, D.; Gilardi, G. Inhibition of apple polyphenoloxidase (PPO) by ascorbic acid, citric acid and sodium chloride. *Journal of Food Processing and Preservation* **1993**, 17, 21-30.
54. Son, S.; Moon, K.; Lee, C. Inhibitory effects of various antibrowning agents on apple slices. *Food Chemistry* **2001**, 73, 23-30.
55. Chiabrando, V.; Giacalone, G. Effect of antibrowning agents on color and related enzymes in fresh-cut apples during cold storage. *Journal of Food Processing and Preservation* **2012**, 36, 133-140.
56. Rojas-Graü, M.; Tapia, M.; Rodríguez, F.; Carmona, A.; Martin-Belloso, O. Alginate and gellan-based edible coatings as carriers of antibrowning agents applied on fresh-cut Fuji apples. *Food Hydrocolloids* **2007**, 21, 118-127.
57. Galus, S.; Kadzińska, J. Food applications of emulsion-based edible films and coatings. *Trends in Food Science & Technology* **2015**, 45, 273-283.
58. Krochta, J.; Mulder, J. Edible and biodegradable polymer films: Challenges and Opportunities. *Food Technology* **1997**, 51, 61-74.
59. Sessa, M.; Ferrari, G.; Donsì, F. Novel edible coating containing essential oil nanoemulsions to prolong the shelf life of vegetable products. *Chemical Engineering Transactions* **2015**, 43, 55-60.
60. Moreira, M.d.R.; Roura, S.I.; Ponce, A. Effectiveness of chitosan edible coatings to improve microbiological and sensory quality of fresh cut broccoli. *LWT-Food science and technology* **2011**, 44, 2335-2341.
61. Nussinovitch, A.; Nussinovitch, A. *Water-soluble polymer applications in foods*; Wiley Online Library: **2003**.
62. Panahirad, S.; Naghshiband-Hassani, R.; Ghanbarzadeh, B.; Zaare-Nahandi, F.; Mahna, N. Shelf Life Quality of Plum Fruits (Prunus domestica L.) Improves with Carboxymethylcellulose-based Edible Coating. *HortScience* **2019**, 54, 505-510.
63. Otoni, C.G.; Pontes, S.F.; Medeiros, E.A.; Soares, N.d.F. Edible films from methylcellulose and nanoemulsions of clove bud (Syzygium aromaticum) and oregano (Origanum vulgare) essential oils as shelf life extenders for sliced bread. *Journal of Agricultural and Food Chemistry* **2014**, 62, 5214-5219.
64. Bravin, B.; Peressini, D.; Sensidoni, A. Development and application of polysaccharide–lipid edible coating to extend shelf-life of dry bakery products. *Journal of Food Engineering* **2006**, 76, 280-290.
65. Gennadios, A. *Protein-based films and coatings*; CRC press: **2002**.
66. Krochta, J.M. Proteins as raw materials for films and coatings: definitions, current status, and opportunities. *Protein-based films and coatings* **2002**, 1, 1-40.
67. Janjarasskul, T.; Sothornvit, R.; McHugh, T. Edible films and coatings for fresh and minimally processed fruits and vegetables. In *Fresh-Cut Fruits and Vegetables*, CRC Press: **2016**; pp. 363-432.
68. Di Pietro, P.F.; Medeiros, N.I.; Vieira, F.G.K.; Fausto, M.A.; Belló-Klein, A. Breast cancer in

southern Brazil: association with past dietary intake. *Nutricíon hospitalaria.[Madrid].* Vol. 22, no. 5 (sept./oct. 2007), p. 565-572 **2007**.
69. Baselice, A.; Colantuoni, F.; Lass, D.A.; Nardone, G.; Stasi, A. Trends in EU consumers' attitude towards fresh-cut fruit and vegetables. *Food Quality and Preference* **2017**, 59, 87-96.
70. Drogoudi, P.D.; Vemmos, S.; Pantelidis, G.; Petri, E.; Tzoutzoukou, C.; Karayiannis, I. Physical characters and antioxidant, sugar, and mineral nutrient contents in fruit from 29 apricot (Prunus armeniaca L.) cultivars and hybrids. *Journal of agricultural and food chemistry* **2008**, 56, 10754-10760.
71. Dea S., G.C., Perez-Gago M.B. and Plotto A. Coatings for minimally processed fruits and vegetables. In *Edible Coatings and Films to Improve Food Quality*, Baldwin E., H.R.a.B.J., Ed. CRC Press: Boca Raton, FL, **2011**; pp. 243-289.
72. Valero, D.; Serrano, M. *Postharvest biology and technology for preserving fruit quality*; CRC press: **2010**.
73. Mahayothee, B.; Rungpichayapichet, P.; Yuwanbun, P.; Khuwijitjaru, P.; Nagle, M.; Müller, J. Temporal changes in the spatial distribution of physicochemical properties during postharvest ripening of mango fruit. *Journal of Food Measurement and Characterization* **2020**, 1-10.
74. Vieira, F.; Borges, G.; Copetti, C.; Gonzaga, L.V.; Nunes, E.C.; Fett, R. Activity and contents of polyphenolic antioxidants in the whole fruit, flesh and peel of three apple cultivars. *Arch Latinoam Nutr* **2009**, 59, 101-106.
75. Janovitz-Klapp, A.; Richard, F.; Nicolas, J. Polyphenoloxidase from apple, partial purification and some properties. *Phytochemistry* **1989**, 28, 2903-2907.
76. Luo, Y.; Lu, S.; Zhou, B.; Feng, H. Dual effectiveness of sodium chlorite for enzymatic browning inhibition and microbial inactivation on fresh-cut apples. *LWT-Food Science and Technology* **2011**, 44, 1621-1625.
77. Antunes, M.D.; Dandlen, S.; Cavaco, A.M.; Miguel, G. Effects of postharvest application of 1-MCP and postcutting dip treatment on the quality and nutritional properties of fresh-cut kiwifruit. *Journal of Agricultural and Food Chemistry* **2010**, 58, 6173-6181.
78. de Souza, B.S.; O'Hare, T.J.; Durigan, J.F.; de Souza, P.S. Impact of atmosphere, organic acids, and calcium on quality of fresh-cut 'Kensington'mango. *Postharvest Biology and Technology* **2006**, 42, 161-167.
79. Arias, E.; López-Buesa, P.; Oria, R. Extension of fresh-cut "Blanquilla" pear (Pyrus communis L.) shelf-life by 1-MCP treatment after harvest. *Postharvest Biology and Technology* **2009**, 54, 53-58.
80. Kader, A. Future of modified atmosphere research. In *Proceedings of IX International Controlled Atmosphere Research Conference 857*; pp. 213-218.
81. Saltveit, M.E. Physical and physiological changes in minimally processed fruits and vegetables. In *Proceedings of Proceedings-Phytochemical Society of Europe*; pp. 205-220.

2 Colloidal Systems

«Logic brings you from A to B, imagination brings you everywhere»
A. Einstein

2.1 Colloidal Systems

In several branches of science and technology, we often deal with colloidal systems. Almost all agricultural and industrial products, especially foodstuffs, contain colloidal structures that determine their rheological properties and textures. Example are founded in living cells, food products, pharmaceuticals, soil and different biotechnological and biomedical appliances. The institution of the colloid science is dated around the mid-nineteenths, when Selmi described the first colloidal particles as ´pseudosolutions´ to explain an anomalous behavior.
In 1850 Faraday focused on colloidal gold sols, i.e. particles of gold in water. In 1861, Thomas Graham introduced the term *colloid*, from the Greek word $\kappa o \lambda \lambda \alpha$ which means *glue*, to describe the systems previously defined by Selmi. With this term Graham emphasized the low rate of diffusion of particles with size of at least few nanometers in diameter and lack of crystallinity. Significant advances in explaining the stability of colloidal sols were made in 1945, with the publication of Derjaguin-Landau and Verwey-Overbeek (DLVO) theory, cornerstone of colloidal science [1].
Colloidal domain generally refers to systems with particle size ranging from a few to few thousand nanometers [2]. Colloidal particles, having intermediate dimensions, possess characteristics related to both the nanoscopic and the macroscopic worlds. At the lower limit, particles of a few nanometers dispersed in a liquid medium show strongly reduced colligative properties, like osmotic pressure and freeze point suppression, as compared to solution of regular-sized molecules of the same mass-concentration. The colloidal behavior is based on a delicate balance of the intrinsic thermal motion and external forces that act upon between the particles.
A colloidal system is a heterogeneous mixture in which one phase is finely dispersed into another, called continuous phase by amphiphilic molecules. Because of the characteristic dimensions of the dispersed phase, colloidal systems develop a large interfacial area. The interfacial properties govern the interaction between colloidal particles and therewith the macroscopic behaviour and the characteristics of colloidal system, like the rheological and optical properties and the stability against aggregation.
Colloids can be distinguished in *hydrophobic* and *hydrophilic* based on their affinity with water; in the first case the water molecules have a higher affinity for one another than for the colloidal particles. While hydrophilic colloids are those that ´love´ water, based on the presence of an electrical charge that allow particles to interact in a positive way with it. On the basis of the constituting phases colloids may be classified, as is done in Table 2.1.

2.1.1 Interaction between particles in colloidal systems

The nature and the magnitude of the surface/interface energy are determined by the physicochemical properties of the particles and the solvent since the particles will have a tendency to undergo aggregation to reduce the surface energy. Colloidal particles in a dispersion medium are always subjected to Brownian motion with frequent collisions between them. Stability and other

Table 2.1: Calssification of colloidal dispersions.

		Dispersed Material		
		Solid (S)	**Liquid (L)**	**Gas (G)**
Medium	**Solid (S)**	Solid suspension (bone, wood, various composite materials)	Solid emulsion (opals, pearls)	Solid foam (loofah, bread, pumice, styrofoam)
	Liquid (L)	Sol, suspension (blood, polymer latex, paint, ink)	Emulsion (milk, rubber, crude oil, shampoo, mayonnaise)	Foam (detergent foam, beer foam)
	Gas (G)	Aerosol (smoke, dust)	Aerosol (fog, sprays)	-

characteristics of dispersion are thus determined by the nature of the interactions between the particles during such collisions. When attractive forces dominate, the particles will aggregate and the dispersion may destabilize. When repulsive forces dominate, the system will remain in a dispersed state [1].

Attractive forces - van der Waals forces

London explained the van der Waals forces (the universal attractive forces) acting between all atoms, molecules and ions on the basis of wave mechanics. These short-range forces result from the interaction between temporary dipoles on some molecules and induced dipoles on the neighboring molecules, and a quantum mechanical effect leading to attraction between nonpolar molecules. They are fairly weak and only important on small scales (crucial for molecules, very important for colloids). Most of the interpretations of London-van der Waals forces in the past have been based on the Hamaker approach, which involves pairwise addition of the microscopic forces acting between two bodies (Eq.2.1):

$$V_A = \frac{-A_H R}{12D^2} \tag{2.1}$$

A_H= Hamaker constant
R= particle radius
D= distance

Repulsive and steric forces

Electrostatic interactions
Electrostatic interactions occur between molecular species that possess permanent electrical charges (ions and polar molecules). It is possible a redistribution of ions in the surrounding solution by droplets. Same charges repel each other, but there is an effective range of repulsion determined by Eq. 2.2:

$$V_E = Kr\Psi^2 e^{-kh} \tag{2.2}$$

V_E= free energy due to electrostatic interactions
K= constant
r= particle radius
Ψ= electrostatic potential
k= reciprocal Debye lenght
h= particle distance

Steric and bridging forces
To explain stability of dispersed systems it is necessary to take in consideration also steric repulsion. If we consider two particles that approach each other, the entropy per adsorbed molecule decreases causing desorption and a concomitant increase in the interfacial energy. This

means that to bring the particles together, additional work has to be made and this shows itself as a repulsive force. Interpenetration and aggregation is possible only if the net change in Gibbs free energy, due to the interpenetration of the polymer chains, is negative.
The Gibbs free energy change is determined essentially by the change in entropy, due to the release of solvent molecules and to the decrease in randomness of the polymer chain, and by the enthalpy of de-solvation of the polymer chains. De-solvation characteristics of the adsorbed polymer species and the dependence of it on solution properties such as temperature and ionic strength will be important in determining aggregation by this mechanism. Ottewill and Walker derived an equation (Eq. 2.3) for the energy change due to an overlap of the adsorbed layers by using Flory´s liquid lattice model for polymer solutions [3,4].

$$V_{steric}(a) = \frac{4\pi kTC_V^2}{3v_1^2\rho_2^2}(\psi_1 - k_1)(\delta - a)^2(3R + 2\delta + \frac{a}{2}) \tag{2.3}$$

C_v= concentration of material in the adsorbed layer
v_1= molecular volume of solvent molecules
ρ_2 = density of the adsorbate
ψ_1 and k_1= entropy and enthalpy parameters
δ= adsorbed layer thickness
R= particle radius
a= distance separating the surfaces

In an emulsion system, the steric interaction depends on the separation distance between the internal aqueous droplets and the external aqueous phase, the thicknesses of the adsorbed surfactant layer and the size of the internal aqueous droplets and the oil globules. All these aspects determine the extent of the compression of the adsorbed surfactant molecules. The thickness of surfactant layers has the same effect on the steric repulsion, and stronger steric interaction can be achieved with thicker adsorbed layers, which can effectively prevent coalescence between the internal aqueous droplets and the external aqueous phase. Increasing the internal aqueous droplet size can produce stronger steric repulsion; however, larger oil globules will weaken the steric repulsion, indicating that a more stable emulsion system can be achieved by preparing the system with smaller oil globules and larger internal aqueous droplets. Polymers are known as protective against coagulation and they lead to the steric stabilisation of a colloid. They can provide bridging between particles particularly under conditions where particles are not totally coated by the polymeric species. To stabilize systems with polymers, where the surface area-to-volume A/V is high, it is important to add sufficient amount of polymer that will be adsorbed on the surfaces of the particles to fully covered it. If the polymer has a reasonably high molecular weight, it is possible that an adsorbed polymer molecule at a particle surface may stretch over and adsorb to another particle surface, thus creating a bridge. If the bridging force is strong enough, the outcome will be flocculation or coagulation of the dispersion. The phenomenon is favoured in systems with unsaturated particle surfaces and high molecular weight polymers that adsorb relatively strongly to the particles.

DLVO theory

Colloidal stability refers to the long-term integrity of a dispersion and its ability to resist phenomena such as sedimentation or particle aggregation. Stability of the colloidal systems is well described by the DLVO theory; this theory was elaborated by Derjaguin and Landau and, independently, by Verwey and Overbeek [5]. Two types of forces are considered in DLVO theory: long-range van der Waals attraction forces (V_A) and repulsive electric forces (V_R) which increase exponentially with decreasing distance (h). Thus the total interaction potential can be written

as (Eq. 2.4):

$$V(h) = V_A(h) + V_R(h) \tag{2.4}$$

Depending on the relative strength of the attractive and repulsive terms, it is possible to generate an interaction potential as function of the distance between surfaces that is illustrated with the force curves in Fig. 2.1B.

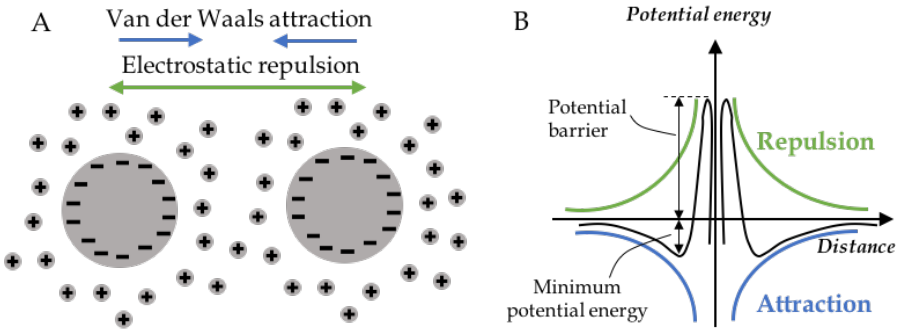

Figure 2.1: *Attractive and repulsive forces (A) interaction potential vs distance curves (B).*

The interaction potentials have the character of free energies and contain both energetic and entropic contributions. The attractive term $V_A(h)$ dominates the repulsive term $V_R(h)$ when h is very large or very small. At intermediate separations the double-layer force gives rise to a potential energy barrier if the surface is sufficiently charged and if the electrolyte ions do not screen too much. If the sum of the repulsion forces is higher than that one of the attraction forces, the system described can be considered stable. If the attractive forces, caused by permanent dipole-dipole interaction (Keesom), permanent dipole-induced dipole forces (Debye) and the transitory dipole-dipole forces (London), are stronger than the repulsive forces, the particles adhere each other and, as a result, flocculation occurs.

2.2 Emulsions - Structural complexity

Emulsions are colloidal dispersions of two immiscible liquids in which one is present as fine droplets (usually in lower amount) in a continuous medium (liquid as well) held together by the emulsifying agents (having both hydrophilic and hydrophobic characteristics) that are located at the oil/water interface. Emulsification appeared, as an industrial process, at the beginning of the XX century, with a technologic-gastronomic aim: give better texture to food products, incorporations of flavour, colorant and so on. Emulsions can be classified in two different ways:

1. Based on the dispersed phase:
    - O/W (oil in water): where lipid (oil) is the dispersed phase in a water continuous phase;
    - W/O (water in oil): where water is the dispersed phase and oil the continuous one;
    - O/W/O (oil in water in oil) or W/O/W (water in oil in water): multiple emulsions.
2. Based on dimensions of the dispersed phase:
    - Macroemulsions: 1 to 100 um (weakly kinetically stable);
    - Nanoemulsions: 20 to 500 nm (kinetically stable);
    - Microemulsions: 10 to 100 nm (thermodynamically stable).

Food emulsions can be characterized by high complexity both in their composition and structure if compared to the simple three components (oil, water and surfactant). Main components can be polysaccharides, lipids, proteins and surfactants. The interaction between droplets and other dispersed particles, contribute to the structural complexity. The polysaccharides have basically a controlling effect of viscosity of the continuous medium. The interaction between droplets and other dispersed particles (proteins, gases bubbles, starch grains, fat or water crystals and so on) contribute to the structure complexity. Each production, in turn, has its own structural organization that control its stability, depending on time and amount of ingredients. Between the two components O and W it is possible to have: solid particles, monolayer of surfactant or proteins, multilayers of surfactant, gels or various liquid crystals. The formation of emulsion is not a spontaneous process, so in order to form it, is necessary to give energy proportionally to the increase of the interfacial area.

$$\Delta G = \Delta A \gamma_{w/o} - T\Delta S_{conf} \tag{2.5}$$

$\Delta A\gamma_{w/o}$= energy required to expand the interphase
$T\Delta S_{conf}$= configurational entropy

The free energy (ΔG) of formation is positive because $\Delta A\gamma_{w/o}$ is always positive and higher than $T\Delta S_{conf}$, so the formation process of emulsion is not spontaneous. The entropic term is negative, thus allowing the formation of emulsion, but its absolute value is lower than the $\Delta A\gamma_{w/o}$, so to produce an emulsion it is necessary to modify this parameter. This is possible adding a surface active agent to the mixture (decrease of interfacial energy, stabilization of the emulsion). The surface tension (γ) decrease also using mixture of surfactant or co-surfactant, molecules that dispose at the interface making the system more stable. In case of microemulsion the surface tension is reduced at $\Delta A\gamma_{w/o}$ values lower or equal to $T\Delta S$, so the free energy is negative or equal to zero. Being $\Delta G \leq 0$ microemulsions are thermodynamically stable. To prepare emulsions it is necessary to give energy in a *mechanic* or *chemical* way. The first one can be provided through mixing by any means, while the second one is given by the ingredients, and is available when there is a contact between them. The energy required for emulsification of a liquid with volume v, in a solvent, considering R as the radius of the droplets is given by:

$$\Delta G_{em} = \frac{\gamma 3v}{R} \tag{2.6}$$

The theoretical value obtained from the Eq. 2.6 is lower if compared to the real one, due to the fact that part of the supplied energy is converted to heat, due to friction, and the energy to supply needs to be higher than the energy barrier against destabilization. Two competitive processes will determine the final structure of emulsion, so the formation of direct or inverse structures: the *migration of surfactant* to the interface and *coalescence*. The first one is a stabilizing process, while the second one brings to an irreversible instability. The continuous phase will be the one with higher rate of coalescence. Another factor that influence the structure is the order in which the ingredients are mixed. The amount of emulsifier, together with the capacity of the equipment is a limiting factor in the production of emulsions with a determinate particle size. Different type of emulsification will lead to the production of different distribution and average particle size. So, as discussed, nanoemulsions are thermodynamically unstable systems and appropriate stabilizers are required to form and stabilize them.

2.2.1 Stabilizer - Surfactant

Surfactants (SURFace ACTive ageNTS) are amphiphilic molecules with low molecular weight (usually <1000 Dalton) with detergent, solubilizing, foaming and wetting properties. These

compounds have several important roles in formation and stabilization of emulsions. Examples of the main roles are: lowering the surface tension, giving higher stability to the emulsion, acting on the free energy, avoiding the rupture of the film layer surrounding the dispersed phase, reducing the coalescence and so on.
The surface active agents (Fig. 2.2) are constituted by a hydrophilic part, defined as polar head with affinity for polar media, and a hydrophobic part, tail, with affinity to non-polar media. These two parts give rise to the amphiphilic character of surfactants.

Figure 2.2: *Schematic representation of surface active agents with single or double ¨tails¨.*

Surfactants are molecules that act on the surface, and in presence of immiscible phases are positioned in such a way that the hydrophilic heads face the hydrophilic area, while the tails are organized in the hydrophobic one. Properties of surfactants depend on:

- the position of the polar head;
- the length of the carbon-chains;
- the relative dimension of the two parts;
- the ramification of the apolar chains.

Based on the charge of the groups present in the polar head, it is possible to classify surfactants into anionic (negatively charged - carboxylate, sulphate or phosphate), cationic (positively charged - ammine or quaternary ammonium), zwitterionic (with the presence of negative and positive charge - derivate N-alchilic of aminoacid) and non-ionic (no charge).
The electrical properties of an emulsifier have major impact on the formation, stability and functional properties of nanoemulsions. In this work of thesis non-ionic surfactant has been used. Nonionic surfactants are generally less toxic, less hemolytic and less irritating to cellular surfaces than other anionic or cationic surfactants and, in solution, they tend to maintain pH close to physiological values. They have uncharged hydrophilic head-groups and solubilize in water through H-bonding. The hydrophilic part contains the polyoxyethylene, polyoxypropylene or polyol derivatives. The hydrophobic part contains saturated or unsaturated fatty acids or fatty alcohols. Among the non-ionic surfactants are sorbitane monooleate or sucrose monopalmitate, polyoxyethylene sorbitane esters of monoglyceride (Tweens - Fig. 2.3).

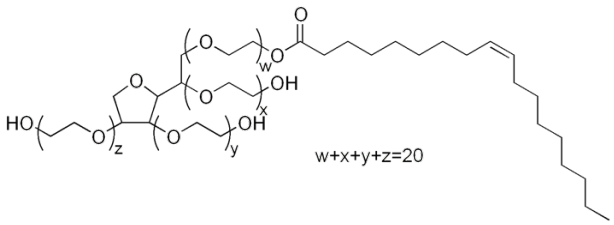

Figure 2.3: *Chemical structure of Tween 80 - Polyoxyethylene (20) sorbitan monooleate.*

Certain polysaccharides have surface-active properties and can be used as emulsifiers, with lower efficiency if compared to proteins or small molecule of surfactant.

Surfactant choice

Two parameters are fundamental in the choice of surfactant:

- HLB (Hydrophilic-Lipophilic Balance);
- Packing parameter.

HLB is a semi-empirical concept based on the structure of the surfactant, in particular on the percentage of hydrophilic and lipophilic groups. This parameter can be calculated with Griffin equation (Eq. 2.7):

$$HLB = 20(1 - \frac{S}{A}) \tag{2.7}$$

S= number of saponification of ester
A= acid number of fatty acid

Another formula that can be used to determine HLB taking in consideration the hydrophilic group number (n_H) and the lipophilic group number (n_L) is the Davis equation (Eq. 2.8):

$$HLB = 7 + \sum n_H(i) - \sum n_L(i) \tag{2.8}$$

HLB measures the relative wettability of the surfactant in each of the phases: the curvature of the O/W interface will become convex towards the phase that preferably moisturizes the emulsifier (analogously to solid particle stabilization). If the surfactant has a low HLB it will form W/O emulsions, while at higher value of HLB O/W emulsions will be formed. *Packing parameter* (N_s) is inversely correlate to the HBL. Taking in consideration a surfactant with a hydrophobic chain of volume v characterized by an effective area per headgroup a_0 and hydrocarbon chains with length l it is possible to calculate N_s as:

$$Ns = \frac{v}{la_0} \tag{2.9}$$

the volume of the hydrocarbon core of a saturate hydrocarbon chain (nm^3) is:

$$v = 0.027(n_c + n_{Me}) \tag{2.10}$$

where n_c is the total number of carbon atoms and n_{Me} is the number of methyl groups, which are twice the size of an ethylene group. Also, the maximum length (nm) of a fully extended hydrocarbon chain can be estimate from Eq. 2.11.

$$l = 0.15 + 0.127n_c \tag{2.11}$$

The most problematic quantity to define is the area per headgroup; for ionic surfactant, a_0 depends on both electrolyte and surfactant concentration. For non-ionic or zwitterionic surfactant, a_0 is less sensitive to external conditions. Packing parameter relates the properties of the molecule to the preferred curvature properties of the aggregates (Fig. 2.4). Small values of N_s imply highly curved aggregates (spherical micelles, cylinders), when it is close to the unit, planar bilayers usually form. For values higher than 1 inverted cylinders and micelles will be obtained.

2.2.2 Emulsions Instability

A freshly prepared emulsion changes its properties with time, owing to a series of different events that occur on a microscopic scale. Depending on the particular molecular characteristics

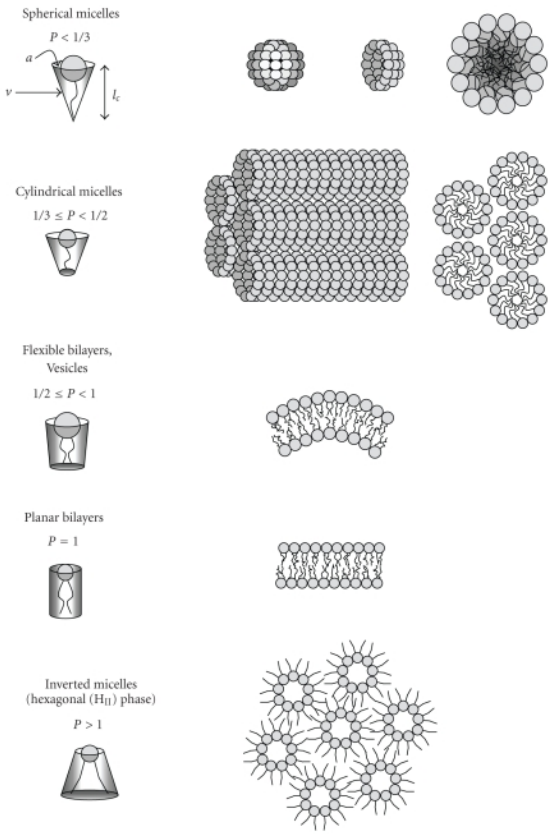

Figure 2.4: *Structures predicted by the Packing parameter (P).*

involved, these events rapidly lead either to the overall equilibrium state with macroscopically separated phases (´unstable emulsion´) to a metastable state (´stable emulsion´). The difference between a stable and unstable system is qualitative and could depend on the context [1]. An emulsion is potentially unstable, such as the other colloidal systems. Principal processes of destabilization are due to different forces: gravitational forces (creaming and sedimentation), inter-particular forces at molecular scale (flocculation), flow and molecular forces (coalescence). Fig. 2.5 depicts the main mechanism of emulsion destabilization, depending on the size of droplets and emulsion concentration. At high concentration the small distance among droplets favour the coalescence, especially if droplets have big dimensions, while at lower concentration the creaming and flocculation occur mostly, for big and small droplets respectively.

Creaming and Sedimentation

Creaming and sedimentation are the result of the movement of droplets under forces such as gravity or centrifugal one. The destabilization phenomenon takes the name of creaming when the action of external forces creates a concentrate layer on the surface of the vessel, while when the droplet comes to the bottom the phenomenon is called sedimentation. These destabilization processes do not occur when the Brownian diffusion of droplets (kT) is greater than the gravitational force, g, in a vessel with l length and in an emulsion with difference of density $\Delta\rho$ between the two phases, as express by the following relation:

$$kT > \frac{4}{3}\pi R^3 \Delta\rho g l \tag{2.12}$$

During creaming (as well as in sedimentation) we can distinguish two steps of the process; in

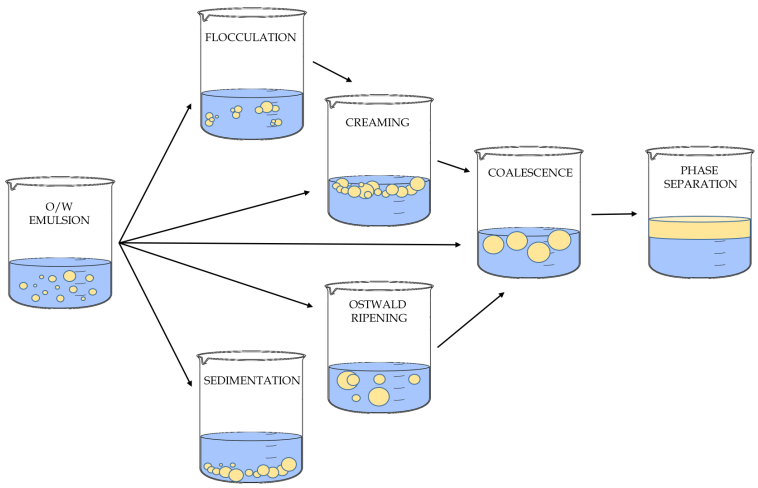

Figure 2.5: *Different mechanisms of emulsion destabilization, depending on the particle size and dispersed phase concentration.*

the first one there is a vertical gradient of droplets concentration. In the second step it is possible to see two different phases: the upper phase or cream, and the lower phase or serum (opposite for sedimentation). If we consider a single drop, with radius r and density ρ in a continuous medium, with density ρ_0 and viscosity η_0, and g as the acceleration due to the gravity, with the application of balance of forces it is possible to obtain Stoke´s law (Eq.2.13), used to obtain the creaming velocity (v_s)

$$v_s = -\frac{2gr^2(\rho - \rho_0)}{9\eta_0} \tag{2.13}$$

with this equation it is possible to determine the factor to change in order to minimize the creaming:

- reducing the particle size (through homogenization);
- reducing the difference of density between droplet and continuous phase (multiple emulsions);
- adjusting the viscosity of the continuous phase (incorporation of hydrocolloids).

Flocculation

The phenomenon consists in the droplets aggregation, caused by van der Waals forces (V_A), without varying their individual size. The potential of two equal particles of radius R, at distance h is given by:

$$V_A = \frac{-A_H R}{2h} \tag{2.14}$$

where A_H is the Hamaker constant, which is related to the polarizability of the molecules at the interface. Since V_A increases decreasing h, in the absence of repulsive forces, large droplet aggregates are formed. Repulsive forces can be established in the presence of ionic surfactants that create a double electrical layer between the droplets or using non-ionic surfactants that are adsorbed at the interphase with the hydrophobic parts, creating a hydrophilic layer in the bulk. This layer prevents that the droplets come close to each other by steric interaction.

Coalescence

Coalescence happens after that the films separating the droplets are thinned and broken, so two droplets coming in contact and consequently they blend. The mechanism of this phenomenon can be explained in terms of disjoining pressure, π. This pressure is the result of the summing of three contributions due to the van der Waals forces (A), electrostatic forces (E) and steric forces (S):

$$\pi = \pi_A + \pi_E + \pi_S \tag{2.15}$$

Since electrostatic and steric forces are repulsive forces, in order to reduce coalescence, it is necessary to have a positive disjoining pressure:

$$\pi_A < \pi_E + \pi_S \tag{2.16}$$

Ostwald ripening

The Ostwald ripening can be described as the growth of droplets size at the expense of the small one due to the mass transport of the soluble dispersed material in the continuous medium. The thermodynamic driving force is the decrease of the chemical potential of the components of the dispersed phase when the radius of curvature of the drop increase. The driving force is inversely proportional to the droplet size. So droplets with smaller radius are more soluble than the one with lower curvature. It is mathematically described by Ostwald relation (Eq. 2.17) here reported:

$$\frac{RT}{M} \ln \frac{S_1}{S_2} = \frac{2\gamma}{\rho}(\frac{1}{R_1} - \frac{1}{R_2}) \tag{2.17}$$

S = solubility ($S_1 > S_2$ if $R_1 < R_2$)
R= radius
M= molecular weight
ρ = droplets' density

As the force which regulates the process is γ, the addition of a surfactant reduces the process. When the dispersed phase is multicomponent it is characterized by different solubility, so the rate of ripening is reduced.

Phase inversion

This phenomenon is basically the inversion of the continuous phase and dispersed one; an emulsion made as O/W become a W/O. To happen it is necessary a high amount of energy, as mechanical energy. This process is really complex, and it involves primary process such as flocculation, coalescence, creaming and probably colloidal intermediate states structurally complicated: foams, multiple emulsions and so on. Based on Bancroft rules, it is possible to change the composition of an emulsion from O/W to W/O working on the HBL and Packing parameter.

2.2.3 Nanoemulsions

The concept of nanotechnology was introduced by Feyman in 1959, defining this as ´the design, characterization, production and application of structures, devices and systems by controlling the shape and size at nanometric scale´ [6]. As said before for emulsions, in O/W nanoemulsions oil droplets are dispersed in an aqueous medium and stabilized by an emulsifier layer. Appropriate food-grade surfactants (polysorbates, sugar esters, lecithins) together with other types of stabilizer, such as biopolymers, may be incorporated in food applications not only as an emulsifier but also to impart to the nanoemulsions some desired features, such as specific

interfacial behaviour (electrostatic forces, steric repulsion, and rheology), loading capability, as well as response to environmental stresses. What makes nanoemulsions interesting are their distinctive and unique properties due to their nanometric size. In fact, differently from emulsions, which are thermodynamically unstable systems, naturally tending to physical separation, nanoemulsions show physical meta-stability thanks to the Brownian motion effects dominating over gravitational forces. In addition, the strength of the net attractive forces acting between droplets usually decreases with decreasing droplet diameters, reducing aggregation phenomena in nanoemulsions [7]. Moreover, nanoemulsions do not scatter light strongly and form transparent or only slightly turbid systems, due to the droplet diameters that are much smaller than the wavelength of the visible light. In particular, these colloidal systems, exhibit optical transparency for mean droplet sizes<40 nm independently on the oil fraction, whereas, in the range between 40 and 100 nm nanoemulsions appear hazy, with a marked dependence on the oil content, and for sizes >100 nm they appear white due to significant multiple scattering [8]. Together with the decrease of droplets size, also the biological activity of the lipophilic compounds encapsulated in nanoemulsions increases because of the enhanced transport of active molecules through biological membranes. This happen also for the increased surface area/volume ratio, leading to improved reactivity [9]. Therefore, the encapsulation of lipophilic functional components into nanoemulsions offer several advantages.

Nanoemulsions preparation methods

The fabrication methods of nanoemulsions can be classified based on the energy used, so in high and low energy method, or in *top-down* and *bottom-up* approaches [10,11]. Fig. 2.6 depicts some of the possible routes to the fabrication of oil-in-water nanoemulsions, suggesting the approximate correlation between the process energy involved, the required amount of surfactant with respect to the oil phase, and the expected mean droplet size. Top-down approaches aimed

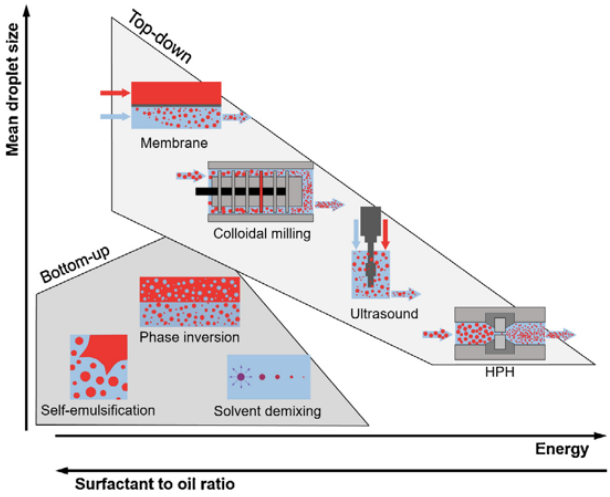

Figure 2.6: *Schematics of the different fabrication methods of o/w nanoemulsions, correlating their requirements in terms of energy and surfactant to oil ratio with the expected mean droplet size.*

at the disruption of the oil phase into homogeneously sized, fine droplets, while the bottom-up approaches, aimed instead at driving the direct assembling of molecular building blocks into structured systems. *Top-down* methods include mechanical size reduction techniques, where fluid-mechanical stresses are generated. Within these approaches, the emulsification process occurs in two phases: the first one is the break-up of coarse droplets into smaller ones while

the second is the absorption of the emulsifier onto the newly formed interfaces, to prevent coalescence phenomena and promote kinetic meta-stability. Systems used for the fabrication of O/W nanoemulsions are high shear homogenization (HSH), ultrasonication (US) and high pressure homogenization (HPH), which requires that large amounts of energy are transferred to the process fluid (50-500 MJ/m^3) [12]. However, less energy-intensive top-down approaches are also possible, such as membrane emulsification. High shear homogenization or colloid milling, includes all those devices equipped with high-speed rotor/stator systems (Ultra-Turrax), where the emulsification process is controlled by the intense shear stresses, friction, and high-frequency vibrations developed [13]. Despite HSH systems are cost-effective, easily scalable methods of emulsification, the resulting emulsion droplet size is limited by the lower intensity of the fluid-mechanical stresses than other systems.
Usually, HSH is extensively used as a preliminary step to produce the coarse emulsions, subsequently processed by HPH or US [14]. Even when using HSH devices with high emulsification efficiency, high surfactant to oil ratio (SOR) values are required. Ultrasonication (US) is based on the perturbation induced by cavitation phenomenon of the oil-water interface and consequent formation of fine droplets. The alternating low-pressure and high-pressure waves generated by ultrasounds at high frequency (>18 kHz) induce in liquids the rapid shifts from conditions of vapor bubble formation to vapor bubble its collapsation; bubbles, imploding lead to the intense shock waves of cavitation, reaching local pressures in the surrounding liquid as high as 1.35 MPa [15]. When associated to high SOR values, US ensures the rapid production of extremely fine nanoemulsions [16], also in very small processing batches. However, it is necessary to bearing in mind that with this technique local hot spots are induced that might degrade reactive or thermo-labile molecules, with a significant reduction in their activity.
Also *bottom-up* methods (solvent de-mixing, spontaneous emulsification and phase inversion) are able to efficiently produce very fine droplets, using simple to implement and scale-up, low-cost equipment, and preventing the encapsulated molecules from being degraded during processing. These approaches included physicochemical processes based on the spontaneous association of surfactants around the oil molecules, driven by the balance of attractive and repulsive forces tending to thermodynamic equilibrium. The self-assembly of oil droplets depends strongly on the properties of the molecules present, and in particular, their solubility, molecular geometry and surface activity [17]. Factors, such as temperature, concentration, pH and ionic strength of the system are exploited to control the entity of the involved forces, whereas mechanical energy is required only to ensure thorough system uniformity through agitation [14,18]. However, strict limitations apply to the types of oils and surfactants that can be used to form stable nanoemulsions, as well as to the required SOR, which are significantly higher than in top-down methods [14].

Nanoemulsions applied in food field

Due to their unique properties described above, nanoemulsions can be applied in several fields, from the pharmaceutical to the food industries. Basic research studies have highlighted the potential advantages derivate from the use of nanoemulsions to design smart food. The important consequence of the oil droplet size to the nano-range (increasing the surface area of the disperse phase) is the transport of active substances to cellular membrane, which in case of antimicrobials or nutraceuticals with lipophilic characteristics, result in a greater bactericidal effect [19].
The liphophilic character of nanoemulsions allows them to be used for the encapsulation of bioactive compounds, increasing the bioavailability of compounds with low-water solubility [20]. *In-vitro* digestion studies using bioactive-fortified nanoemulsions were conducted, showing that these systems protect lipophilic compounds, improving their bio accessibility and bioavailability [21]. As well as nanoemulsions are suitable for addition to clear beverages, sauces, soups, and syrups, their use is also growing in the food packaging fields, as it will be well described in the

following chapters.

References

1. Fennell Evans, D.; Wennerstrom, H.; Rajagopalan, R. The colloidal domain: where physics, chemistry, biology, and technology meet. *Journal of Colloid and Interface Science* **1995**, 172, 541-541.
2. Norde, W. *Colloids and interfaces in life sciences and bionanotechnology*; CRC Press: **2011**.
3. Flory, P.J.; Volkenstein, M. Statistical mechanics of chain molecules. *Biopolymers: Original Research on Biomolecules* **1969**, 8, 699-700.
4. Slater, R.; Kitchener, J. Characteristics of flocculation of mineral suspensions by polymers. *Discussions of the Faraday Society* **1966**, 42, 267-275.
5. Christenson, H.K. DLVO (Derjaguin–Landau–Verwey–Overbeek) theory and solvation forces between mica surfaces in polar and hydrogen-bonding liquids. *Journal of the Chemical Society, Faraday Transactions 1: Physical Chemistry in Condensed Phases* **1984**, 80, 1933-1946.
6. Castro, F. Legal and Regulatory concerns facing Nanotechnology. *Chi.-Kent J. Intell. Prop.* **2004**, 4, 140.
7. Rao, J.; McClements, D.J. Formation of flavor oil microemulsions, nanoemulsions and emulsions: influence of composition and preparation method. *Journal of agricultural and food chemistry* **2011**, 59, 5026-5035.
8. Mason, T.G.; Wilking, J.N.; Meleson, K.; Chang, C.B.; Graves, S.M. Nanoemulsions: formation, structure, and physical properties. *Journal of Physics: condensed matter* **2006**, 18, R635.
9. Salvia-Trujillo, L.; Rojas-Graü, A.; Soliva-Fortuny, R.; Martín-Belloso, O. Physicochemical characterization and antimicrobial activity of food-grade emulsions and nanoemulsions incorporating essential oils. *Food Hydrocolloids* **2015**, 43, 547-556.
10. Mason, T.; Graves, S.; Wilking, J.; Lin, M. Effective structure factor of osmotically deformed nanoemulsions. *The Journal of Physical Chemistry B* **2006**, 110, 22097-22102.
11. Khare, A.R.; Vasisht, N. Nanoencapsulation in the food Industry: technology of the future. In *Microencapsulation in the food industry*, Elsevier: **2014**; pp. 151-155.
12. Donsì, F.; Annunziata, M.; Ferrari, G. Microbial inactivation by high pressure homogenization: Effect of the disruption valve geometry. *Journal of Food Engineering* **2013**, 115, 362-370.
13. Schultz, S.; Wagner, G.; Urban, K.; Ulrich, J. High-pressure homogenization as a process for emulsion formation. *Chemical Engineering & Technology: Industrial Chemistry-Plant Equipment-Process Engineering-Biotechnology* **2004**, 27, 361-368.
14. Sessa, M.; Donsì, F. Nanoemulsion-based delivery systems. In *Microencapsulation and Microspheres for Food Applications*, Elsevier: **2015**; pp. 79-94.
15. Maa, Y.-F.; Hsu, C.C. Performance of sonication and microfluidization for liquid–liquid emulsification. *Pharmaceutical development and technology* **1999**, 4, 233-240.
16. Sugumar, S.; Ghosh, V.; Nirmala, M.J.; Mukherjee, A.; Chandrasekaran, N. Ultrasonic emulsification of eucalyptus oil nanoemulsion: antibacterial activity against Staphylococcus aureus and wound healing activity in Wistar rats. *Ultrasonics sonochemistry* **2014**, 21, 1044-1049.
17. McClements, D.J.; Rao, J. Food-grade nanoemulsions: formulation, fabrication, properties, performance, biological fate, and potential toxicity. *Critical reviews in food science and nutrition* **2011**, 51, 285-330.
18. Silva, H.D.; Cerqueira, M.Â.; Vicente, A.A. Nanoemulsions for food applications: development and characterization. *Food and bioprocess technology* **2012**, 5, 854-867.
19. Topuz, O.K.; Özvural, E.B.; Zhao, Q.; Huang, Q.; Chikindas, M.; Gölükçü, M. Physical and antimicrobial properties of anise oil loaded nanoemulsions on the survival of foodborne pathogens. *Food*

chemistry **2016**, 203, 117-123.
20. Salvia-Trujillo, L.; Martín-Belloso, O.; McClements, D.J. Excipient nanoemulsions for improving oral bioavailability of bioactives. *Nanomaterials* **2016**, 6, 17.
21. Cuomo, F.; Perugini, L.; Marconi, E.; Messia, M.C.; Lopez, F. Enhanced Curcumin Bioavailability through Nonionic Surfactant/Caseinate Mixed Nanoemulsions. *Journal of food science* **2019**, 84, 2584-2591.

3 Experimental Techniques

«Science is simply the word we use to decribe a method of organizing our curiosity»
T.Minchin

3.1 Emulsions Characterization

3.1.1 Dynamic Light Scattering

Dynamic Light Scattering (DLS) is a non-invasive technique used for the determination of size of particles dispersed in a medium typically in the sub-micron region. This technique has several positive characteristics: it is a fast and convenient tool for particle size analysis of non-interacting spherical colloids [1]. In general light scattering is a consequence of the interaction of light with the field of small particles. In experiment that involves light-scattering, sample is exposed to a monochromatic wave of light, that pass through the sample and after it is detect by an appropriate detector. When the monochromatic beam of light encounters macromolecules solutions, light scatter in all direction, depending on the size and shape of macromolecules. In static light scattering, the intensity of scattered light is analysed as time-averaged intensity, on the other hand, if the intensity fluctuations, caused by the Brownian motion, of scattered light is analysed, the diffusion coefficient that is related to the hydrodynamic size of macromolecules can be obtained. The intensity of scattered light from a colloidal system depends on the scattering angle (θ) and observation time (t) [2]. DLS is based on two different phenomena of the colloidal systems, namely Tyndall effect and Brownian motion. The speed at which the particles are diffusing due to Brownian motion is measured. This is done by measuring the rate at which the intensity of the scattered light fluctuates when detected using a suitable optical arrangement. The larger the particle, the slower the Brownian motion will be, while smaller particles move more rapidly in the solvent. The Brownian motion is also influenced by the temperature and viscosity, so both parameters are considered in the equation used for the calculation of diameter measured with DLS. The temperature needs to be stable, otherwise convection currents in the sample will cause non-random movements which prevents accurate size interpretation, and for the control of viscosity that is related to this parameter. The velocity of the Brownian motion is defined by a property known as the translational diffusion coefficient (D), calculated by the Stoke- Einstein equation (Eq.3.1):

$$d_h = \frac{kT}{3\pi\eta D} \tag{3.1}$$

d_h= hydrodynamic diameter
D= translational diffusion coefficient
k= Boltzmann's constant
T= absolute temperature
η= viscosity of the continuous phase

The diameter that is measured in DLS, is a value that refers to how a particle diffuses within a fluid therefore it is referred to as a *hydrodynamic diameter*. So the obtained value with this technique is the diameter of a sphere that has the same translational diffusion coefficient as the particle. The translational diffusion coefficient will depend not only on the size of the particle

´core´, but also on any surface structure, as well as the concentration and type of ions in the medium. DLS allow us to measure particles that are much smaller than the λ used for the determination. Three are the factors that affect the hydrodynamic diameter:

- *ionic strength*: ions in the medium as well as the total ionic concentration could change the thickness of the electric double layer, called Debye length (κ^{-1}), so affecting the particle diffusion speed. If the concentration of ions is low, an extend double layer is produced around the particle, thus resulting in an apparent hydrodynamic diameter. Higher concentration of ion salts, so high conductivity media, will suppress the electrical double layer reducing the measured hydrodynamic diameter;

- *surface structure*: if a polymer is absorbed around the particle a change in the surface will occur, causing a change of the apparent size of the particle. An adsorbed polymer layer projecting out into the medium will reduce the diffusion speed more than if the same polymer is lying flat on the surface. The polymer conformation is affected by the nature of the surface and the polymer, as well as the ionic concentration of the medium. This conformation can change the apparent size of particles of several nanometers;

- *non-spherical particles*: sphere is an object whose size can be described by a single figure. Each technique could be affected by different properties of the particle, even the size in a microscope image will depend on parameters set. The hydrodynamic diameter of non-spherical particle is the diameter of a sphere that has the same translational diffusion speed as the particle taken in consideration. If the shape of particle changes in a way that affects the diffusion speed, then the hydrodynamic size will change.

Theories behind Light Scattering: Rayleigh Scattering and Mie Theory

Rayleigh Scattering
It is a response based on the dimensions of particles. If particles are small compared to the wavelength of the laser used (less than d=λ/10 or 60nm for He-Ne laser), the scattering of a particle illuminated by a vertically polarized laser will be isotropic (i.e. equal in all directions). The Rayleigh approximation tells that the intensity of scattered light (I) is directly proportional to the diameter of the particle (I$\propto d^6$) and inversely proportional to the wavelength (I$\propto 1/\lambda^4$).
Mie Theory
When the size of particles becomes roughly equivalent to or greater than the wavelength used for illuminate our systems, a complex function of maxima and minima with respect to angle is observed. This theory works well with diffusion centres of any size, with the limit that these are smaller than the incident wavelength. So when particles become larger than λ/10, the scattering changes from being isotropic to a distortion in the forward scattering direction. The particles that are suspended interact with the radiation that comes from the laser and they act as slit [3]. Mie theory is used in software for the conversion of the intensity distribution into volume and number for all sizes of particles.

How DLS works

As said before, the DLS measures the speed at which particles are diffusing due to the Brownian motion, so it practically measures the rate at which intensity of the scattered light fluctuates when detected using a suitable optical arrangement. Thus, when a cuvette containing stationary particles is illuminated by a laser and a frosted glass screen is used to view the sample cell, a speckle pattern would be seen. This pattern will be stationary both in the speckle size and position due to the fact that all the system is stationary. For a system of particles undergoing Brownian motion, a speckle pattern is observed where the position of each speckle is seen to be

in constant motion. This is because the phase addition from the moving particles is constantly evolving and forming new patterns. The rate at which these intensity fluctuations occur will depend on the size of the particles.

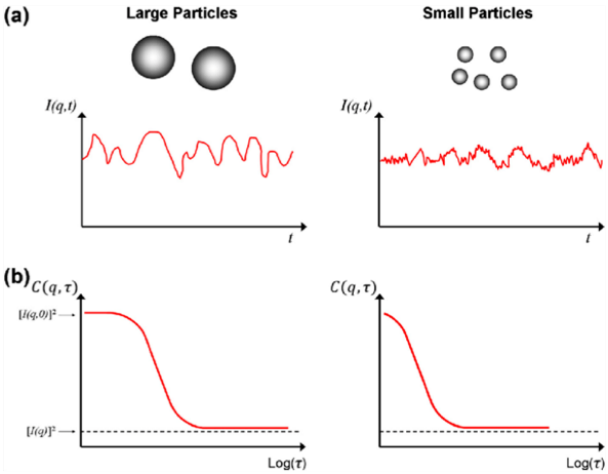

Figure 3.1: *Schematic illustration of intensity measurement and the corresponding autocorrelation function in DLS of dispersion composed of large and small particles. Intensity fluctuation of scattered light with time (a) and the variation of autocorrelation function with delay time (b).*

Fig. 3.1 schematically illustrates typical intensity fluctuations arising from a dispersion of large particles and a dispersion of small particles. The small particles cause the intensity to fluctuate more rapidly than the large ones. To understand obtained data is necessary to use a correlator. It is a signal comparator that measures the degree of similarity between two signal or the same signal in different time intervals. If the intensity of a signal is compared with itself at a particular point in time and a time much later, then for a randomly fluctuating signal it is obvious that the intensities are not going to be related in any way, i.e. there will be no correlation between two signals. Knowledge of the initial signal intensity will not allow the signal intensity at the time $t = \infty$ to be predicted. This will be true of any random process such as diffusion. However, if the intensity of signal at a certain time (t) is compared to the intensity at very small time later $(t + \delta t)$, there will be a strong correlation between intensities of the two signals, that could be strongly or well correlated, even if it is compared to the signal at $t + 2\delta t$. Of course, the correlation is reducing with time, so the period of time δt is to be considered very small, maybe nanoseconds or microseconds and it is called the sample time of the correlator. When we consider $t = \infty$ maybe the order is of a milliseconds or tens of milliseconds. Perfect correlation is indicated by unit 1 and no correlation by 0. If particles are large the signal will be changing slowly and the correlation will persist for a long time, while if they are small, so particles move rapidly, the correlation will reduce more quickly. The time at which the correlation starts to significantly decay is an indicator of the mean size of the sample. The steeper the line, the more monodisperse the system is. Conversely, a more extended decay indicates a higher polydispersity of the sample.
The correlator will construct a function called correlation function G(τ) of the scattered intensity. Considering τ the time difference (sample time) of the correlator and I(t) the scattered intensity at an arbitrary time, it is possible to write:

$$G(\tau) =< I(t).I(t+\tau) > \tag{3.2}$$

For a large number of monodisperse particles in Brownian motion, the correlation function is

an exponential decaying function of the correlator time delay (τ):

$$G(\tau) = A[1 + Bexp(-2\Gamma\tau)] \tag{3.3}$$

A= baseline of the correlation function
B= intercept of the correlation function
$\Gamma = Dq^2$ decaying constant

q is the magnitude of the *scattering vector* and it is calculated as follow:

$$q = (4\pi\frac{n}{\lambda_0})\sin\frac{\theta}{2} \tag{3.4}$$

For polydisperse samples, the Eq. 3.3 can be written as:

$$G(\tau) = A[1 + Bg_1(\tau)^2] \tag{3.5}$$

In this equation $g_1(\tau)$ is the sum of all the exponential decays contained in the correlation function [4]. This function contains the diffusion coefficient information required to be entered into the Stokes-Einstein equation. Size is determined from the correlation function by using various algorithms (through cumulant or distribution analysis). The size distribution obtained is a plot of the relative intensity of light scattered by particles in various size classes and is therefore known as an intensity size distribution. The polydispersity index is a dimensionless measure of the broadness of the size distribution calculated from the cumulants analysis and its value ranges between 0 and 1 (0.08<PDI<0.7 mid-range value of PDI)[5].

3.1.2 ζ-Potential

ζ-Potential, or potential at the solid-liquid interface, is a fundamental parameter in models of electrical double layers and their associated properties. The potential applied to an electrode is inherently well-defined and easily measured, hence the zeta potential is a natural parameter used to describe electrochemical properties and the surface charge of particles in suspension, that give us information about the stability of systems [6]. The net charge density on a microfluidic substrate in contact with an aqueous solution gives rise to an electrical double layer (EDL) due to the ions in suspension that surround the interfacial region, resulting in an increased concentration of counterions (ions of opposite charge to that of the particle) [7]. Usually, protonation, deprotonation, adsorption and other reaction equilibria define a net charge density on the surface. This charge density creates an electric field, drawing counterions towards it and driving like-charged ions (co-ions) away. The liquid layer surrounding the particle exists as two parts:

- inner region, called *Stern layer*, where the ions are strongly bound;
- outer region, diffuse, where ions are less firmly attached. Within the diffuse layer there is a notional boundary inside which the ions and particles forms a stable entity.

The existence of the Stern layer helps to describe both the dependence of electrode capacitance and counterion size and the functional form of electrode capacitance at high counterion concentration. Counterions in the Stern layer do not move normal to the surface, but measurement of the so-called anomalous conductivity suggest that the ions may still move laterally in certain situations [8]. When a particle moves, ions within the boundary move with it, but any ions beyond the boundary do not travel with the particle. This boundary is called the surface of

hydrodynamic shear or *slipping plane*. The potential that exists at this boundary is known as *zeta potential*.

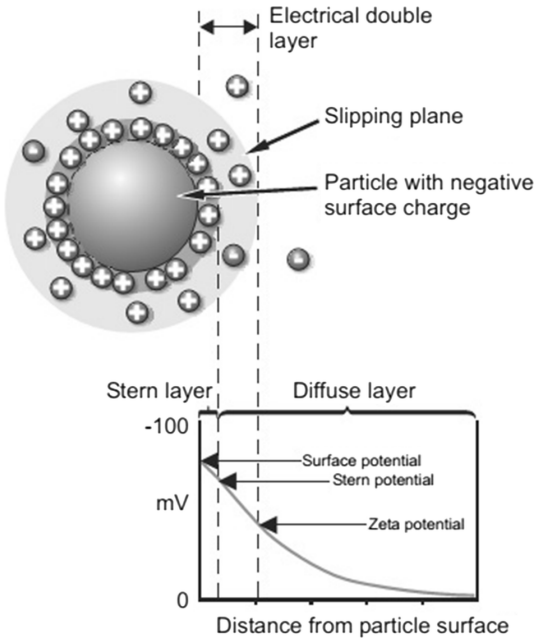

Figure 3.2: *Schematic representation of Zeta Potential.*

The magnitude of this value gives an indication of the stability of colloidal systems. If all the particles in suspension have a large negative or positive potential (generally more positive than +30 mV and more negative than -30 mV), then they will tend to repel each other and there is no tendency to flocculate. However, if the particles have low ζ-potential values, then there is no force to prevent the particles coming together and flocculating. pH, conductivity and the concentration of the different ions in the medium are important factors that influence the ζ-potential. The Stern layer with the diffuse layer has a certain width that can change in presence of ions and salts. At the same concentration if there are ions with higher valence the effect on the layer will be higher. So, when ions are added they can be absorbed in two different ways:

- specific: stronger interaction that can change the isoelectric point also with small addition;
- non-specific: there are no effects on the isoelectric point even if the ζ-potential changes.

Techniques for measuring ζ-potential

In general, zeta-potential is measured indirectly using one of three means: electroosmotic mobility, streaming current or potential and response of a small spherical particle in applied E-field [6]. An important consequence of the existence of electrical charges on the surface of particle is that they will exhibit certain effects under the influence of applied electric field, such as electrophoresis, electroosmosis, streaming potential and sedimentation potential. These effects are collectively defined as electrokinetic effects [9].
Electrophoresis
When an electric field is applied across an electrolyte, charged particles suspended in the electrolyte are attracted towards the electrode of opposite charge. Viscous forces acting on the particles tend to oppose this movement. When equilibrium is reached between these two opposing forces, the particles move with constant velocity. The velocity is dependent on the strength of electric field or voltage gradient, the dielectric constant of the medium, the viscosity of the

medium and the zeta potential. The velocity of a particle in a unit electric field is referred to as its electrophoretic mobility. Zeta potential is related to the electrophoretic mobility by the Henry equation (Eq. 3.6):

$$-UE = \frac{2\epsilon z f(\kappa a)}{3\eta} \tag{3.6}$$

UE= electrophoretic mobility
z= zeta potential
ϵ= dielectric constant
η= viscosity
f(κa)= Henry's function

The units of κ, termed the Debye length, are reciprocal length and κ^{-1} is often taken as a measure of the ´thickness´ of the electrical double layer. The parameter ´a´ refers to the radius of the particle and therefore ´κa´ measures the ratio of the particle radius to electrical double layer thickness (Fig. 3.3). Electrophoretic determinations of zeta potential are most commonly made in aqueous media and moderate electrolyte concentration. F(κa) in this case is 1.5, and this is referred to as the Smoluchowski approximation. Therefore, calculation of zeta potential from the mobility is straightforward for systems that fit the Smoluchowski model, i.e. particles larger than about 0.2 microns dispersed in electrolytes containing more that 10^{-3} molar salt. For small particles in low dielectric constant media, like non-aqueous media, f(κa) becomes 1.0 and allows an equally simple calculation. This is referred to as the Huckel approximation.

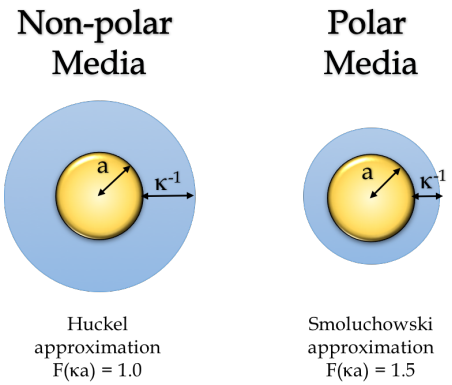

Figure 3.3: *Huckel and Smoluchowski´s approximations used for the conversion of electrophoretic mobility into zeta potential.*

Measuring Electrophoretic Mobility
The essence of a classical micro-electrophoresis system is a capillary cell with electrodes at either end to which a potential is applied. Particles move towards the electrode, their velocity is measured and expressed in unit field strength as their mobility. A laser beam passes through a sample undergoing electrophoresis and the scattered light from the moving particle is frequency shifted. The frequency (Δf) shift is equal to:

$$\Delta f = 2\nu \frac{\sin(\theta/2)}{\lambda} \tag{3.7}$$

ν= the particle velocity
λ= laser wavelenght
θ= scattering angle

Since the frequency of light is so high (10^{14} Hz), the shift in frequency can only be measured

by an optical mixing or interferometric technique. This is done by using a pair of mutually coherent laser beams derived from a single source. One of these beams must pass through the sample (scattering beam), while the other (reference beam) is routed around the cell.

Configuration of the Nano Instrument for DLS and ζ-potential measurements

The components of the DLS are quite easy as reported in Fig. 3.4. In general, the instrument is composed by six main components: a laser (usually He-Ne, 633 nm) that provides a light source to illuminate the sample contained in a cell, an attenuator, a Peltier system (for the control of temperature), a detector used to measure the scattered light, that can be placed at two different angles (90 and 173°) depending on the particular model, a correlator and a computer for collecting data.

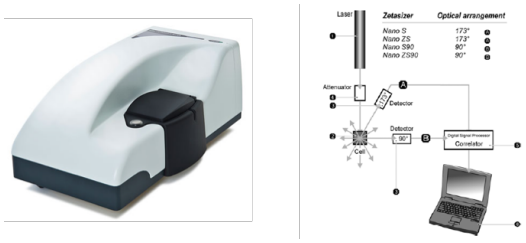

Figure 3.4: *Malvern instrument Nano S90 and optical configuration for determination of average size.*

The intensity of scattered light needs to be within a specific range for the detector to successfully measure it. In case of too much light is scattered, the attenuator will provide, reducing the intensity of the laser source and hence reduce the intensity of scattering. Also if sample does not scatter much light, the attenuator will allow more laser light to pass through the sample. Sample characterized by large particles or concentrated scatter more light, so the intensity of the scattered light must be decrease, and the system automatically determine the appropriate position of the attenuator. The correlator then compares the scattering intensity at successive time intervals to derive the rate at which intensity is varying. Also the measurement of ζ-potential can be carried out by the same instrument (Fig. 3.4). Firstly, the laser is used to provide a light source to illuminate the particles within the sample. For zeta potential measurements, this light source is split to provide an incident and reference beam. The incident laser beam passes through the centre of the sample cell, and the scattered light at an angle of about 13° is detected. When an electric field is applied to the cell, any particles moving through the measurement volume will cause the intensity of light detected to fluctuate with a frequency proportional to the particle speed and this information is passed to a digital signal processor and then to a computer. The software produces a frequency spectrum from which the electrophoretic mobility and hence zeta potential is calculated. The intensity of the detected, scattered light must be within a specific range for the detector to successfully measure it. This is achieved using the attenuator, which adjusts the intensity of the light reaching the sample and hence the intensity of the scattering. To correct for any differences in the cell wall thickness and dispersant refraction, compensation optics are installed to maintain optimum alignment [10].

3.1.3 Conductance and conductivity

Conductivity is the ability of a solution to conduct current. It is typically measured in aqueous solutions of electrolytes. Electrolytes are substances containing ions such as solutions of ionic salts or of compounds that ionise in solution. The ions formed in solution are responsible for carrying the electric current. Acid, bases and salts are electrolytes and they can be strong or

weak. The fundamental measurement used to study the motion of ions is that of the electrical resistance, R, of the solution. Resistance is calculated with Ohm´s law (Eq. 3.8):

$$V = RI \tag{3.8}$$

V= voltage (Volts)
I= current (Amperes)
R= resistance of the solution (Ω)

The conductance (Λ) of a solution is the reciprocal of the electrical resistance and as resistance is expressed in Ohms (Ω), the conductance of a sample is expressed as Ω^{-1}, known as Siemens (S). The conductance of a sample decreases with its length l and increases with its cross-sectional area A. These features are related by Eq. 3.9.

$$\Lambda = \kappa \frac{A}{l} \tag{3.9}$$

κ= conductivity
A= cross-sectional area
l= length

With the conductance in Siemens and the dimensions in metres, it follows that the units of κ is Sm^{-1}. The conductivity of a solution depends on the number of ions present, and usually another feature is introduced, called molar conductivity λ_m ($\mathrm{Sm}^2\mathrm{mol}^{-1}$), defined as:

$$\lambda_m = \frac{\kappa}{c} \tag{3.10}$$

where c is the molar concentration of the added electrolyte. The molar conductivity is found to vary with the concentration. One reason for this variation is that the number of ions in the solution might not be proportional to the concentration of the electrolyte. For instance, the concentration of ions in a solution of a weak acid depends on the concentration of the acid in a complicated way, and doubling the concentration of the acid added does not double the number of ions. Moreover, because ions interact strongly with one another, the conductivity of a solution is not exactly proportional to the number of ions present [11]. The conductivity of an electrolyte solution is measured by means of a conductivity meter which applies an alternating current (I) at an optimal frequency to two active electrodes and measures the potential (V). Both the current and the potential are used to calculate the conductance. The conductivity meter then uses the conductance and cell constant to display the conductivity as reported in Eq. 3.9. Conductance is the reciprocal of resistance and can be determined by the Wheatstone bridge (Fig. 3.5), known as Kohlraush conductance bridge, in which the conductivity cell forms one arm of the bridge.
The solution whose conductance is to be determined is placed in the conductivity cell. When the bridge is balanced, assuming that the conductivity cell behaves as a pure resistance, then the voltage between the opposite points of detector is equal to zero. The circuit allows determining resistance R from which conductivity is determined, once known the cell constant. The electrodes in the cell are not exactly 1 cm apart, thus the value of observed conductivity is not equal to specific conductance but it is proportional to it and for this reason it is introduced the cell constant. The cell constant (K) is the ratio of the distance (d) between the electrodes to the area (a) of the electrodes and it is calculated as follows:

$$K = \frac{d}{a} \tag{3.11}$$

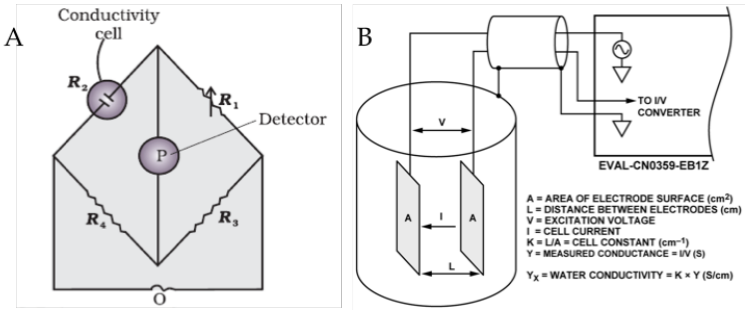

Figure 3.5: *Wheatstone bridge circuit for measurement of conductivity (A), conductivity cell with one are of a resistance bridge for measurement of conductivity of an electrolyte (B).*

It has been observed that the conductivity of solution increases with dilution until it reaches its limiting value at infinite dilution. Kohlrausch made a systematic study of λ_m^0 that is the limiting molar conductivity, the molar conductivity in the limit of zero concentration (when the ions are effectively infinitely far apart and do not interact with one another). He found that λ_m^0 was the sum of the independent contributes of cations and anions present in the solution known as low of the independent migration of ions (Eq. 3.12).

$$\lambda_m^0 = \sum_i^0 \lambda \tag{3.12}$$

3.1.4 Rheology

The word rheology originates from the Greek word ´$\rho\epsilon\omega$´ that means ´to flow´ and ´$\lambda o\gamma\iota\alpha$´ meaning ´the study of´, thus literally rheology is the science of deformation and flow. The quote ´$\pi\alpha\nu\tau\alpha\ \rho\epsilon\iota$´ of Eraclito is the motto of the Society of Rheology, which chose the symbol of a clepsydra to underlines the importance of time in the study of rheology.

Flow and Deformation

Rheology can be applied to liquid and semi-solid materials analysing their flow, while when it is applied to solid materials it studies the deformation of bodies [12]. Deformation is also called strain, and it is possible to define a tensile deformation (E) and shear deformation (γ). Deformation is the ratio between the variation of sample size and its original size. If the applied stress is perpendicular to the surface of the body it is named normal stress, while when it is parallel to the surface it is called shear stress.
In flow, elements of the liquid are deforming and adjacent points in the liquid are moving relative to another. Therefore, materials that clearly show flow behaviour are referred to as fluids, and on the basis on how their component move each other it is possible to distinguish two types of flow: *shear* and *extensional*. In shear flow, component elements flow over or past each other, while in extensional flow fluid components flowing away or towards from one another. The shear flow can be visualised alternatively as the movement of hypothetical layers sliding over each other, with each layer moving faster than the one below. In response of this force the upper layer will move of a given distance x while the lower layer is stationary. So the displacement gradient between the layers (x/h) of the sample taken in consideration can be defined as shear strain. The gradient of velocity in the normal direction to the flow is called shear rate, or strain rate ($\dot{\gamma}$) considering the infinitely small velocity difference (dv) between two neighbouring flow layers, and infinitely small thickness (dh) of a single flowing layer (Eq. 3.13).

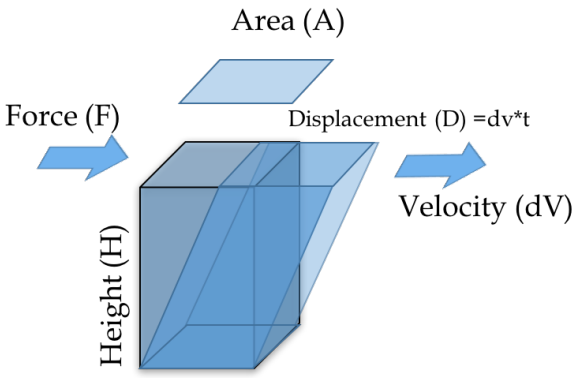

Figure 3.6: *Behaviour of material after the application of a strain.*

$$\dot{\gamma} = \frac{dv}{dh} \tag{3.13}$$

While the force (F) per unit area (A) creating or produced by the flow is the shear stress (τ or σ):

$$\tau = \frac{F}{A} \tag{3.14}$$

The shear rate has the units of velocity divided by distance (s^{-1}), while the shear stress is measured in Nm^{-2} so, as reported in the SI, it is expressed in Pa. The stress applied to a fluid is equivalent to a rate of momentum transfer to the upper layer of fluid. That momentum is transferred through the layers of fluid by collision and interactions with other fluid components giving a reduction in fluid velocity and kinetic energy. The coefficient of proportion between the shear rate and the shear stress, measure of the internal frictions, is called *shear viscosity* or *dynamic viscosity*. For a solid that behaves like a single block of material the strain will be finite and no flow is possible for any stress applied. For a fluid, where the components can move one relative to another, the shear strain will continue to increase for the period of applied stress. The perception of a material (solid or liquid) depends also on the time of observation. The concept of observation time in rheology is defined by the Deborah number, D_e, which is the ratio between the relaxation time (Λ) and the time of observation (t) over which stress is applied. Λ is the time that molecules binding needs to show a response after the application of an external stress, while t is the time of application of a stress to induce a response. Consequently, D_e>1 indicates solid-like behaviour, while D_e<1 indicates liquid-like behavior. Each material behaves in a certain way based on the structure or the time of analysis, and ideal elastic solid and ideal viscous liquid are used as two extreme to explain material's behavior. An ideal solid, when a force is applied, will deform elastically: the energy used for the deformation is preserved as potential elastic energy, used when the force is removed. On the contrary, an ideal viscous liquid is subject to a total irreversible deformation and all the energy used to deform the liquid will be lost as heat, so it will be impossible to return it. The behavior of all real materials is based on the combination of both viscous and elastic portion and therefore is called viscoelastic behavior. Fig. 3.7 reports a schematization of the different behaviors correlated to Deborah number. The *Hooke* and *Newton* laws are the basic principle describing the behavior of an ideal elastic solid and ideal viscous liquid when they are subjected to a deformation.

Elastic Behavior - ideal solid

Structured fluids have a minimum energy state associated with their ´at rest´ microstructure. This state may relate to inter-entangled chains in a polymer solution, randomly ordered particles

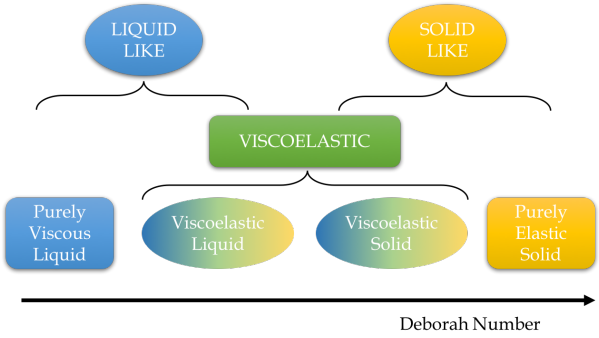

Figure 3.7: *Schematic representation of different fluids depending on Deborah number*

in a suspension, or jammed droplets in an emulsion. Applying a force or deformation to a structured fluid will shift the equilibrium away from its energy state, creating an elastic force that tries to restore the microstructure to its initial state. This is analogous to a stretched spring that attempts to return to its un-deformed state. A spring is representative of an ideal elastic solid and follows the Hooke's law where the applied stress is proportional to the resultant strain as long as the elastic limit is not exceeded. The spring, when the stress is removed, will return to its initial shape, but if the elastic limit is exceeding it will permanently be deformed. The same principle can be applied to a simple shear deformation. In case of simple shear elastic deformation, the constant of proportionality is called elastic modulus (G). It is a measure of the stiffness or resistance to deformation and, just as the viscosity, measures the resistance to flow. For a pure elastic material, there is no time dependence response, so when the stress is applied, an immediate strain is observed, and when it is removed the strain disappears. The behaviour of these materials can be described by Hooke's law:

$$\tau = G\gamma \tag{3.15}$$

G is the shear modulus (Pa) that reveals information about the rigidity of material. The values of the shear modulus of Hookean solids are independent of the degree and duration of the shear load applied.

Viscous Behavior - ideal liquid

Viscous material can be represented by a dashpot which, differently from spring, follows Newton's law (Eq. 3.16). The dashpot is a mechanical device characterized by a plunger moving through a viscous Newtonian fluid. As soon as a stress is applied to a dashpot it immediately starts to deform and goes on deforming until the stress is removed. The energy required for deformation is dissipated within the fluid (usually as heat) and the strain is permanent. The strain evolution in an ideal liquid is given by the following expression:

$$\tau = \eta\dot{\gamma} \tag{3.16}$$

The viscosity is the constant of proportionality between the shear rate and shear stress. The application of an increasing shear rate and the contemporary measure of the shear stress is defined as flow curve or test viscosimetry. For an ideal viscous fluid, the shear depends on time and it is irreversible. It means that all the mechanical energy used to induce the flow is entirely dissipating as heat and friction. Viscosity is influenced by different parameters, such as the chemical structure of substances, temperature, pressure and time.

Viscoelastic Behavior

Viscoelastic behavior describes materials that show characteristics between that of an ideal liquid (viscous) and of an ideal solid (elastic). There are a number of rheological techniques for

probing the viscoelastic behavior of materials, including creep testing, stress relaxation and oscillatory testing, that will be discuss later. Materials that show rheological behavior between that of liquids and solids are therefore classified as viscoelastic materials. Consequently, it is possible to describe them using a combination of spring and dashpot, as illustrated in Fig. 3.8, in series to describe a viscoelastic liquid (Maxwell model) or parallel, in case of viscoelastic solid (Kelvin-Voigt model). If a stress is applied to a Maxwell model, after a very short time the

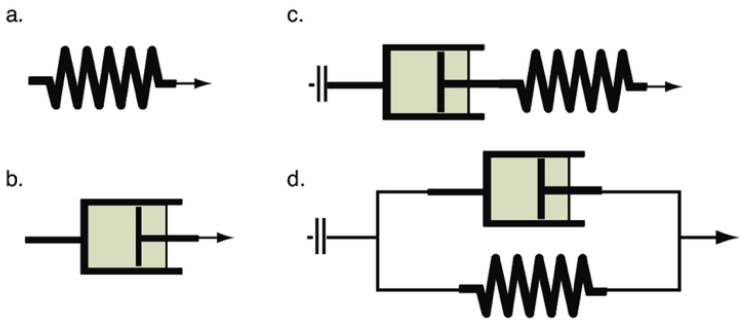

Figure 3.8: *Spring (a), dashpot (b) and combination of them in series (c) and parallel (d) to illustrate behaviour of material.*

elastic response is predominant, and governed by G, while the viscous behavior prevails at much longer time and it is governed by η.

$$\sigma = G\gamma + \eta\dot{\gamma} \tag{3.17}$$

If, in the other case, the stress is applied to a Kevin-Voigt model, the response is delayed because the presence of the dashpot retards the response of the spring and the system behaves like a viscous liquid initially and then elastically over longer time scale because the spring becomes more stretched. The time scale or the rate at which this deformation occurs depends on the retardation time λ that represents the delay in elasticity response. The model that better describe the behaviour of viscoelastic systems in response to an applied stress is the Burger model, which is the result of the Maxwell and Kevin-Voigt models connected in series.

Fluids behavior: Newtonian and non-Newtonian

The correlation between shear stress and shear rate defining the flow behavior of a liquid is graphically displayed in a diagram of τ on the ordinate and $\dot{\gamma}$ on the abscissa. This diagram is called *flow curve*, while when viscosity is reported on the ordinate, *viscosity curves* are obtained. Depending on their behavior when a stress is applied, fluids can be classified in Newtonian or non-Newtonian.

Newtonian fluids are those for which the viscosity - although varying with temperature and pressure - does not vary with deformation rate or time, so the shear rate and the shear stress are linearly related, hence the viscosity is a constant. Typical fluids that have a Newtonian behavior are water, simple hydrocarbons or diluted colloidal dispersions. Of course, the behavior of a liquid depends on the range of the shear rate that we use to study it. Another class of fluid are those one for whom the viscosity varies as a function of the applied shear rate or stress, and they are called *non-Newtonian*. Based on how the viscosity is related to the stress and rate it is possible to classify different kinds of fluids, as reported in Fig. 3.9 [13].

Pseudoplastic: fluids for which the viscosity decreases, so they become ´thinner´, as the shear rate increases, for this they are also called shear-thinning fluids. Emulsions, suspensions or dispersions belong to this group. It should be mentioned that shear thinning/pseudoplastic flow behavior of fluids is not uniform; at low shear rates range the Brownian motion keeps all molecules of particles at random despite the initial effects of shear orientation. At very low

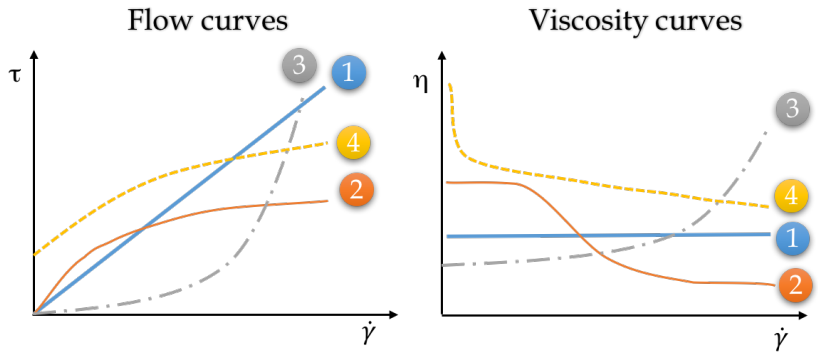

Figure 3.9: *Flow and viscosity curves of common fluid flow behavior: 1) Newtonian liquid, 2) Pseudoplastic liquid, 3) Dilatant liquid, 4) Pseudoplastic liquid with yield point.*

shear rate pseudoplastic liquids behaves like Newtonians, having a defined viscosity η_0 (zero shear viscosity) independent of shear rate. At a critical shear rate the viscosity drops drastically, which signify the beginning of the shear thinning region. This region can be described mathematically by a power law relationship which appears as a linear section when the plot of flow curve is in logarithmic scale. Reaching extremely high shear rates the viscosity will approach asymptotically a finite constant level: η_∞. Going to even higher shear rates it is impossible to cause further shear-thinning since the optimum or perfect orientation is reached and is influenced by the solvent viscosity and related hydrodynamic forces. In the low and high shear rate region, called first and second Newtonian ranges, even the viscosity of non-Newtonian liquids is independent of shear rates.

Pseudoplastic with yield point (Plastic): it describes pseudoplastic liquid characterized by the presence of a yield point indicate as τ_0 or σ_0. Plastic fluids can be classified with good reasoning to belong to both groups of liquids and solids. When below a critical stress the viscosity of materials becomes infinite and hence characteristic of a solid. This type of flow response is known as plastic and is characterized by an ever increasing viscosity as the shear rate approaches zero (no visible plateau). Some authors prefer to describe it as *apparent yield point* since it depends strongly on the tests condition and other factors. Materials that behave in this way are mostly dispersions which at rest can build up an intermolecular network of binding forces. These forces restrict positional change of volume elements and give the substance a solid character with an infinitely high viscosity. Only when the outside forces are strong enough to overcome the network forces so surpass the thresholds shear stress, σ_0, the network collapse. In this way, volume elements change the position irreversibly: the solid turns into a flowing liquid. The consequence of these rearrangements is a decrease in molecular/particle interaction and an increase in free space between dispersed components, which both contribute to the large drop in viscosity. Typical substances showing this behaviour are food colloids such as ketchup and mayonnaise and natural rubber polymers, while Bingham is a plastic fluid that shows Newtonian behavior after yielding, but this is not really common. This explain the behavior of shear-thinning material in general, so a micro-structural rearrangements occurring in the plane of applied shear and is commonly observed as said before for dispersions, as well as polymer solution and melts. An illustration of the orientation is reported in Fig. 3.10 [14].

Dilatant: fluids that increase their viscosity as the shear rate increase. This phenomenon refers to a specific mechanism for shear thickening associated with a volume increase. This behavior is found, for example, in highly concentrated suspensions (i.e. emulsion-PVC) in which solid particles are mixed with liquids such as plasticizer to form plastisol. At rest, or at low shear rate, the plasticizer fully lubricates the particle surfaces and thus allows an easy positional change of them when forces are applied: this suspension behaves as a liquid at low shear rates. At higher

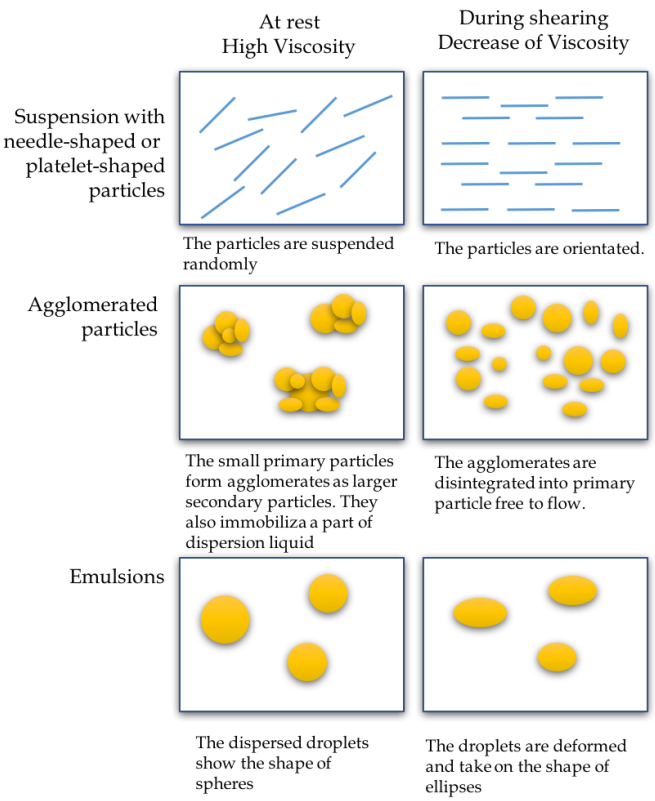

Figure 3.10: *Rearrangements of the microstructure of different fluids at low and high shear rate.*

shear rates, particle will wedge apart causing general volume increases. Since the plasticizer is no longer sufficient to fill all voids and to keep the particle surfaces fully lubricated, the plastisol becomes more viscous. Dilatancy in liquid is rare, and when it occurs it is often wise to reformulate the recipe in order to reduce it. For some suspensions, shear thickening generally occurs in materials that show shear thinning at lower shear rates and stresses.

Thixotropy

Thixotropy is related to the time dependent microstructural rearrangements occurring in a shear thinning fluid following a step change in applied shear. For most fluids, shear thinning is reversible so once being sheared, samples will eventually gain to their original viscosity when the shearing force is removed. When this recovery process is sufficiently time dependent the fluid is considered thixotropic. A shear thinning material can be thixotropic, but a thixotropic material will always be shear thinning. Paints and coatings need to be thixotropic because they should be thick when stored for long time to prevent separation, but should thin down easily when stirred for a period of time. Often the structure of the fluid is not rebuilt instantaneously on ceasing stirring, it takes time for the structure and hence viscosity to rebuilt to give enough working time. Thixotropy is required for levelling coating/paint. In fact, sample should have low enough viscosity at application shear rates to be distributed with a roller or brush, but once applied should recover its viscosity in a controlled manner. The recovery time should be short enough to prevent sagging but long enough to allow the application and the creation of a levelled film. This property also influences the thickness of material after it has been processed at a given shear rate, which may influence the consumer perception, or whether a dispersion is prone to separation and/or sedimentation after high shear mixing for example [15]. Methods for determination of thixotropic behaviour will be showed in the following paragraphs.

How to determine rheological behaviour: Rheometry

Through rheometry it is possible to carry out various tests and determine rheological data using instruments equipped with specific measuring systems. Both liquid and solid materials can be studied with rotational and oscillatory tests performed with the use of rotational rheometer [13]. Based on the sample it is possible to choose among different sensor systems: coaxial cylinders, cone-plate and parallel plate. For the specific thesis the last two systems (Fig. 3.11) have been used.

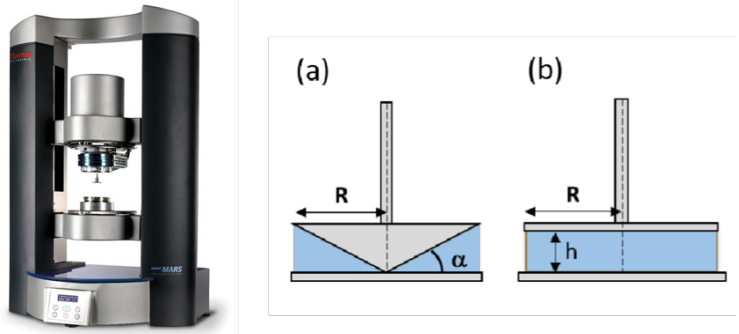

Figure 3.11: *Rotational rheometer and different geometry: cone and plate (a) and parallel plate (b).*

For both the sensors, the upper probe is directly linked to the rotor of the instrument. The lower plate is connected to a Peltier system or a water bath for the control of the temperature because, as said before, viscosity and in general rheological behaviour is influenced by this feature. The rheometer allows to control the torque, the angular speed and the angular sliding. When tests are carried out, the sample is placed on the lower plate while the upper moves toward the lower plate up to a fixed gap distance (h). Cone plate geometry allows to work with smaller amount of sample than the parallel plates. During tests the lower plate is fixed, while the upper devices can rotate (in case of *rotational tests*) or oscillate (for the *Small Amplitude Oscillatory Strain* Test).

Rotational tests

These tests are performed to determine the behavior of fluids when subjected to a shear stress or strain. In case of control rate (CR) mode, an increasing shear rate is applied and the response in terms of shear stress is measured by the rheometer. Flow behavior is illustrated graphically by flow curves that can be fitted with several mathematical model.
Model fitting
An adequately model with straightforward equations needs to be chosen to describe the shape and the curvature of the flow curves and to predict in this way the behavior at unmeasured shear rates. The benefit of this approach is the use of relatively small numbers of fitting parameters. In addition to the Newton's law, that allows to fit liquids with Newtonian behaviour, Cross, Ostwald de Waele and Sisko are the most common models for fitting flow curves of shear-thinning materials [16,17]. Herschel-Bulkley, Casson and Bingham are instead used to fit curves that shows yield point [18,19]. Here are reported two models: Ostwald de Waele or Power Law (Eq. 3.18) and Herschel-Bulkley (Eq. 3.19) models.

$$\sigma = k\dot{\gamma}^n \tag{3.18}$$

$$\sigma = \sigma_0 + k\dot{\gamma}^n \tag{3.19}$$

In both cases two parameters are present: the *consistency coefficient (k)* and the *flow index (n)*. k can be interpreted as an indication of the viscosity values, while n gives information on the behavior of fluids. For $n = 1$ we can consider that the behavior is Newtonian, for n higher than 1 a shear thickening behavior is observed while when n is lower than 1 it indicates a pseudoplastic behavior.

Oscillatory tests

Dynamic methods in sinusoidal regime, allow to extend the characterization of material in a wide range of frequencies.

Small Amplitude Oscillatory Shear Testing

The most common method for measuring viscoelastic properties using a rotational rheometer is Small Amplitude Oscillatory Shear (SAOS) testing. To perform oscillation testing the upper plate oscillates back and forth at a given stress or strain amplitude and frequency. Since oscillatory motion is closely related to circular motion, a full oscillation cycle can be considered equivalent to 360°. The amplitude of oscillation is equal to the maximum applied stress or strain, and the angular frequency represents the number of oscillation per second. This motion can be represented as a sinusoidal wave with the stress or strain plotted on the y axis and the time on the x axis (Fig. 3.12). In a controlled stress measurement an oscillating torque is applied to the upper plate and the resultant angular displacement is measured, from which the strain is calculated.

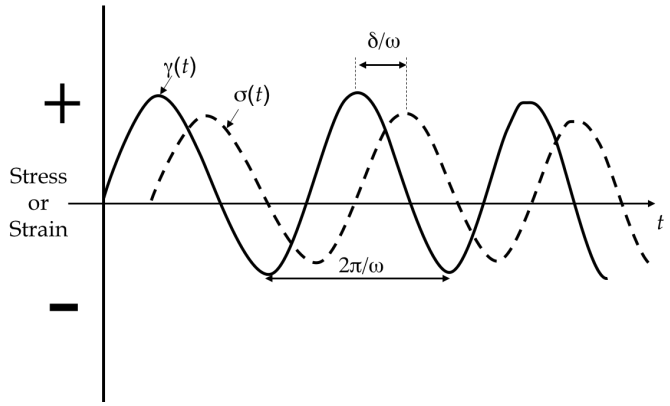

Figure 3.12: *Stress (dotted line) and strain (black line) during SAOS tests.*

In a mathematical way the deformation imposed can be described by Eq. 3.20:

$$\gamma(t) = \gamma_0 \sin(\omega t) \tag{3.20}$$

If the material is viscoelastic it will respond with a stress σ (Eq. 3.21), also sinusoidal, displaced by an angle δ called phase angle, with respect to the applied deformation, whose value depends on the characteristics of the material.

$$\gamma(t) = \gamma_0 \sin(\omega t + \delta) \tag{3.21}$$

From the above equations it is possible to write the equivalent relation (Eq. 3.22) where G', elastic modulus, and G", viscous modulus, are introduced:

$$\sigma(t) = \gamma_0 G' \sin(\omega t + \delta) + \gamma_0 G'' \cos(\omega t + \delta) \tag{3.22}$$

$$G' = \frac{\sigma_0}{\gamma_0}\cos\delta \tag{3.23}$$

$$G'' = \frac{\sigma_0}{\gamma_0}\sin\delta \tag{3.24}$$

It is the phase difference which allows the viscous and elastic components contributing to the total material stiffness to be determined; δ is the relative measure of the material viscous/elastic characteristics. For a pure elastic material, where stress is proportional to strain, the maximum stress occurs at maximum strain (when deformation is greatest) and both stress and strain are said to *be in phase* ($\delta = 0$). In case of pure viscous material, the maximum stress occurs when the strain rate is maximum, and stress and strain are *out of phase* by 90° (or $\pi/2$ a quarter of cycle). For a viscoelastic material the phase difference between stress and strain will fall somewhere between 0° and 90°, with 45° as boundary between solid and liquid-like behavior (Fig. 3.13).

In a controlled strain experiment the angular displacement is controlled and the torque required

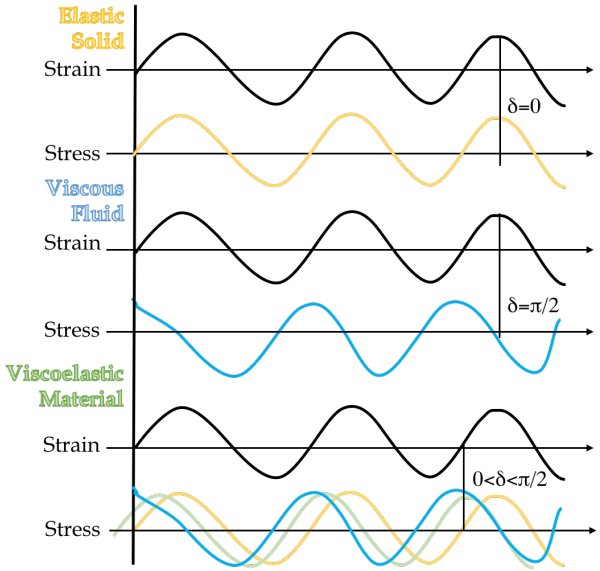

Figure 3.13: *Schematic stress response to oscillatory strain deformation for the different materials.*

to give that displacement is measures, from which the shear stress can be calculated. The ratio of the applied stress (or strain) to the measured strain (or stress) gives the complex modulus (G*), which is a quantitative measure of material stiffness or resistance to deformation at given frequency ω.

$$G^* = \frac{\sigma_{max}}{\gamma_{max}} \tag{3.25}$$

An alternative mathematical representation makes use of complex number notation since G* is a complex number and i is the imaginary number equal to $\sqrt{1}$. Using this notation, considering Eqs. 3.23-3.24, it is possible to write the following relation:

$$G^* = \frac{\sigma_0}{\gamma_0}e^{i\delta} = \frac{\sigma_0}{\gamma_0}(\cos\delta + i\sin\delta) = G' + iG'' \tag{3.26}$$

G' can be considered to represent the real part and G" the imaginary part of G*. In fact, using trigonometry, it is possible to determine the viscous and elastic contributions to G* as shown by the vector diagram reported in Fig. 3.14.

G' describe the capacity of material to store elastic energy, therefore it is called also storage

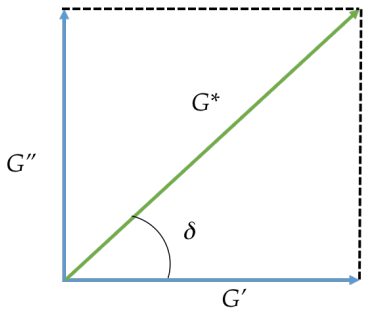

Figure 3.14: *Phasor diagram (vectorial representation of G' and G").*

modulus, while G" is linked to the capacity of dissipate energy, from this the name loss modulus. The ratio between the energy loss and stored is defined as loss tangent (tanδ - Eq. 3.27).

$$tan\delta = \frac{G''}{G'} \tag{3.27}$$

When loss tangent is equal to 1, so G' and G" moduli have the same value, a *cross-over* point is observed. This value represents a boundary; after that a completely change in the behavior is observed so if the material behaves as a viscous fluid it will change for a solid behavior and *vice versa*. Usually values of $tan\delta$ are more useful when working with polymer systems than the values of δ. The inverse of the cross over point frequency represents the characteristic relaxation time (λ_c) of the material. The concept of relaxation time is directly related to the ´entangled´ structure of concentrated polymer solutions, thus a structure made of long entangled chains linked through physical and/or chemical bonds. When the deformation is slow, these structures can be untidy, while when the deformation occurs too quickly, the entanglements behave as rigid knots of a tri-dimensional network. Knowing the relaxation time of a material could be helpful for predicting the viscoelastic response of a material stressed for a given time. It is possible also to define a complex viscosity η^*, which is the measure of the resistance to flow expressed as function of angular frequency ω and it is given by the ratio between maximum stress amplitude and maximum strain rate amplitude (Eq. 3.28)

$$\eta^* = \frac{G^*}{\omega} \tag{3.28}$$

As with G*, also complex viscosity can be divided in two parts, which include the dynamic (η') and storage (η'') viscosity.

Linear Visco-Elastic Range

When measuring viscoelastic characteristics of a material, it is important that the applied stress does not exceed a value for which the material response depends by it. The range in which stress and strain do not affect the viscoelastic properties is called Linear Visco-Elastic (LVE) range (o region). In LVE region, applied stress is not enough strong to cause structural breakdown and hence the microstructural properties can be measured. As soon as applied stress exceed the yield stress, non-linearity appears and measurements can no longer be correlated to the microstructural properties. A test at constant frequency called amplitude sweep is carried out to determine this LVE region. The point at which the structure begins to yield is the limit of the linearity as reported in Fig. 3.15 (so when G' is not constant anymore, but starts to be stress or strain dependent).

Oscillatory Frequency Sweep

G' and G" are not material constant, but they are time dependent. Oscillatory frequency tests

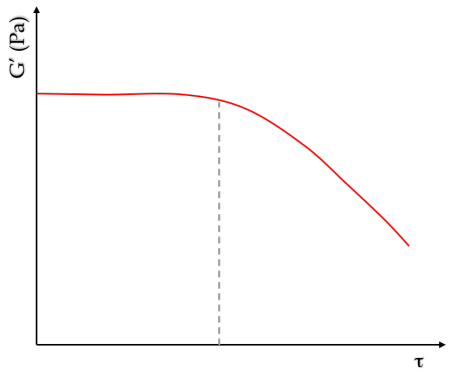

Figure 3.15: *Amplitude sweep oscillation, grey dot line indicates the end of the LVE.*

allow to measure time dependence of the two moduli, by varying the frequency (inverse of time, $\omega = 1/t$) of the applied stress or strain. So, at high frequency it is possible to investigate behavior of materials at short time scale, and low frequency correspond to longer time scale. G' and G" vary with the angular frequency according to the following expressions (Eq. 3.29-3.30):

$$G' = \frac{G(\omega\tau)^2}{1 + (\omega\tau)^2} \tag{3.29}$$

$$G'' = \frac{\eta\omega}{1 + (\omega\tau)^2} \tag{3.30}$$

If the G' modulus is higher than G", a solid-like behavior is predominant ($\delta < 45°$), while if the viscous modulus is higher than the elastic one, a liquid-like behavior is expected, characterized also by δ value higher than 45°.

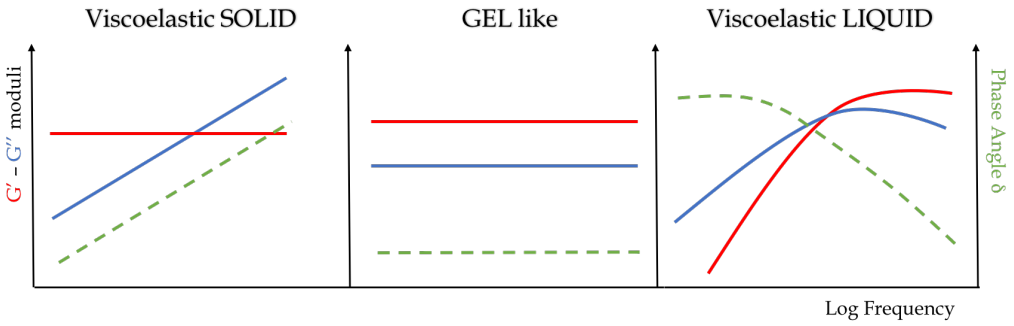

Figure 3.16: *Mechanical spectra of various materials were G' (red) and G" (blue curves) are reported as function of log frequency. In green is reported the phase angle δ.*

Creep-Recovery Test

Creep recovery tests are used to analyse the viscoelastic (VE) behavior performing two shear stress steps. This method is suitable to evaluate the behavior of chemically cross-linked polymers, gels and dispersions showing a physical-chemical network of forces. The test must be performed in the LVE range where the microstructure remains intact [20]. The test is carried out in two steps: a creep phase in which a constant stress is applied, and deformation during time is followed. Once the stress is removed, the second phase starts and it is possible to analyse the recovery, so what happen after the deformation during time. The measured response in a creep

test is presented in terms of creep compliance (J) which is the ratio between the strain (γ) and the applied stress (τ). If an ideally elastic solid is tested, an immediate step-like deformation will be observed and, once removed the load, it will recover totally. Opposite, as long as loaded by constantly acting stress, ideally viscous liquids are showing continuously increasing deformation. After removing the load, they finally remain deformed to the same extent as they showed in the end of the load phase, since these material do not have any elastic portion. For viscoelastic materials under a constant stress, the resulting deformation can be divided in two portion: the first one immediately and the second delayed. When the load is removed, delayed reformation takes place, in a partially or completely way. The degree of reformation/recovery depends on the elastic portion. To interpret creep-recovery curves, several model can be used depending on the behavior of samples. Here the Burger model will be introduced, used for the characterization of obtained hydrogel (see Chapter 5). A typical profile of the creep recovery for a viscoelastic material showing Burger type behavior, a combination of Voigt and Maxwell elements, is reported in Fig. 3.17. It is characterized by an initial elastic response, behavior of

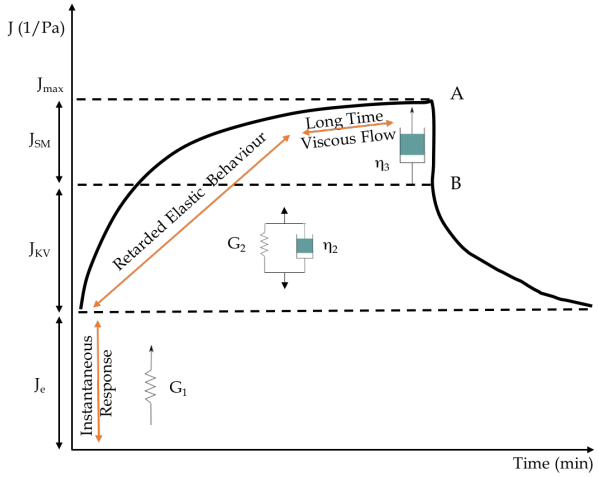

Figure 3.17: *Creep-recovery curve explained with Burger model. J_{max} maximum compliance, J_{SM} Maxwell Spring compliance, J_e compliance of dashpot, J_{KV} Kelvin-Voigt element.*

the spring G_1, followed by a viscoelastic deformation, so a combination of the delayed elastic response and finally a steady state (linear) viscous response at longer times (spring and dash-pot G_2 and η_2). The gradient of this line is equal to the strain and can therefore be used to calculate the zero shear viscosity of the fluid. If the steady state linear response is extrapolated back to zero time, then the intercept is equal to the equilibrium compliance (J_e) associated with just the elastic components of the material (spring in the Burger model). J_{SM} is influenced by the viscous deformation, that will reach a steady-state behavior, showed on the curve by a constant slope. The total deformation, J_{max}, at the end of the stress phase is given by the sum of the singular compliance here described ($J_e + J_{KV} + J_{SM}$). Once the stress is removed, a recovery phase starts, after the steady state has been attained and the strain is monitored. The creep function, describing the time-dependent deformation behavior during the stress phase, can be formulated as:

$$J(t) = \frac{1}{G_1} + \frac{1}{G_2}(1 - exp(-\frac{t}{\lambda_2}) + \frac{t}{\eta_3}) \tag{3.31}$$

With the shear modulus G_1 corresponding to the spring constant and visible in the creep curve as an immediate deformation step due to the purely elastic behavior. Here is also reported the retardation time, λ, correlated to Kelvin-Voigt model. λ determines the time-dependent deformation and reformation behavior of the parallel connecter components spring and dashpot

for both intervals, stress and rest phase, and it is necessary to take in consideration also the reformation of the first spring G_1. η_2 will then be infinite and the creep compliance will reach the plateau to the equilibrium compliance (J_e). However, since the spring recoils immediately, there is no influence on the value of λ. Only the elastic deformation of the sample can fully recover, because the viscous deformation is permanent and J_r, the recovery compliance, should be eventually equal to J_e. To model the response of a real system is often necessary to use multiple Kevin-Voigt elements. If a material has a true yield stress, then no steady state response is observed.

Thixotropic tests

In order to study the thixotropic behavior, linked to the structural rearrangement as reported above, it is possible to carry out two different tests. The first one is a rotational test also called hysteresis loop test [21] characterized by three steps; as for the determination of the flow behavior, shear rate is increased from zero to a predetermined maximum level of shear to obtain an upward curve.

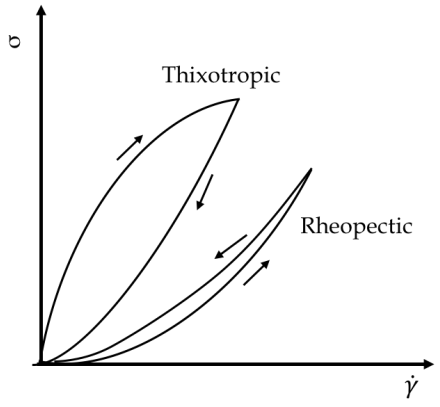

Figure 3.18: *Curves showing thixotropic and rheopectic behavior after hysteresis loop test.*

After that, a phase at constant shear rate follows, where the shear is maintained for a fixed time. The last step is a downward curve, so the shear is decreased back to zero (Fig. 3.18). If the upward curve and downward curve collapse one on the other, the material is not thixotropic, while when the two curves are distinct, they create an area called thixotropic area called also hysteresis loop. If the down-curve is lower than the up one, it means that the material is rheopectic, a rare phenomenon. Another suitable test for assessing thixotropy is a three step shear test (Fig 3.19) that can be carried out in control rate or control stress. In this case, a low shear rate/stress is applied in stage one, until a steady viscosity value is attained, trying to replicate the behavior at rest. Then, in the second stage, the shear rate/stress is increased to a value ideally corresponding with the shear of interest i.e. during stirring, rolling, painting, spraying, and pumping. In the third phase the measuring parameters of the first stage are restored. This last interval allows the sample to recover its structure/viscosity. Generally, in case of shear rate is used in this test, viscosity will be monitored, while when the test is conducted in an oscillation mode, values of the elastic modulus G' are collected. To compare thixotropic behavior between samples the time required to recover a defined amount of the initial viscosity/elastic modulus can be used. This time can therefore be viewed as a relative measure of thixotropy. If it is too short, it indicates a small thixotropic behavior of sample.

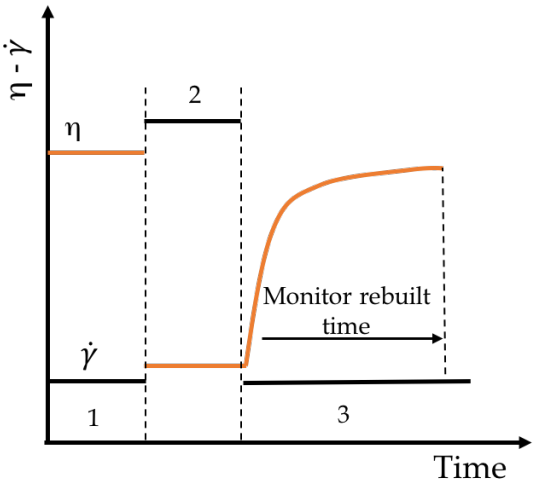

Figure 3.19: *Schematics showing a three-step shear rate profile (black line) to assess thixotropy and the material response.*

3.2 Edible Film characterization

3.2.1 Mechanical Properties

The study of the mechanical properties of a material is necessary to understand the deformation of it under the influence of the applied forces. The mechanical behavior of polymeric films is function of their microstructure or morphology, therefore of the chemical composition, surrounding conditions and test conditions. The micro-structure produced during film processing influences the viscoelastic nature and thus the response to applied stresses during testing. Tensile or mechanical properties are important for the identification and characterization of materials. These properties may vary with specimen thickness, method of preparation, speed of testing, type of grips used, and manner of measuring extension. In this sense, interesting is the study of the material response to unidirectional stress such as in the tensile tests, one of the most widely used mechanical tests. By measuring the force required to elongate a specimen to breaking point, it is possible to determine the properties useful for designing the final quality of the products obtained. The load or stress is determined at the fixed end by means of a load transducer as a function of the elongation, which is measured by means of mechanical strain devices. The experimental data are generally stated as stress (σ) vs. strain (ϵ). The engineering stress is defined as the ratio between the applied load (F) and the original cross-sectional area (A_0)over the specimen (Eq.3.32):

$$\sigma = \frac{F}{A_0} \tag{3.32}$$

while the engineering strain is given by the difference between the instantaneous gauge length (L) and the original length (L_0) (Eq. 3.33):

$$\epsilon = \frac{L - L_0}{L_0} \tag{3.33}$$

The information given by tensile tests allow to quantify the elastic and plastic response of the material through its resistance and ductile properties. Data collected during tests allow obtaining the stress-strain curve where the applied stress is reported as function of the deformation of material, that increases at a constant rate. It is important to distinguish stiffness, which is the measure of the load needed to induce a given deformation in the material, from the strength,

which usually refers to the material's resistance to failure by fracture or excessive deformation. The stiffness is usually measured by applying relatively small loads, well short of fracture, and measuring the resulting deformation. When a material is subjected to small stresses, it responds elastically. This means that the strain produced is reversible with stress and the magnitude of the strain is directly proportional to the magnitude of the stress for the material. In this case we can say that the material exhibits a Hookean behavior, from Hooke's observation that first described the linear relation between a certain load and its resulting deformation, as long as the loads were sufficiently small. The relation between the two features, known as Hooke's Law, can be written algebraically as:

$$E = \frac{\sigma}{\epsilon} \tag{3.34}$$

where E is a constant of proportionality called the Young's modulus or the modulus of elasticity, indication of the stiffness and having units of N/m. The stiffness as defined by E is not a function of the material alone, but is also influenced by the specimen shape. A useful way to adjust the stiffness so as to be a purely materials property, is to normalize the load by the cross-sectional area; i.e. to use the tensile stress rather than the load. The strength properties of solids are more simply illustrated by the stress-strain diagram which describes the behavior of homogeneous brittle and ductile specimens of uniform cross section subjected to uniaxial tension [22]. As described for the rheological properties, within the linear region the strain is proportional to the stress and the deformation is reversible. If the material fails and ruptures at a certain tension and a certain small elongation, it is called *brittle*. If permanent or plastic deformation sets in after elastic deformation at some critical stress, the material is called *ductile*, that does not make it tough.

Tensile testing on a Texture Analyser

The instrument used for the determination of tensile properties is a universal test machine (Fig. 3.20) working with standard methods that can be followed for the measurements of mechanical properties.

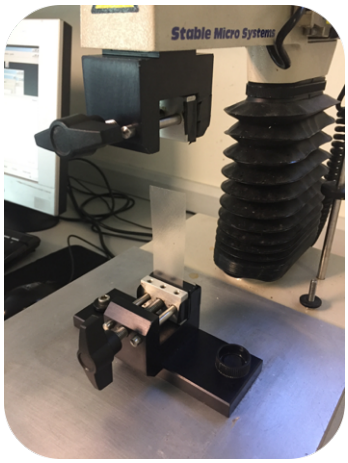

Figure 3.20: *Texture Analyzer.*

Tensile testing involves a specimen, having length L and cross-sectional area A, held in two grips at a predetermined distance. Specimen needs to be conditioned at defined temperature and relative humidity before being tested. The loading arm, attached to the top grip, moves up at a constant speed to deform the sample, first deforming it elastically then plastically. If the force required to break the sample is within the limit of the load cell, fracture will occur. During the test, the applied force, the distance moved by the probe and the time are

recorded. The force-distance graph usually begins with a straight section that corresponds to elastic (reversible) deformation, then most samples show a curved section that shows plastic (irreversible) deformation. Once the y-axis has been changed to show stress and the x-axis strain, the resultant true stress-Henky strain curves can be used for the determination of material properties. Depending on the nature of the sample, some or all of the features can be shown as illustrated in the stress-strain graph in Fig. 3.21. Different materials show different graph shapes. Several useful parameters can be calculated from a tensile stress-strain graph, using the standard engineering equations for stress and strain. If the force is measured in Newton and distance in metres, stress has units of Pascal and strain has no units (it is a ratio).

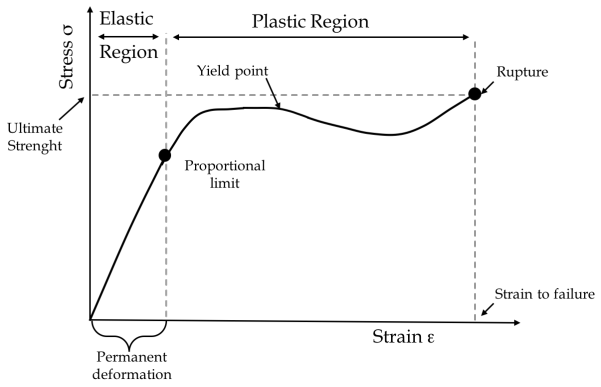

Figure 3.21: *Example of stress vs strain curve for a polymeric material.*

Tensile Strength (σ_{max}), the maximum strength that the sample can support, is obtained from Eq. 3.32 and it is expressed in MegaPascal (MPa). Occasionally it is possible to refer at this also as ultimate tensile strength. Some materials break very sharply, without plastic deformation, in what is called a brittle failure. Others, which are more ductile, including most metals, experience some plastic deformation and possibly necking before fracture. The key of toughness, that is the ability to absorb energy and undergo extensive plastic deformation without rupturing (area under the stress-strain curve), is a good combination of strength and ductility. A material with high strength and high ductility will have more toughness than a material with low strength and high ductility. This feature can be better explained through the calculation of *elongation at break* ($\%\epsilon$), the percentage of the longitude that the sample change starting from its original length to the rupture. It is determined as difference between the final length and initial one.
Young's modulus, is measured as the slope of the initial linear section of the stress-strain graph, where there is a linear regression. Practically, it is given by the ratio between the tensile strength and the elastic region. A stiff material has a high value of this modulus, while materials such as rubber, highly viscoelastic, cannot be said to have a Young's modulus as they show no linear elastic behavior. This value is useful for calculating the compliance of structural materials that follow Hooke's law when subjected to uniaxial loading. But for materials that follow nonlinear elastic stress-strain behavior, the values of tangent, secant or chord moduli are useful in estimating the change in strain for a specified stress range. From the graph it is also possible to recognize two regions: one is the *elastic region*, where the stress-strain curve up to the yielding point. In the elastic region stress and strain are related to each other linearly and the elastic deformation is recoverable. The other is called *plastic region* which starts after the yielding point. Here a plastic deformation takes place and it is permanent. The yield stress is the stress at which the sample begins to deform plastically, so in a permanent way. It is defined as the end of the linear section. Yield stress can only be located if there is a linear section then a clear gradient decrease, and it will be more accurate if there are more points collected per second. The deformation of many materials depends strongly on strain rate, as the processes that allow

deformation to occur are time dependent. The strain rate of a test can be calculated from the gradient of the strain - time graph [23].

3.2.2 Optical properties

Color is defined as the subjective appearance of light detected by the eye and is inherent to the light that leaves a source of emission; but most of the time, before it reaches the eye it interacts with matter of many types: gases, liquids and solids. The color observed is thus a function of both the source radiation and the interactions that have occurred [24]. Color cannot exist without the presence of three elements: light, an object and the observer. In elementary optics, light can usually be considered to consist of light rays. The way in which light interacts with a material can be described in terms of scattering or absorption. To a first approximation, scattering is well treated assuming that the light behaves as an electromagnetic wave, while absorption is better treated in terms of photons. The term scattering itself is usually reserved for the interaction of light with randomly distributed small particles. Elastic scattering from a surface is normally called reflection, while elastic scattering into a transparent solid is called refraction. In classical optics, the interaction of the light with a transparent solid, is concerned with the scattering of the light. This leads to phenomena of reflection, refraction and so on. In these processes, color is produced by an interaction between various light waves, and consideration on energy exchange hardly matter. When the light hits an opaque object, the portion of light that is not absorbed is reflected by the product, with higher or lower intensity depending on the structure of the surface of the object. The color of the object can be therefore measured through *reflectance*. For transparent objects, in which light is absorbed or transmitted, the determination can be made by *transmission*. In case of translucent object, so object that are not totally opaque or transparent, the light is absorbed, reflected, transmitted or lost, so the determination of color is difficult. When the radiation emitted by a light source, is delivered to a material, different optical phenomena occur, such as reflection, refraction, absorption, dispersion or transmission. Fig. 3.22 shows a diagram of the optical phenomena that occur when a light source strikes a material.

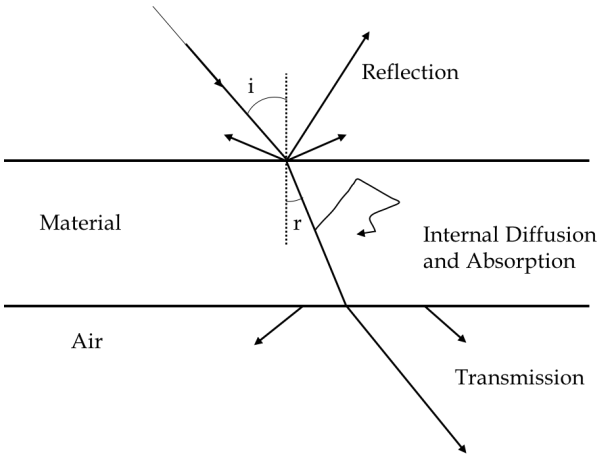

Figure 3.22: *Optical phenomena that happens when a light source strikes a material.*

These optical phenomena are difficult to separate, but more or less selective, depending on the nature of the medium and the position of the observer. Generally, the beam of light incident on the surface of the object, is reflected with a certain intensity in a specular or diffuse way, depending on the roughness of the surface, and suffers a phenomenon of refraction towards the interior of the material. Depending on the absorbent compounds present in the medium,

absorption and/or internal dispersion phenomena occur within the material. The heterogeneity of the material, with one or more dispersed phases of different particle size, together with the differences in the refractive index, between these phases, causes phenomena of light scattering within the material. Finally, and for material with enough homogeneity in the refractive index, there is also the transmission of a certain intensity of light throughout the entire thickness of the product on a regular diffuse basis. Based on the predominant optical phenomenon, it is possible to classify object in:

- transparent: when the specular transmission predominates and the color is defined through a spectrum of product transmission;
- opaque: if the reflection is higher, the spectrum of reflection of the product is used to define the color;
- translucent: where diffusion reflection or transmission predominates depending on their characteristics. Kubelka-Munk theory is applied to define the color of the object [25,26].

Both transmission and reflection spectra can be easily obtained using conventional instruments such as spectrophotometers in case of transparent object and spectrocolorimeter in case of opaque materials. The Kubelka-Munk theory [27] of multiple dispersion is based on the fact that the light that affects a translucent object can be absorbed or dispersed depending on the absorption coefficient (K) and the dispersion coefficient (S) of the material. If the measurements of the reflection spectra are made on a white background and on a black background, the K/S ratio can be determined through the following equation:

$$\frac{K}{S} = \frac{(1 - R_\infty)^2}{2R_\infty} \tag{3.35}$$

R_∞ is the reflectance of an infinite sample sheet (with sufficient thickness so that the bottom does not affect the measurement), calculated through Eqs. 3.36 to 3.38, where R is the reflectance of the sample determined on a white background of a known reflectance R_g and R_0 is the reflectance of the sample determinate on an ideal black background. The internal transmission (T_i) of the sample can be obtained by Eq. 3.39.

$$R_\infty = a - b \tag{3.36}$$

$$a = \frac{1}{2}(R + \frac{R_0 - R + R_g}{R_0 R_g}) \tag{3.37}$$

$$b = \sqrt{a^2 - 1} \tag{3.38}$$

$$T_i = \sqrt{(a - R_0)^2 - b^2} \tag{3.39}$$

The Kubelka-Munk theory provides parameters that explain the behaviour of translucent objects better than the conventional color measurements. In general, high values of K/S are related to an open structure and transparent materials, while low values are related to closed structure and less transparent materials. On the other hand, from the value of R_∞ it is possible to calculate the color through coordinates (explained later) that allow to describe the color of the object. These coordinates are not directly related to the sensorial perception of the object, but they help to control and describe the color of the sample. So the color can be defined in a physic way, with serious limitation if the color need to be used as a quality tool control (because it is the impression in the observer that define the characteristics of rejection or acceptability of a product). It is also possible to define a color as set of signals that arrive to the brain through the sense of sight (perceived color). However, this perception is influenced by a series of different attributes of the product (shape, size, type of surface etc.) and for a set of psychological perceptions, such as the environment of the object where the type of light that it receives plays a very important role.

Despite the complexity inherent in the concept of color and its perception, it has been found that all colors can be precisely specified by three parameters then conveniently represented by points in a three-dimensional coordinate system. There are many diagrammatic ways of representing the three attributes called *color spaces*. The way in which the coordinates of any color in the color space are derived is called a color model. Based on this, the CIE (Commission Internationale de l' clairage) introduced the concept of psychophysical color, which allows to relate objective measures of it (physical color) and takes into account the response of the observer (perceived color)[28]. Psychophysical color is described by the use of coordinates, which allow different color space to be constructed. These coordinates allow quantifying the perception of color through a physical determination of it, in terms of amount of red (X), green (Y) and blue (Z) that is perceived. The value of these coordinates will depend on the external light stimulus and on the observer. The external stimulus will depend in turn on the physical interaction of the object with the light (visible spectrum) and on the spectral distribution of the illuminant used for the observation. To calculate the coordinates, it is necessary to specify which is the illuminant used and the observer because the perception of color depends on them. Taking in mind these two variables, the CIE describes different illuminants (A, B, C, D55, D65 etc.) and observer, based on a viewing angle (2° and 10°) [28]. Due to the fact that the illuminant and observer used for the calculation of color coordinates are prefixed for the CIE, there are tables with the value of the spectral distribution and several equations that allow to determine in a mathematic way the tri-stimuli coordinates XYZ (it is simply the sum of the product between the spectral value of the object at each wavelength and the spectra of the source of light and observer). The complex nature of color make it necessary to understand its three-dimensional nature. Interpretation of color data was simplified by the CIE L*a*b* (CIELAB) system and is now used as the universal system for colorimetry. The CIELAB color space is a derivation of color space from the values

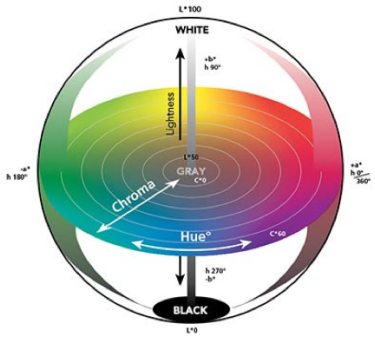

Figure 3.23: *Sphere representing the distribution of color parameters including L*, a*, b* and hue and chroma.*

of X, Y, Z, with L*, a*, and b* coordinates. It is based on a Cartesian system consisting of 3 axes [29], the vertical axis L*, represents the measure of lightness of a colour, attribute of visual sensation according to which a surface emits more or less light, varying from 0 (black) to 100 (white). The horizontal axis a* represents a measure of the red or green content of a color. If a color has red, a* will be positive, while, if a color has green, a* will be negative. The horizontal axis b*, perpendicular to the axis a*, represents a measure of the yellow or blue content of a colour. Positive values of b* indicate yellow content, while negative values of it indicate blue content. In this color space two more attributes are used to describe objects, together with lightness: hue and chroma. Hue (h*) is the attribute of visual sensation according to which a surface seems similar to one, or proportions of two, of the colors perceived red, orange, yellow, green, blue and purple; and chroma (C*) is the attribute of the visual sensation which

corresponds to the amount of white light mixed in with the hue and allows pale 'washed out' colors to be described. These color attributes h* and C* can be obtained from the values of L * a * b * (Eqs. 3.40-3.41).

$$C^*_{ab} = \sqrt{a^{*2} + b^{*2})} \tag{3.40}$$

$$h^*_{ab} = \arctan\left(\frac{b^*}{a^*}\right) \tag{3.41}$$

$$\Delta E = \sqrt{(L^*_0 - L^*_s)^2 + (a^*_0 - a^*_s)^2 + (b^*_0 - b^*_s)^2} \tag{3.42}$$

When two or more objects are compared, it is possible to calculate a total difference between color coordinates called ΔE (Eq. 3.42) and represent the distance between two points in the L*a*b* color space. The greater the difference, the larger the color difference value. The spectrophotometer can estimate tri-stimulus values through the measure of the transmittance and reflectance as a function of wavelengths, from 380 to 780 nm, equivalent to the ones that can be sensed by the human eye. Color measurement software can perform calculation in the different color systems, so tri-stimulus values XYZ can be converted into chromaticity coordinates and manipulated through color space transformations.

3.2.3 Thermogravimetric Analysis (TGA)

Thermogravimetric (TG) is a branch of thermal analysis that examine the mass changes of a sample and with the expression thermogravimetric analysis (TGA) we refer to a method of thermal analysis in which changes in physical and chemical properties of materials are measured as a function of increasing temperature (with constant heating rate, scanning mode), or as a function of time (with constant temperature, isothermal, and/or constant mass loss) [30]. Sample is subject to a program of change in temperature and changes in its mass can be due to various chemical reactions (decomposition, loss of crystallization water, combustion, reduction of metal oxides) and physical transition (desorption, sublimation, vaporization, drying). Therefore, TGA is used in the analysis of volatile and gaseous products lost during the reactions in thermoplastics, elastomers, composites, films, fibers, coatings, paints, etc. Based on how the analysis is carried out it can be:

1. Isothermal or Static TGA: sample is maintained at a constant temperature for a period of time during which change in weight is recorded;

2. Quasi-static TGA: sample is heated to a constant weight at each of a series of increasing temperature;

3. Dynamic TGA: sample is subjected to condition of a continuous increase in temperature at a constant heating rate (usually linear with time).

The instrument used for TGA analysis is a thermo-balance, programmed precision balance for a rise in temperature. Thermo-balance consists of an electronic microbalance, a furnace, a temperature programmer and a recorder. The main choices on performing a TGA experiment are the sample pans (platinum or ceramic), sample size, temperature program, including positive isothermal steps, and the gas environment. The plot of mass change in percentage versus temperature or time (known as TGA curves) is the typical result of this analysis as shown in Fig. 3.24. Two are the main temperatures in the reaction: T_i, temperature at which the decomposition starts, and T_f, final temperature, representing the lowest temperature at which the onset of a mass change is seen and the lowest temperature at which the process has been completed, respectively. The reaction temperature and interval (T_f - T_i) strongly depend on the conditions of the experiments. According to their shape it is possible to recognize different types of TGA curves as reported in Fig. 3.25.

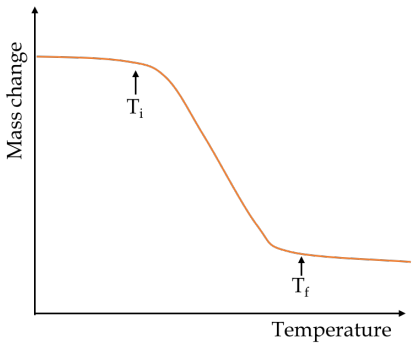

Figure 3.24: *The plot of mass change with temperature.*

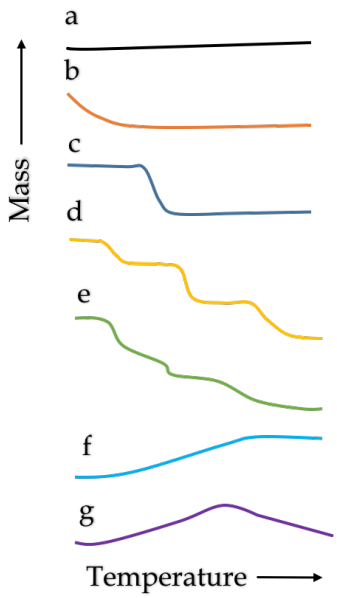

Figure 3.25: *TGA curves*

- *a*, no mass change over the entire range of temperature, indicating that the decomposition temperature is greater than range of the instrument;
- *b*, the mass loss is large and it is followed by mass plateau. This is formed when evaporation of volatile products during desorption, drying or polymerization takes place;
- *c*, this curve is typical of single-stage decomposition temperatures having T_i and T_f;
- *d*, a multi-stage decomposition processes is represented as a result of various reactions;
- *e*, Similar to *d*, but either due to fast heating rate or due to no intermediates;
- *f*, this curve shows the increase in mass. This may be due to the reactions such as surface oxidation reactions in the presence of an interacting atmosphere;
- *g*, it is similar to curve *f*, but product decomposes at higher temperatures. For example, the reaction of surface oxidation followed by decomposition of reaction product(s).

TGA can provide precise and accurate compositional analysis that can be used for quality and process control. This analysis is generally used to study the thermal stability of the related

materials that can be compared at elevated temperatures under the required atmosphere. In addition to TGA curves, other different curves can be used to aid interpretation, such as the first derivative curves (DTG curve), where the rate of change of mass is reported. Many complex materials/mixtures can be analyzed by decomposing or removing their components. TGA can be also used to carried out kinetic and corrosion studies [31].

3.2.4 Field Emission Scanning Electron Microscopy (FESEM)

The word FESEM is the abbreviation of Field Emission Scanning Electron Microscope and it is developed based on a technology for high-resolution imaging and different contrasting methods aiming for a comprehensive characterization of specimens. The first true scanning electron microscope (SEM) was described and developed in 1942 by Zworykin, who showed that secondary electrons provided topographic contrast by biasing the collector positively relative to the specimen. He reached the resolution of 50nm when using an electron multiplier tube as pre-amplifier of the secondary electrons emission current. Since then, many improvements have been made until the first commercial SEM was made [32]. The SEM that uses a field emitter gun (FEG) to emit electrons is called FESEM and it is used to visualize very small topographic details on the surface or entire or fractioned objects, so in general it is possible to observe structures that may be as small as nanometers. For these reasons it is employed for the study of biological material, synthetic polymers, coatings and so on.

FESEM components

An FESEM is composed by a cylindrical column that hosts the electron beam and lenses. Knobs for the regulation of the electron beam can be found at various levels on the column. There are also tubes present to maintain the vacuum and the temperature in the instrument. The microscope is operated from the steering panel. An exchange chamber in front, below the columns is used to introduce the object into the high vacuum area. The object can be observed on a monitor while it is scanned and it is possible to see the object chamber. For image archiving and processing there is a computer connected to the system.

How FESEM works

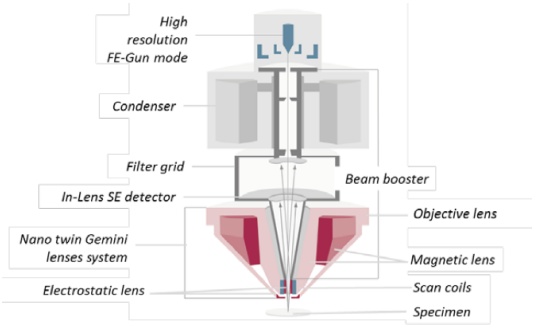

Figure 3.26: *Electron optic column design for GeminiSEM 500.*

As said, electrons are liberated from a field emission source made up of tungsten wire and accelerated in a high electrical field gradient. Sometimes tungsten can be replaced by a crystal of lanthanum hexaboride LaB_6. This modification results in a higher electron density in the beam and a better resolution than with the conventional device. In a field emission scanning electron microscope no heating but a so-called ´cold´ source is employed, so it is possible to use this technique also with samples that are heat intolerant. The extremely thin and sharp tungsten needle (tip diameter $10^{-7} - 10^{-8}$ m) functions as a cathode in front of a primary and secondary anode. The voltage between cathode and anode is in the order of magnitude of 0.5 to 30 KV. Because the electron beam produced by the FE source is about 1000 times smaller than in a

standard microscope, the image quality is markedly better. As field emission necessitates an extreme vacuum in the column of the microscope, a device is present that regularly decontaminates the electron source by a current flash. Within the high vacuum column these so-called primary electrons are focussed and deflected by electronic lenses to produce a narrow scan beam that bombards the object. As a result, secondary electrons are emitted from each spot on the object. Electron optic is used to de-magnify the size of electron source to form smallest possible probe for high resolution. The demagnification is achieved using a series of lens known as ´probe-firming´ lens, comprising the condenser and the objective lens. The scan coils deflect the electron beam over the object according to a zig-zag pattern. The formation of the image on the monitor occurs in synchrony with this scan movement. The scan velocity determines the refreshing rate on the screen and the amount of noise in the image. The smaller the scanned region on the object, the larger the magnification becomes at a constant window size. Scan coils often consist of upper and lower coils, which prevent the formation of a circular shadow at low magnification. The objective focuses the electron beam on the sample. At a short working distance, so when the object is closer to the objective lens, it needs to apply a greater force to deflect the electron beam. The shortest working distance produces the smallest beam diameter, the best resolution, but also the poorest depth of field. The stigmator coils are utilized to correct irregularities in the x and y deflection of the beam and thus to obtain a perfectly round-shaped beam. A preliminary phase of sample preparation is necessary in order to observe objects. First it is indispensable to coat samples with an extremely thin layer of gold or platinum to make it conductive. Further on, objects must be able to sustain the high vacuum and should not alter it. To observe transversal section of film these are fractured after being immerse in liquid nitrogen and coated for direct observation in the FESEM. After the object has been covered it is mounted on a special holder. The object, inserted through an exchange chamber into the high vacuum part of the microscope, can be repositioned in the chamber by means of a joy stick that steers in left-right axis, or forward and backward. In addition, the object can be tilted and rotated. The ´secondary electron emission´ detector (scintillator) is located at the rear of the object holder in the chamber. The angle and velocity of these secondary electrons relates to the surface structure of the object. A detector catches the secondary electrons and produces an electronic signal. The signal produced by the scintillator is amplified and transduced to a video signal that is fed to a cathode ray tube in synchrony with the scan movement of the electron beam. The contrast in the ´real time´ image that appears on the screen reflects the structure on the surface of the object. Parallel to the analogue image, a digital image is generated which can be further processed.

References

1. Dahneke, B.E. *Measurement of suspended particles by quasi-elastic light scattering;* John Wiley & Sons: **1983**.

2. Hassan, P.A.; Rana, S.; Verma, G. Making sense of Brownian motion: colloid characterization by dynamic light scattering. *Langmuir* **2014**, 31, 3-12.

3. Berne, B.J.; Pecora, R. *Dynamic light scattering: with applications to chemistry, biology, and physics*; Courier Corporation: **2000**.

4. Pecora, R. *Dynamic light scattering: applications of photon correlation spectroscopy*; Springer Science & Business Media: **2013**.

5. ISO13321, I. Methods for determination of particle size distribution part 8: Photon correlation spectroscopy. *International Organisation for Standardisation* (ISO) **1996**.

6. Kirby, B.J.; Hasselbrink Jr, E.F. Zeta potential of microfluidic substrates: 1. Theory, experimental

techniques, and effects on separations. *Electrophoresis* **2004**, 25, 187-202.
7. Overbeek, J.T.G. The interaction between colloidal particles. *Colloid science* **1952**, 1, 245-277.
8. Hunter, R.J. *Zeta potential in colloid science: principles and applications*; Academic press: **2013**; Vol. 2.
9. Lyklema, J. *Fundamentals of interface and colloid science: soft colloids*; Elsevier: **2005**; Vol. 5.
10. Bhattacharjee, S. DLS and zeta potential-what they are and what they are not? *Journal of Controlled Release* **2016**, 235, 337-351.
11. Atkins, P.W.; De Paula, J.; Keeler, J. *Atkins' physical chemistry*; Oxford university press: **2018**.
12. Barnes, H.A. A handbook of elementary rheology. **2000**.
13. Schramm, G. *A practical approach to rheology and rheometry*; Haake Karlsruhe: **1994**.
14. Mezger, T.G. *The rheology handbook: for users of rotational and oscillatory rheometers*; Vincentz Network GmbH & Co KG: **2006**.
15. Barnes, H.A. Thixotropy-a review. *Journal of Non-Newtonian fluid mechanics* **1997**, 70, 1-33.
16. Ma, J.; Lin, Y.; Chen, X.; Zhao, B.; Zhang, J. Flow behavior, thixotropy and dynamical viscoelasticity of sodium alginate aqueous solutions. *Food Hydrocolloids* **2014**, 38, 119-128.
17. Nindo, C.; Tang, J.; Powers, J.; Takhar, P.S. Rheological properties of blueberry puree for processing applications. *LWT-Food Science and Technology* **2007**, 40, 292-299.
18. Coussot, P.; Raynaud, J.; Bertrand, F.; Moucheront, P.; Guilbaud, J.; Huynh, H.; Jarny, S.; Lesueur, D. Coexistence of liquid and solid phases in flowing soft-glassy materials. *Physical review letters* **2002**, 88, 218301.
19. Bhattacharya, S.; Bal, S.; Mukherjee, R.; Bhattacharya, S. Rheological behaviour of tamarind (Tamarindus indica) kernel powder (TKP) suspension. *Journal of food engineering* **1991**, 13, 151-158.
20. Dolz, M.; Hernández, M.; Delegido, J. Creep and recovery experimental investigation of low oil content food emulsions. *Food Hydrocolloids* **2008**, 22, 421-427.
21. Ferron, R.P.; Gregori, A.; Sun, Z.; Shah, S.P. Rheological method to evaluate structural buildup in self-consolidating concrete cement pastes. *ACI materials journal* **2007**, 104, 242.
22. Van Krevelen, D.W.; Te Nijenhuis, K.*Properties of polymers: their correlation with chemical structure; their numerical estimation and prediction from additive group contributions*; Elsevier: **2009**.
23. Labossiere, P. Mechanical properties and performance of materials. *Mechanics of materials laboratory. Lecture notes, university of washington* **2013**.
24. Tilley, R.J. *Colour and the optical properties of materials*; John Wiley & Sons: **2020**.
25. Berger-Schunn, A. *Practical color measurement: a primer for the beginner, a reminder for the expert*; Wiley-Interscience: **1994**.
26. Kuehni, R.G. *Color: An introduction to practice and principles*; John Wiley & Sons: **2012**.
27. Hutchings, J. Food color and appearance 2nd edition. USA: *Aspen Pulisher Inc* **1999**.
28. Schanda, J. *Colorimetry: understanding the CIE system*; John Wiley & Sons: **2007**.
29. Hunter, R. Accuracy, precision, and stability of new photoelectric color-difference meter. In Proceedings of Journal of the Optical Society of America; pp. 1094-1094.
30. Prime, R.B.; Bair, H.E.; Vyazovkin, S.; Gallagher, P.K.; Riga, A. Thermogravimetric analysis (TGA). Wiley Online Library: **2009**; pp 241-317.
31. Menczel, J.D.; Prime, R.B. *Thermal analysis of polymers*; Wiley Online Library: **2009**.
32. Cik, R.C.H.; Foo, C.T.; Nor, A.F.O. Field Emission Scanning Electron Microscope (FESEM) Facility in BTI.

4 Rheological characterization and antifungal properties of alginate - essential oil nanodispersions

«Everything flows if you wait enough...even mountains»
Prophet Deborah

Abstract

Due to its favorable structural properties and biocompatibility, alginate is recognized as a suitable versatile biopolymer for use in a broad range of applications ranging from drug delivery, wound healing and tissue engineering applications and food formulations such as nanodispersions. Rheological analysis plays a crucial role in the design of suitable nanoemulsions based coatings. To this aim, different essential oil (EO) and alginate nanodispersion compositions stabilized by Tween 80 were analyzed for rheological and conductometric properties as well as for the antifungal activity. The results confirmed that the nanoformulations shared a pseudoplastic non-Newtonian behavior that was more evident with higher alginate concentration (2%). Nanodispersions made of alginate and essential oil exhibited a slight thixotropic behavior, demonstrating the aptitude to instantaneously recover from the applied stress or strain. Oscillatory frequency sweep tests showed a similar fluid-like behavior for 1% and 2% alginate nanodispersions. Nanodispersions at concentration of EO higher than 1% were effective in inhibiting the growth of species belonging to *Penicillium, Aspergillus* and *Rhizopus* genera. Finally, it was demonstrated that advantages coming with the use of the essential oil are added to the positive aspects of the use of alginate with no dramatic modification on the flow behavior.

4.1 Introduction

Alginate is a versatile polyelectrolyte, as already reported in Chapter 1, that when dissolved in aqueous environment confers to the suspension interesting mechanical properties. This aspect allows alginate to be a good candidate for designing many applications in different fields. A further improvement of the features provided by the use of alginate is offered by the formation of composite systems based on the nanodispersion of essential oil (EO) in alginate suspensions. EO, indeed, have outstanding properties that in nanoemulsion formulations are added to those carried by alginate. Rheological characterization of nanodispersions based on hydrocolloids is one of the most important steps of material characterization because it is well recognized that rheological properties play a role in the design, evaluation and modelling of the production process [1,2]. This is the reason why the data obtained from rheological tests are required as quality indicator, since they are used for the calculation in processes involving fluid flow, and for the analyses of flow condition in food processes. Therefore, complete knowledge of the apparent viscosity at different shear rates, is requested by industries to calibrate and optimize production method and processes [3]. Together with the flow behavior, thixotropy can provide clues to product stability after the application of a certain strain or stress, for example after stirring, while dynamic frequency sweeps give information on the physical structure by analyzing data related to the energy reserve (G') and consumption (G") [4]. Among the positive aspects of nanodispersions containing EOs, there is the antimicrobial and antifungal activity, that made them suitable for the application as edible coatings and films for food applications. Essential oils on their own, have activity against several food pathogens and undesirable microorganisms [5]. Anyway, to obtain an inhibitory effect, it is sometimes necessary to use a high concentration of these substances, leading to negative consequences on the sensorial properties of food matrices on which they are applied. From literature the positive action of EOs against several pathogens as *Escherichia coli* and *Staphylococcus aureus*, is reported for EOs encapsulated or not [6-8]. Concerning fungus, *Aspergillus* and *Penicillium* spp. are mycotoxin producing fungi responsible for about 50% of post-harvest losses in tropical and under-developed countries [9]. About 25% of food commodities are contaminated by mycotoxins and it constitutes a threat to the health and the economy of many countries [10]. *Penicillium expansum* is a post-harvest fungus responsible for the deterioration of fruits, in particular apples on which it causes the so-called ´blue rot´. This fungus synthesizes the patulin, a mycotoxin whose toxicity to humans and animals has been demonstrated [11,12]. In the present study, different nanodispersions have been prepared and characterized to analyze the rheological properties of formulations having alginate 1% or 2% in the continuous phase and essential oil concentration varying from 0% to 2%. Considering the use of alginate as edible coating, the goal of this investigation was to understand how the essential oil dispersion in alginate suspension affects the structural and fluid behavior. Moreover, the in vitro antifungal activity of nanodispersions against mycotoxin fungus, like *P. expansum* and *A. niger*, was assessed as well as the antifungal activity against two strains of *Rhizopus oligosporus* species.

4.2 Materials and Methods

4.2.1 Materials

Food-grade sodium alginate was from Farmalabor, Tween 80 was purchased from Sigma Aldrich, lemongrass (*Cymbopogon nardus*) essential oil (100%) was from Erbamea (Lama di San Giustino, PG, Italy).

4.2.2 Nanodispersions preparation

Dispersions made of different concentrations of sodium alginate (1-2% w/v) were prepared by dissolving polyelectrolyte powder in water bath at 70 °C through gentle stirring with magnetic bar. Nanodispersions were prepared using sodium alginate dispersion (1 or 2% v/v) as the continuous phase and lemongrass essential oil (EO) at different concentrations (0, 0.5, 1, 2% v/v) as the dispersed phase. All the nanodispersions were stabilized by Tween 80 (1% v/v). Coarse emulsions were prepared by mixing the aqueous phase with EO and Tween 80 using a laboratory mixer, T25 digital Ultra-Turrax, working at 24000 rpm for 4 minutes. All the emulsions were then sonicated using an Ultrasonic Homogenizer (Model 300 VT) for 1 min at 120 W with 50% pulsed frequency to reduce particle dimensions.

4.2.3 Rheological characterization

Rheological measurements of alginate suspensions and nanodispersions were made through a rotational rheometer, Haake MARS III (Thermo Scientific, Karlsruhe, Germany) two days after their preparation. All rheology measurements were made using a 60 mm diameter parallel plate geometry (PP60). The temperature was controlled by a Peltier system in combination with a water bath system (Phoenix II, Thermo Scientific, Karlsruhe, Germany). The samples (2.9 mL) were carefully poured onto the surface of the lower plate and the upper plate was lowered to 1 mm gap distance. Before testing, samples were left equilibrating for 10 min to allow for mechanical and temperature equilibrium. Flow curves were made in control rate mode (CR) varying the shear rate (0.1- 150 s^{-1}) at 25°C. Frequency sweep tests were carried out using a fixed shear stress from the linear viscoelasticity (LVE) range previously determined (through amplitude sweep measurements), and in a frequency range from 0.01 to 100 Hz. Thixotropy curves were obtained through hysteresis loop experiments carried out in three steps: (1) rotational CR test with shear rate varying from 0 to 100 s^{-1} in 100 s; (2) plateau curve at the maximum shear rate (100 s^{-1}) for 30 s; (3) downward curve from 100 to 0 s^{-1} in 100 s.

4.2.4 Conductivity measurements

Conductivity values were recorded using a CDM230 conductivity meter (Radiometer Analytical) equipped with a two-pole conductivity cell tailored for small volumes (CDC 749), calibrated with a standard solution of KCl 1x10^{-2} M. The conductivity was measured at 25 °C.

4.2.5 Antifungal activity

Antifungal effect of nanodispersions at different concentration of essential oil was tested evaluating the presence of the inhibition halo by contact method for *Penicillium expansum, Aspergillus niger* and two strains of *Rhizopus oligosporus* (A and B). The moulds were obtained from the Institute of Food Sciences of the National Research Council of Italy (Avellino). Moulds were maintained on Potato Dextrose Agar (PDA) (Oxoid, Milan, Italy) at the temperature of 25 °C. Fungal spores obtained from 10-day-old cultures of the moulds were used to inoculate 20 mL of PDA medium poured into sterilized Petri dishes at a concentration of approximately 10^4-10^5 spore/mL. After solidification of the medium, 40 μl of the nanodispersions at different concentration of EO (1.0, 1.5, 2.0%), were spread on the surface of the substrate. To establish the antifungal activity of the nanodispersions, the system with only polymer and surfactant was used as control (B2), as well as it was made a spot with the essential oil simply mixed in water. Inoculated plates were incubated at 25°C for ten days for fungal recovery. The efficacy of inhibition of the samples is to be considered positive when the halo is present, so no growth is visible.

4.3 Results and Discussion

Food grade nanodispersions were prepared by mixing different concentrations of lemongrass essential oil with suspensions containing either 1 or 2% of alginate. The effect of the oil mixing with alginate was measured with ionic conductivity. Fig. 4.1 illustrates the conductivity values

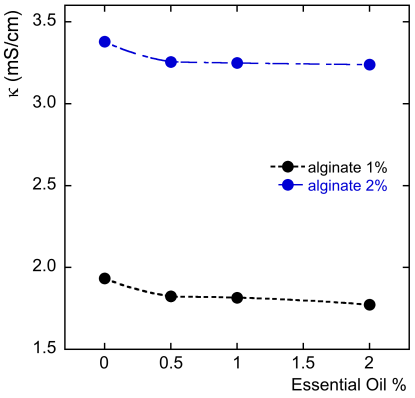

Figure 4.1: *Ionic conductivity as function of lemongrass essential oil concentration. Nanodispersions having 1% and 2% alginate as continuous phase are represented with black and blue symbols, respectively.*

according to variations of essential oil concentration in 1 and 2% alginate dispersions. Shown in the graph, the conductivity of the dispersions decreases with the oil content increase. Among the nanodispersions ingredients, alginate, being a polyelectrolyte, is the only one bearing charges and as can be seen from Fig. 4.1, the ionic conductivity of the nanoemulsions based on 2% alginate was higher than conductivity at 1% alginate. However, the addition of essential oil was able to reduce the alginate charge mobility, regardless the alginate concentration. From these results the relevance of the amount of polymer that influences the phase behavior of the system appears obvious. Such changes in electrical conductivity can be interpreted as a consequence of the polymer-induced increase in connectivity of aqueous domains [13]. These results indicate that the hydrocolloid and the lipid fraction interact with each other.

The rheological behavior was investigated according to the increasing oil concentration through both rotational and oscillatory tests. Native alginate suspensions (without oil and surfactant) exhibited a non-Newtonian pseudo-plastic behavior (data not shown) showing shear rate dependence of the apparent viscosity. As reported in Fig. 4.2A, B, an analogous behavior was observed for the alginate/essential oil nanodispersions. The flow curves of all the o/w nanodispersions showed the apparent viscosity values decreasing along with the shear rate increase. In the insets of Fig. 4.2, the shear stress values as function of the shear rate are reported. Apparent viscosity curves for 1% alginate nanodispersions (Fig. 4.2A) presented a small increase for essential oil content of 0.5% (A1 - EO 0.5) and overall, the values measured were one order of magnitude smaller than the values of the 2% alginate nanodispersions (Fig. 4.2B). Among the nanodispersions made with 2% alginate, loading 1% of essential oil (A2 - EO 1) gave the lowest viscosity values.

Flow curves of all the nanodispersions were fitted to the Ostwald-de Waele model [14,15] according to Eq. 4.1:

$$\tau = k\dot{\gamma}^n \tag{4.1}$$

where τ is the shear stress (Pa), $\dot{\gamma}$ is the shear rate (s^{-1}), k is known as the consistency index (Pas^n) corresponding to the fluid consistency and n as the flow behavior index (dimensionless number). When the value of n equals 1 the fluid behaves as a Newtonian fluid and the con-

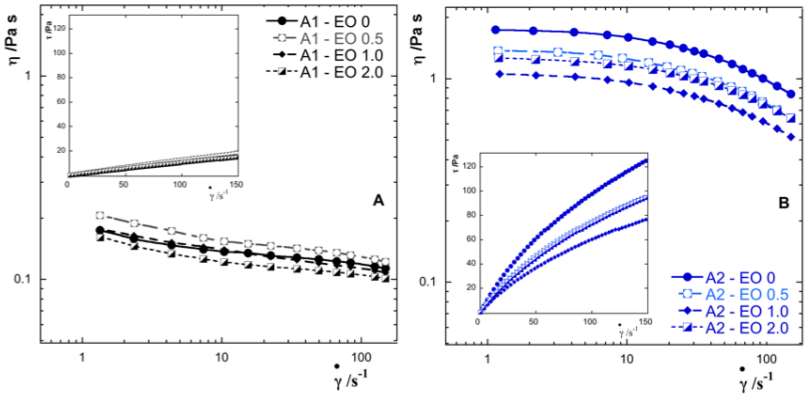

Figure 4.2: *Apparent viscosity curves of alginate/lemongrass essential oil nanodispersions as function of the shear rate. Nanodispersions having 1% and 2% alginate as the continuous phase are represented with black (**A**) and blue (**B**) symbols, respectively. Insets of (**A**) and (**B**) panels are the flow curves (shear stress as functions of the shear rate) for nanodispersions based on 1% and 2% alginate.*

sistency index will coincide with the viscosity value, for n values smaller than 1 the fluid is considered a shear thinning pseudoplastic fluid; for n values higher than 1 the fluid rheogram will show the behavior of a shear thickening or dilatant fluid. The values of consistency and flow indices, calculated from the flow curve fittings for all the nanodispersion systems at either 1 or 2% of alginate, are shown in Fig. 4.3A, B, respectively. As shown, the flow index values are

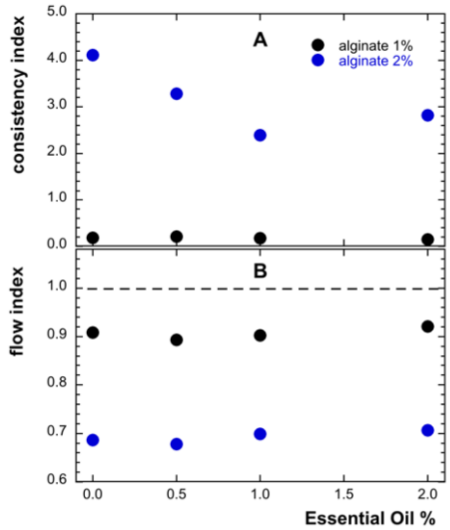

Figure 4.3: *Consistency index (**A**) and flow index (**B**) as function of the nanoemulsion oil content calculated by fitting the nanodispersion flow curves to the Ostwald-de Waele model. Nanodispersions at 1 and 2% of alginate are represented with black and blue dots respectively.*

all smaller than 1, indicating a deviation from the Newtonian behavior that was higher for 2% alginate based nanodispersions. On the other hand, the trend observed for the viscosity values is replicated in the trend seen in the index of consistency values. These values indicate that the flow behavior of the nanodispersions was more influenced by the hydrocolloid concentration than by the oil content. This aspect together with the shear thinning behavior is important since the continuous phase prevents the creaming phenomena. A relevant aspect regarding the

handling of fluids is their time dependent behavior that can result in a thixotropic (viscosity decrease) or rheopectic (viscosity increase) response to shearing time.

A common method for studying the thixotropic behavior of fluids like paints and coatings

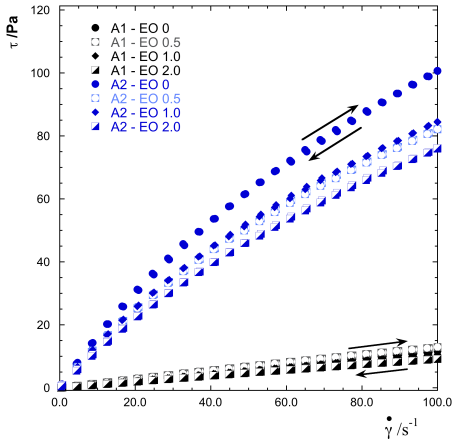

Figure 4.4: *Curves of hysteresis loop at 1% and 2% alginate (black and blue symbols respectively) and essential oil concentration ranging from 0 and 2%.*

is a loop experiment including a Controlled Rate (CR) ramp up from low to high shear rates (structure breakdown), followed by a steady shear rate phase at the highest shear rate and a CR ramp down to a zero shear rate (structure recovery). For thixotropic materials the difference in the area defined by the upward and the backward curve is the hysteresis area that represents the energy to breakdown the fluid structure. A non-thixotropic material would exhibit identical viscosity curves for ramp up and ramp down and therefore no hysteresis area. This kind of material recovers instantaneously from an applied stress or strain. The larger a hysteresis area the more a material is considered as thixotropic. The nanodispersions made of alginate 1 and 2% and essential oil (varying from 0 to 2%) all exhibited slight thixotropic behavior as shown in Fig. 4.4, and therefore it can be claimed that the nanodispersions viscosity is barely time dependent, but it is mostly function of shear rate and temperature. This means that the here-prepared nanodispersions have a fast structure recovery. A very similar thixotropic behavior was previously observed on aqueous suspensions of alginate at different concentrations [14]. To gain a better understanding of the nanodispersion structures, rheological oscillatory analyses were carried out. Frequency sweep tests, performed within the linear viscoelastic region of each fluid, enabled to determine the viscoelastic behavior in a frequency range from 0.1 to 100 Hz. As shown in Fig. 4.5A, B, the storage modulus (G') and loss modulus (G") were both increasing along with the frequency applied to either 1% or 2% alginate dispersions. The high frequency zone of the mechanical spectra corresponds to short-time behavior that is simulated by the rapid motion, while, the low frequency side, characterized by a slower motion, simulates the long-term behavior. The nanodispersions considered had G" values higher than the G' values, particularly at low frequencies. Additionally, the G' and G" moduli approached each other at high frequency, indicating that the viscous-like behavior dominated, even if in short terms the dispersions become less liquid-like. By comparing the elastic moduli G' of nanodispersions prepared with 1% (Fig. 4.5A) and 2% alginate (Fig. 4.5B) it was evident they were more frequency dependent using 1% alginate nanodispersions, showing it provided a more fluid-like material compared with the samples containing 2% alginate. Overall the rheological investigation on alginate-based nanodispersions has demonstrated that the nanodispersions studied had similar flow properties to the parent alginate suspension free from oil. This shows that the positive features of alginate in the continuous phase were added to the advantages given by the addition of essential oil, with no dramatic modification on the flow behavior. The practice of coating

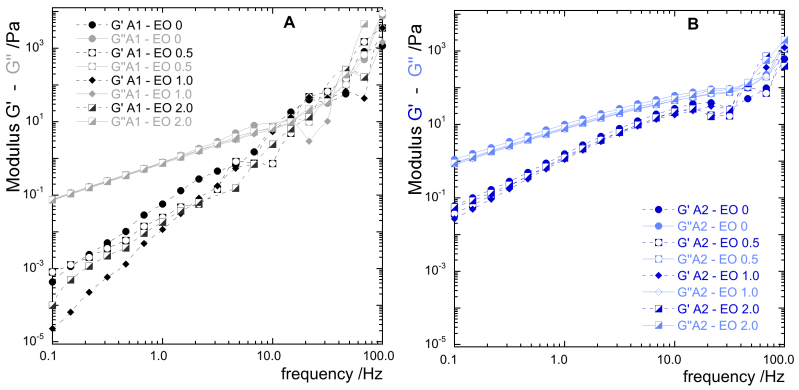

Figure 4.5: *Dynamical oscillatory frequency sweep test curves for alginate/lemongrass essential oil nanodispersions. Storage modulus (G') and loss modulus (G") of 1% alginate nanodispersions (**A**) are shown with black and grey symbols respectively. G' and G" of 2% alginate nanodispersions (**B**) are represented with dark blue and light blue symbols, respectively.*

food products involves the formation of a protective layer on the surface avoiding draining or dripping phenomena to ensure the realization of a continuous film. To achieve this, a step of gelation of the coating on the food surface is usually provided. In this regard, alginate is known for its gelling properties, in the presence of divalent cations (like calcium ions). Therefore, considering the similar properties shown by the alginate essential oil enriched nanodispersions proposed here, similar gelling aptitudes are also expected for the latter. The restrictions on the use of some synthetic food additives, imposed by food industries and regulatory agencies, have led to renewed interest in searching for alternatives antimicrobial compounds to use in food field, such as essential oils [16]. However, the biological activity of EOs could be lost by volatilization of active components or other degradation reactions [17]. Thus, the incorporation of essential oil in nanodispersion systems, to protect and use it in lower quantities, is a valid prospect to overcome the disadvantages that limit the commercial application of EOs. Molds belonging to *Penicillium* and *Aspergillus* genera can affect different commodities, from fruits (´blue rot´ of *Penicillium* on apples) to bakery products (black mold of *Aspergillus* on bread) while there are other molds such as *Rhizopus* spp. that can be found in some foods due to cross-contaminations. Here, the effectiveness of the prepared nanodipersions was tested against *P. expansum, A. niger* and two different strain of *R. oligosporus*. In particular, based on the viscosity values collected only nanodispersions with alginate 1% as continuous phase were tested, while the amount of essential oil varied from 0 to 2%. Fig. 4.6 reports the pictures of Petri dishes after 9 days of incubation, when the growth of fungi was visible. For the two *R. oligosporus* strains (third and fourth row of Fig. 4.6) it is possible to see how nanodispersions at 1% of EO already have inhibitory effects, while for *A. niger* and *P. expansum* it is necessary to reach at least 1.5% of essential oil to achieve an inhibitory effect. The antifungal action has to be associated with the presence of essential oil, since the system with only alginate and surfactant does not show any inhibition (B2 Fig. 4.6). Also, the positive effect of nanodispersion is pointed out by the control made by mixing the same amount of essential oil in water and poured it on the Petri dish (A Fig. 4.6). So, the same concentration of essential oil that causes an inhibition of the growth of the different fungi does not work when simply mixed in water due to the rapid volatilization of the substance.

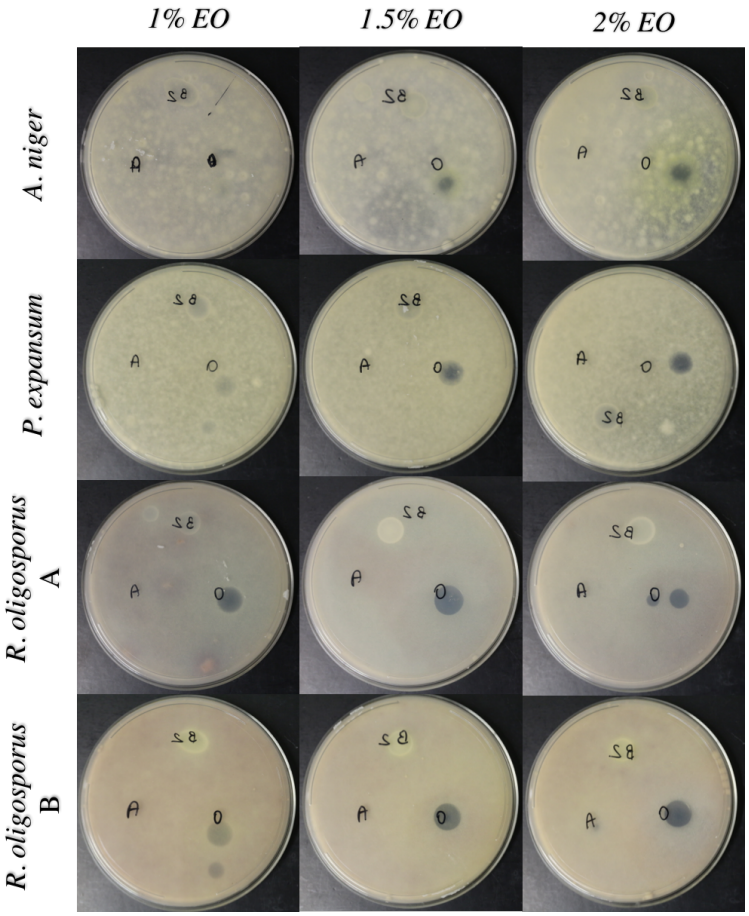

Figure 4.6: *Back of Petri dishes with the growth of A. niger, P. expansum, R.oligosporus A and B after 9 days of incubation: control (B2), nanodispersions (O), essential oil in water (A).*

4.4 Conclusions

In this study the rheological and conductometric properties of nanodispersions based on alginate and lemongrass essential oil were determined and analyzed. Different alginate and essential oil concentrations were considered. A small variation on the ionic conductivity was observed by adding oil up to the 2% to the alginate suspensions. The flow curves of all the nanodispersions were fitted to the Ostwald de-Waele equation and all the preparations shared a pseudoplastic non-Newtonian behavior that was more evident with higher alginate concentration (2%). Through the analysis of thixotropic behavior, it was found that the nanodispersions had the ability to return to their initial structure after the application of a high shear rate. Additionally, through oscillatory frequency sweep tests, the samples showed a similar fluid-like behavior for 1% and 2% alginate nanodispersions. Moreover, these systems showed antifungal effect against moulds such as *P. expansum* and *A.niger* when used at concentration higher than 1% of EO, and at this concentration already inhibits the two strains of *R. oligosporus* considered. This investigation demonstrates that nanodispersions containing essential oil can be handled like the alginate suspensions, with the added value of the benefits offered by the properties of the oil.

References

1. Pal, R. Modeling the Viscosity of Concentrated Nanoemulsions and Nanosuspensions. Fluids **2016**, 1, 11.
2. Malgorzata, J.; Elżbieta, S.; Jan, O. Rheological Properties of Nanoemulsions Stabilized by Polysorbate 80. *Chemical Engineering & Technology* **2015**, 38, 1469-1476, doi:doi:10.1002/ceat.201500069.
3. Cevoli, C.; Balestra, F.; Ragni, L.; Fabbri, A. Rheological characterisation of selected food hydrocolloids by traditional and simplified techniques. *Food hydrocolloids* **2013**, 33, 142-150.
4. Zhu, S.; Yu, X.; Xiong, S.; Liu, R.; Gu, Z.; You, J.; Yin, T.; Hu, Y. Insights into the rheological behaviors evolution of alginate dialdehyde crosslinked collagen solutions evaluated by numerical models. *Materials Science and Engineering: C* **2017**, 78, 727-737.
5. Burt, S. Essential oils: their antibacterial properties and potential applications in foods-a review. *International journal of food microbiology* **2004**, 94, 223-253.
6. Ribeiro-Santos, R.; Andrade, M.; Sanches-Silva, A. Application of encapsulated essential oils as antimicrobial agents in food packaging. *Current Opinion in Food Science* **2017**, 14, 78-84.
7. Oussalah, M.; Caillet, S.; Saucier, L.; Lacroix, M. Inhibitory effects of selected plant essential oils on the growth of four pathogenic bacteria: *E. coli* O157: H7, *Salmonella typhimurium, Staphylococcus aureus* and *Listeria monocytogenes*. *Food control* **2007**, 18, 414-420.
8. Zhang, Y.; Liu, X.; Wang, Y.; Jiang, P.; Quek, S. Antibacterial activity and mechanism of cinnamon essential oil against Escherichia coli and Staphylococcus aureus. *Food Control* **2016**, 59, 282-289.
9. Jeffries, P.; Jeger, M. The biological control of postharvest diseases of fruit. *Biocontrol news and information* **1990**, 11, 333-336.
10. Organization, W.H. Diet, nutrition, and the prevention of chronic diseases: report of a joint WHO/FAO expert consultation; World Health Organization: **2003**; Vol. 916.
11. Morales, H.; Sanchis, V.; Usall, J.; Ramos, A.J.; Marín, S. Effect of biocontrol agents Candida sake and Pantoea agglomerans on Penicillium expansum growth and patulin accumulation in apples. *International journal of food microbiology* **2008**, 122, 61-67.
12. Rosenberger, D. Control of Penicillium expansum during apple harvest and storage. In *Proceedings of Patulin technical symposium*. Feb; pp. 18-19.
13. Lopez, F.; Venditti, F.; Ambrosone, L.; Colafemmina, G.; Ceglie, A.; Palazzo, G. Gelatin microemulsion-based gels with the cationic surfactant cetyltrimethylammonium bromide: A self-diffusion and conductivity study. *Langmuir* **2004**, 20, 9449-9452, doi:10.1021/la048110x.
14. Ma, J.; Lin, Y.; Chen, X.; Zhao, B.; Zhang, J. Flow behavior, thixotropy and dynamical viscoelasticity of sodium alginate aqueous solutions. *Food Hydrocolloids* **2014**, 38, 119-128.
15. Zavaleta-Avejar, L.; Bosquez-Molina, E.; Gimeno, M.; Pérez-Orozco, J.P.; Shirai, K. Rheological and antioxidant power studies of enzymatically grafted chitosan with a hydrophobic alkyl side chain. *Food hydrocolloids* **2014**, 39, 113-119.
16. Hammer, K.A.; Carson, C.F.; Riley, T.V. Antimicrobial activity of essential oils and other plant extracts. Journal of applied microbiology 1999, 86, 985-990.
17. Ayala-Zavala, J.F.; Soto-Valdez, H.; González-León, A.; Alvarez-Parrilla, E.; Martin-Belloso, O.; González-Aguilar, G.A. Microencapsulation of cinnamon leaf (Cinnamomum zeylanicum) and garlic (Allium sativum) oils in β-cyclodextrin. Journal of Inclusion Phenomena and Macrocyclic Chemistry 2008, 60, 359-368.

5 Rheological characterization of hydrogels from alginate based nanodispersions

«The important thing is to never stop questioning»
A.Einstein

Abstract

The interest toward alginate and nanoemulsion-based hydrogels is driven by the wide potential of application. These systems have been noticed in several areas, ranging from pharmaceutical, medical, coating, and food industries. In this investigation, hydrogels prepared through *in situ* calcium ions release, starting from lemongrass essential oil nanodispersions stabilized in alginate aqueous suspensions in the presence of the nonionic surfactant Tween 80, were evaluated. The hydrogels prepared at different concentrations of oil, alginate and calcium were characterized through rheological tests. Flow curves demonstrate that the hydrogels share shear thinning behavior. Oscillatory tests showed that the strength of the hydrogel network increases with the crosslinker increase, and decreases at low polymer concentrations. The hydrogels were thixotropic materials with a slow time of structural restoration after breakage. Finally, by analyzing the creep recovery data, the hydrogel responses were all fitted to the Burger model. Overall, it was demonstrated that the presence of essential oil in the proposed hydrogels does not affect the mechanical characteristics of the materials, which are mainly influenced by the concentration of polymer and calcium as a crosslinker.

5.1 Introduction

Starting from the gelation process that occurs in presence of divalent cations, alginate forms hydrogels, semisolid fluid where a polymer forms a three-dimensional network that swells in water [1,2]. In general, the common property of gel systems is that they have a continuous structure that forms a ´permanent´ infinite network and a solvent medium that diffuses through it. These two components interact in such a way that the network prevents the liquid from flowing away and the liquid prevents the network to collapse [3]. Many research groups have found interest in the study of alginate hydrogel formation. In 1994 Draget et al. [4] studied the influence of unit sequence and the molecular weight of different alginate molecules on the properties of the relative hydrogels and they demonstrated that alginates with a high guluronic acid content provided stronger gels compared to alginates rich in mannuronate. Stokke et al. [5] prepared homogeneous Ca-alginate hydrogels through the *in situ* release of calcium ions and studied the hydrogels through X-ray scattering and rheology. With this study, it was shown that the final characteristic of the hydrogels are dependent on alginate concentration and composition (ratio M/G) as well as on calcium concentration. Liu et al. [6] studied the rheological parameters of the sol-gel transition of alginate suspensions induced by the *in situ* calcium release. Lately, increasing interest has been focused toward complex hydrogels, mainly produced by the gelation of emulsion/nanoemulsion in order to design more stable materials able to encapsulate and deliver hydrophobic compounds in a hydrophilic network; these have found application in, among others, pharmacological and food fields. In 2010 Josef et al. [7] proposed the use of composite hydrogels prepared through gelation of the continuous phase of oil-in-water microemulsions for the sustained delivery of hydrophobic drugs. The oil phase of the emulsion allowed the solubilization of hydrophobic drugs, and the crosslinked matrix made the continuous phase, containing alginate, similar to a solid phase. Ketoprofen was used as a model hydrophobic drug. Analyzing the nanostructure by small-angle X-ray scattering (SAXS), the authors demonstrate that the oil droplets exist in the hydrogel matrix, and through release studies they reveal that the rate of drug release is influenced by the network properties. A successive formulation for the delivery of ketoprofen has been proposed for its transdermal delivery [8]. Different nanoemulsion were selected and Carbomer 940 was added as gelation agent for the nanoemulsion. The systems have been characterized for their structure, viscosity, spreadability and rheological behavior, and permeation studies have demonstrated that the new formulation was more effective for the transdermal delivery of ketoprofen compared with nanoemulsion and marketed formulation. Very recently, Kaur et al. [9] proposed a hydrogel based on nanoemulsion containing Polyphenon 60 and cranberry, developed for the treatment of urinary tract infection and delivered via intravaginal route. The results of the in vitro studies suggested that the hydrogel could be effective for delivering the active drug toward the organs of the urinary tract. Moving toward food application for the delivery of therapeutical molecules through the gastrointestinal tract, Nagakawa et al. [10] proposed a typology of hydrogel containing oil for encapsulation of curcumin. The hydrogel is prepared with a ternary system made of chitosan, k-carrageenan, and carboxymethylcellulose. Freezing the blend of polymers caused the sol-gel transition with successful encapsulation of the curcumin. The release behavior of the model food ingredient is investigated in aqueous systems and the results are influenced by the freezing conditions. An alginate hydrogel was proposed by Lei et al. [11] to encapsulate nobiletin loaded in nanoemulsion droplets. Nobiletin is a flavonoid isolated from citrus peels with excellent bioactivities, such as anti-inflammatory, anti-cancer, anti-dementia. Through *in vitro* release and *in vitro* digestion studies, the authors concluded that nanoemulsion-filled hydrogels could achieve the sustained release and absorption of nobiletin and prevent its precipitation in the gastrointestinal tract. Among the lipophilic phases used to formulate nanoemulsions hydrogels, a particular interest is directed to the use of essential oils. Essential oils, besides being able

to solubilize lipophilic substances, have antimicrobial and antioxidant properties, characteristics that make them suitable ingredients to preserve cosmetic preparations [12,13]. In 2015, Chen and coworkers [14] demonstrated that the presence of essential oils in a hydrogel formulated for transdermal administration enhances the ibuprofen penetration through skin. The presence of essential oils was demonstrated to be effective against microbial proliferation in composite wound dressing films of sodium alginate containing essential oils [15]. The authors characterize different alginate/glycerol matrices enriched with different essential oils and testes them against *Escherichia coli* and *Candida albicans*. Thanks to their outstanding properties, as said previously, the use of essential oils is finding room also in the food packaging field, in particular in fresh fruit coating. In a recent application, lemongrass essential oil has been included in alginate-based edible coating formulations [16] applied on fresh-cut apples pieces through gelation, and it has been demonstrated that the presence of the lemongrass essential oil inhibits the proliferation of *E.coli*. In this scope, understanding of the rheological properties of such gelled systems containing emulsifying or stabilizing agents becomes necessary for improving the systems' characteristics. In light of the current increasing interest in composite hydrogels, here we present a study on the rheological characterization of hydrogels prepared from nanodispersions made of an essential oil stabilized in alginate aqueous suspensions by a nonionic surfactant: Tween 80. The rheological characterization of the starting nanodispersions [17] was reported in Chapter 4. Here, we consider the in situ gelation of the alginate-based nanodispersions and the difference in the mechanical response, along with the variation of oil, alginate and calcium content.

5.2 Materials and Methods

5.2.1 Materials

Tween 80, D-glucono-δ-lactone (GDL), ethylenediaminetetraacetic acid (EDTA) and $CaCl_2$ were purchased from Sigma Aldrich (St. Louis, MO, USA). Lemongrass (*Cymbopogon nardus*) essential oil (100%) was from Erbamea (Lama di San Giustino -PG - Italy) and food-grade sodium alginate was from Farmalabor (Canosa di Puglia, Italy).

5.2.2 Preparation of nanodispersions

Sodium alginate was dissolved in ultrapure water at 70 °C under gentle stirring. Nanodispersions were prepared with a final polyelectrolyte concentration of 0.5 or 1 wt% as the continuous phase, and lemongrass essential oil (EO) at different concentrations (0, 0.1 and 0.5 wt%) as the dispersed phase. All the nanodispersions were stabilized by 1 wt% Tween 80. Coarse emulsions were prepared by mixing the aqueous phase with EO and Tween 80 using a laboratory mixer, T25 digital Ultra-Turrax (IKA, Staufen, Germany), working at 24000 rpm for 4 minutes. All the emulsions were then sonicated using an Ultrasonic Homogenizer (Model 300 VT, BioLogics Inc., Manassas, VA, USA) in order to reduce the dimension of the particles.

5.2.3 Gelation of nanodispersions

Homogeneous Ca-alginate nanodispersions gels were prepared at room temperature, through the *in situ* gelation of sodium alginate induced by release of Ca^{2+} (added as $CaCl_2$) from the Ca-EDTA chelate complex. The chelating constant of Ca-EDTA is high at pH 7, where Ca^{2+} is completely complexed, and is extremely low at pH 4, where Ca^{2+} is totally released. The pH was lowered through the slow hydrolysis of GDL. The mole ratio of GDL/Ca-EDTA to adopt in order to yield pH 4 after equilibration for about 24 h after addition of GDL was calculated through

a calibration curve (Fig. 5.1). The mole ratio selected was GDL/Ca-EDTA= 1.5. Specifically, hydrogels were prepared from 5.2 g of alginate nanodispersions that were mixed with 2.3 mL of Ca-EDTA solution (pH 7) and 2.5 mL of GDL solution, in order to achieve the desired Ca^{2+} after 24 h. $CaCl_2$ concentrations were in the range of 4-10 mM. Hydrogels compositions are listed in Table 5.1 and for the sake of shortness were recalled considering the calcium levels: low ($[Ca^{2+}]$ = 6 mM), medium ($[Ca^{2+}]$ = 8 mM), high ($[Ca^{2+}]$ = 10 mM) and medium* ($[Ca^{2+}]$ = 4 mM).

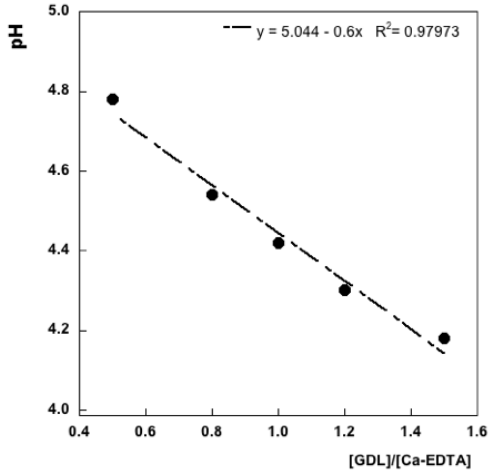

Figure 5.1: Calibration curve for the pH variation as function of GDL and Ca-EDTA complex.

Table 5.1: Hydrogels compositions. Tween 80 concentration was kept constant at 1% wt%. *These samples were considered with a medium calcium level because they have the same ratio of alginate/Ca^{2+} as samples 4, 5, 6.

Hydrogels	**Alginate wt%**	**Essential Oil wt%**	**$CaCl_2$ mM**	**Calcium Level**
1	1	0	6	
2	1	0.1	6	Low
3	1	0.5	6	
4	1	0	8	
5	1	0.1	8	Medium
6	1	0.5	8	
7	1	0	10	
8	1	0.1	10	High
9	1	0.5	10	
10	0.5	0	4	
11	0.5	0.1	4	Medium*
12	0.5	0.5	4	

5.2.4 Rheological characterization

Rheological measurements of the gelled nanodispersions were carried out through a rotational rheometer, Haake MARS III (Thermo Scientific, Karlsruhe, Germany) 10 days after their preparation. All rheology measurements were made using a 20 mm diameter cone (1° angle) and plate

geometry. The temperature was controlled at 20°C by a cooling and heating system (Phoenix II, Thermo Scientific, Karlsruhe, Germany) in combination with a Peltier heating system. The samples were carefully placed onto the surface of the lower plate, and the upper cone was lowered to 0.052 mm gap distance. Before testing, samples were left equilibrating for 5 minutes, in order to allow mechanical and temperature equilibrium. Flow curves were made in control rate mode (CR) varying the shear rate (0.005-500 s^{-1}) over 300 s at 20°C [18]. For the oscillatory tests an amplitude strain sweep was carried out at frequency of 1 Hz and deformation ranging from 0.001 to 10. The frequency sweep was made in controlled deformation (fixed from the range of linear viscoelasticity -LVE- determined through amplitude sweep measurements), and in a frequency range from 0.1 to 10 rad/s. In the oscillatory three-step thixotropy test, steps 1 was made in controlled stress oscillation at τ 0.005 Pa and frequency of 1 Hz for 1 min. Step 2 was made in CR at shear rate of 1000 s^{-1} for 30 s. Step 3 was made in controlled stress oscillation at τ 0.005 Pa and frequency of 1 Hz for 6 min. Creep recovery experiments were carried out by applying a constant stress (τ=3 Pa for samples 1-9 and τ=1 Pa for samples 10-12) for 180 s and following the deformation (loading phase). The stress was then removed and the recovery phase was registered for 360 s.

5.3 Results and Discussion

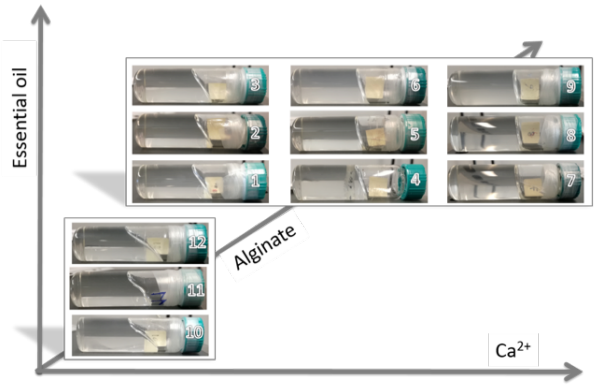

Figure 5.2: *Photographs of alginate based nanodispersion gels with increasing concentration of $CaCl_2$ (x-axes), essential oil (y-axes) and alginate (z-axes). The $CaCl_2$ concentrations ranges from 4 up to 10 mM, the essential oil concentration ranges from 0 up to 0.5 wt% and the alginate concentrations were 0.5 or 1 wt%. Tween 80 was kept constant at 1 wt%.*

As reported in Table 5.1, alginate gels based on nanodispersion were prepared by varying $CaCl_2$, essential oil and alginate concentration. The aspect of the hydrogel formed from the alginate-based nanodispersions is shown in Fig. 5.2, where the vials containing the gels (10 days after the gelification) were placed in horizontal position to display the different gel/air interface profile. At the top of Fig. 5.2 (from left to right), gels sharing the same content of alginate (1 wt%), but different Ca^{2+} concentration are displayed (samples 1-9). In particular, samples 1, 2 and 3 were gelled with 6 mM of Ca^{2+}; samples 4, 5 and 6 with Ca^{2+} 8 mM; and samples 7, 8 and 9 with Ca^{2+} 10 mM. Moreover, samples 1, 4 and 7 did not contain essential oil; samples 2, 5 and 8 contained 0.1 wt% of essential oil and samples 3, 6 and 9 had an oil content of 0.5%. At the bottom of Fig. 5.2 samples formulated with alginate 0.5 wt%, Ca^{2+} 4 mM and various oil content (0, 0.1 and 0.5 wt%) are reported (samples 10, 11 and 12 respectively). Remarkably, considering the alginate and Ca^{2+} concentration, these last samples were prepared with the

same alginate/Ca^{2+} ratio as samples 4, 5 and 6. As can be seen from Fig. 5.2, all the hydrogels had a very clear aspect, indicating that the essential oil was dispersed in nanometric domains, and according to the sample composition, the gel/air interface was mainly influenced by Ca^{2+} and alginate concentrations. Indeed, high and medium calcium content with higher alginate percentage gave flat stiff interfaces, while decreasing both the ingredients resulted in hydrogels with less stiff interfaces. Steady-state flow curves of the alginate-based hydrogels demonstrate that all the hydrogels showed shear rate ($\dot{\gamma}$) dependence and shear thinning behavior. From the apparent viscosity curves reported in Fig. 5.3, a Newtonian region corresponding to the steady plateau at low values of $\dot{\gamma}$ is found for some hydrogels. Specifically, hydrogels prepared without

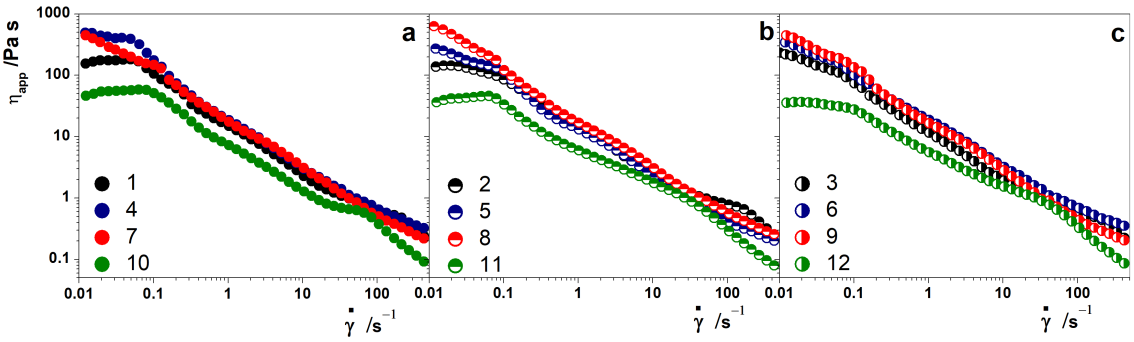

Figure 5.3: *Shear rate dependence of the hydrogels' shear viscosity. Black symbols indicate samples with 1 wt% of alginate and Ca^{2+} 6 mM, blue symbols indicate samples with 1 wt% of alginate and Ca^{2+} 8 mM, red symbols are for samples with 1 wt% of alginate and Ca^{2+} 10mM and green symbols represent samples with 0.5 wt% of alginate and Ca^{2+} 4 mM. (**a**) hydrogels without essential oil; (**b**) hydrogels with 0.1% essential oil; (**c**) hydrogels with 0.5% essential oil.*

oil (Fig. 5.3a) and with low and medium calcium content presented the Newtonian plateau, together with samples prepared with less alginate (0.5 wt%) reported, with green symbols, in Fig. 5.3b, c. A high Ca^{2+} concentration induced a stronger gelation, which was reflected in the increasing viscosity as the shear rate approached zero, indicating that the fluid does not flow at rest (samples 7, 8 and 9 in Figure 5.3 a-c, respectively). Moreover, the presence of essential oil in hydrogels prepared with low and medium Ca^{2+} concentrations seems to have an effect in the region of low shear rate that causes the loss of the Newtonian plateau [9]. The presence or absence of the Newtonian plateau appears, in some way, to be correlated with the shape of the gel/air interface, i.e. the more the interface is flat the less the plateau is present. The results of the dynamic oscillation tests gave important information concerning the effect of Ca^{2+} and polymer concentration on the samples' structure. Strain sweeps confirmed the gel-like behavior, since for all the samples the elastic modulus G' was higher than the viscous modulus G" (data not shown). The linear viscoelastic (LVE) region for each hydrogel can be identified, in Fig. 5.4, in the region where G' results are independent of the applied deformation. Considering the hydrogels prepared at 1 wt% alginate, their mechanical strength was evaluated by comparing the values of G' in the LVE region [19], and the results were mainly influenced by the amount of Ca^{2+} used as cross-linker. Hydrogels with low levels of Ca^{2+} had G' values of about 20 Pa, the presence of medium levels of Ca^{2+} increased the value of the elastic modulus around 50 Pa, and high levels of Ca^{2+} provided a further stronger gel, with a G' value around 100 Pa. In all these samples, the strength measured was strongly dependent on the continuous phase, since no difference was evidenced by the presence of the oil-dispersed phase. Very close G' values were also recorded for hydrogels prepared with 0.5% alginate. Although the green symbols seem more differentiated in Fig. 5.4 due to the logarithmic representation, the G' values ranged between 2 and 5 Pa, resulting in those with the weaker structures among the

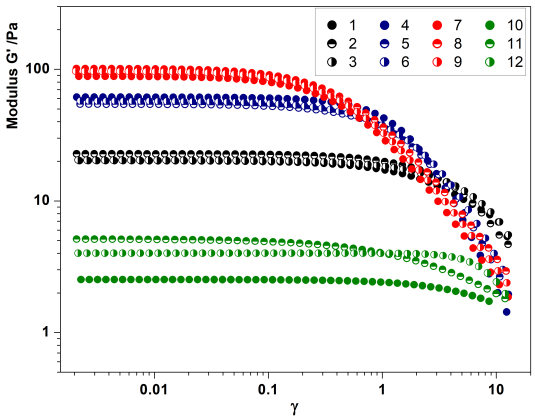

Figure 5.4: *Amplitude strain sweep for hydrogels produced with low Ca^{2+} content (black symbols), medium Ca^{2+} content (blue symbols), high Ca^{2+} content (red symbols) and low alginate and medium* Ca^{2+} content (green symbols). For the detailed sample composition see Table 5.1.*

produced hydrogels. Frequency sweep tests, performed within the linear viscoelastic region of each hydrogel, enabled the determination of the material frequency dependence, in the range of angular frequency between 0.1 to and 10 rad/sec.
The outcomes of the test are reported in Fig. 5.5 a-d. The high frequency region corresponds

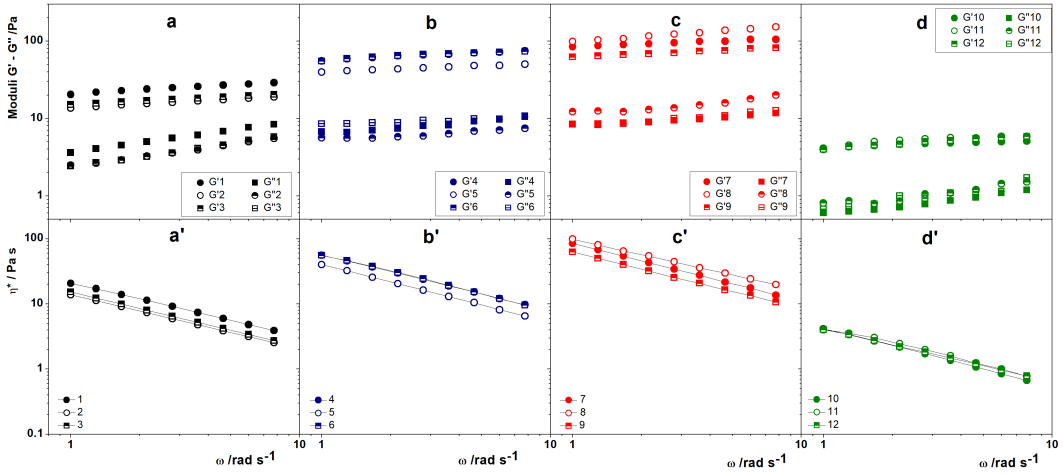

Figure 5.5: *Frequency sweep and complex viscosity (indicated in figure by the letters a-d and a'-d', respectively) for hydrogels produced with (**a-a'**) low Ca^{2+} content (black symbols), (**b-b'**) medium Ca^{2+} content (blue symbols), (**c-c'**) high Ca^{2+} content (red symbols) and (**d-d'**) low alginate and medium* Ca^{2+} *content (green symbols). For the detailed sample compositions, see Table 5.1.*

to short-time behavior (simulated by rapid motion); on the other side, the low frequency zone mimic the long-term behavior. As can be observed from the figures, all the hydrogels exhibited a storage modulus (G') that was always higher than the loss modulus (G"), denoting that the elastic character is always dominant when a load is applied. A very low dependence from the elastic modulus on frequency was found for all the hydrogels, while the G" modulus showed a certain dependence in hydrogels having low Ca^{2+} content (Fig. 5.5a) and low alginate content (Fig. 5.5d). This aspect indicates that for these samples with short-term behavior, the viscous response begins to influence the response of the material. In addition, the distance between the

moduli did not seem to be influenced by the presence of the oil, representing that the existence of oil dispersed phase does not influence the structure of the hydrogels strongly. Remarkably, the complex viscosity value η^*, reported in Fig. 5.5 a'-d' decreased with the increase of the angular frequency, confirming that all the hydrogels were pseudoplastic fluids with shear thinning behavior. In order to understand how the hydrogels' structure responded to high speed shearing, the thixotropic behavior was studied. The study of thixotropy is characterized by a decrease in the values of rheological parameters, such as storage modulus G', as consequence of a mechanical load, and the recovery of the initial state upon reduction of the load [20]. The test is made of a first step, where the sample is under very low shear conditions (rest condition), a second phase where the structure is broken under a high shear rate and a third phase where the condition of the first phase are applied for a longer time. In the last phase, the structure recovery is observed. The results of the thixotropic tests are illustrated in Fig. 5.6, where the elastic modulus is reported before and after the application of the high shear rate, which caused a dramatic viscosity decrease. As shown, the viscosity values correspond to the symbols collected after the first minute of the experiment. The obtained results indicated that the structure

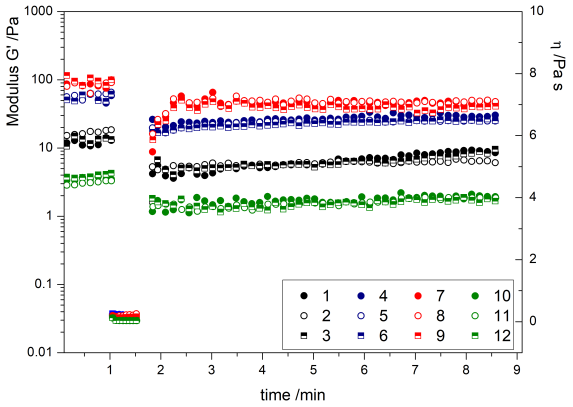

Figure 5.6: *Three-steps thixotropy test of hydrogels produced with low Ca^{2+} content (black symbols), medium Ca^{2+} content (blue symbols), high Ca^{2+} content (red symbols) and low alginate and medium* Ca^{2+} content (green symbols). For the detailed sample compositions, see Table 5.1.*

of all the hydrogels was broken by the high shear rate application, and no full recovery was observed, indicating that the changes induced by the higher shear step could be permanent. The viscoelastic properties of the alginate-based hydrogel were further investigated through creep-recovery experiments. Fig. 5.7 illustrates the creep-recovery curves expressed as compliance variation as a function of time, $J(t)$. The compliance parameter is given by the ratio of the deformation γ to the applied stress τ

$$J = \frac{\gamma}{\tau} \tag{5.1}$$

where the reciprocal of J is G, which is considered as the rigidity of the material. As a consequence, if a material has a high compliance it has a low rigidity and *vice versa*, has high rigidity when exhibiting low compliance. From Fig. 5.7, it is evident that the hydrogels with 0.5 wt% of alginate (Fig. 5.7d) are the less rigid, and moreover that the presence of the oil dispersed phase decreased the compliance by increasing the rigidity. In all the other hydrogels, a higher rigidity is observed according to the increase of Ca^{2+} concentration (Fig. 5.7a-c). The presented data emphasizes that the contribution of the oil phase had a small effect on the rigidity of hydrogels with low and medium Ca^{2+} concentrations, and was negligible in presence of high Ca^{2+} content. In order to analyze quantitatively the materials during the loading step (creep phase), according to the shape of the creep curves the data were fitted to the Burger model (four-

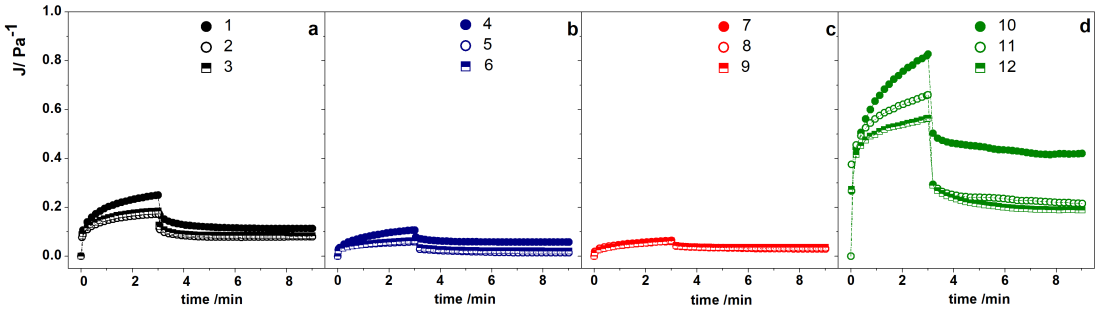

Figure 5.7: *Creep-recovery experiments on hydrogels produced with (**a**) low Ca^{2+} content (black symbols), (**b**) medium Ca^{2+} content (blue symbols), (**c**) high Ca^{2+} content (red symbols) and (**d**) low alginate and medium* Ca^{2+} content (green symbols). For detailed sample compositions, see Table 1.*

parameters Voigt model) [21,22]. The model is made of three elements in series as represented in Fig. 5.8: a spring (elastic element) with shear modulus G_1; a Kelvin-Voigt element (viscoelastic element), made by a spring and a dashpot in parallel, having shear modulus G_2 and viscosity η_2, respectively; and a dashpot (viscous element) with viscosity η_3.

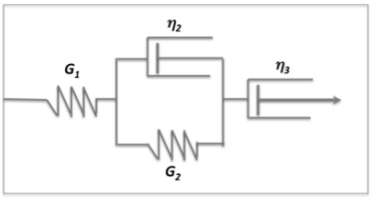

Figure 5.8: *Schematic representation of the Burger model.*

The Burger model expresses the creep compliance J(t) with the following equation:

$$J(t) = \frac{1}{G_1} + \frac{1}{G_1}(1 - exp(-\frac{t}{\lambda_2})) + \frac{t}{\eta_3} \tag{5.2}$$

where G_1 is $1/J_1$, which in the creep curve is the time-independent elastic jump, λ_2 is the retardation time of the viscoelastic element and η_3 is the viscosity of the viscous element. In other words, the compliance, $J(t)$, in the Burger equation is the sum of an instantaneous elastic response, a viscoelastic (delayed elastic) component and the unrecovered viscous flow. The elastic response of the viscoelastic element is given by the G_2 parameter from Eq. 5.2 and the viscosity (η_2) is calculated by the retardation time that is given by the ratio of the viscosity to the elastic storage modulus of the second element, $\lambda_2 = \eta_2/G_2$. The parameters obtained by fitting the creep curves to Eq. 5.2 are listed in Table 5.2.

The elastic component G_1 of the hydrogels from the fittings had a lower value with low alginate concentration and the G_1 values increased in hydrogels with 1 wt% alginate together with the Ca^{2+} content, albeit the values were quite similar for medium and high Ca^{2+} concentrations. The elastic response of the viscoelastic component G_2 follows the same trend as G_1, and a similar trend was also registered for η_2 and for the viscosity of the third element η_3. The data extrapolated, overall, indicate that the presence of the oil in the composition of the hydrogels at a mechanical level did not cause substantial changes, but the differences observed were principally due to the different calcium levels. In the last column of Table 5.2, the values of percentage compliance recovery are reported, and were calculated as the ratio between the compliance in the plateau region of the recovery phase and the maximum compliance value at the end of the creep

Table 5.2: Best-fitting parameters calculated for the creep curves and obtained for each hydrogel, according to Eq. (5.2). The last column reports the percentage recovery of deformation recovery.

Sample	G_1 (Pa)	G_2 (Pa)	η_2 (Pa s)	λ_2 (s)	η_3 (Pa s)	R^2	J_R (%)
1	25.62 ± 3.13	7.64 ± 0.28	83.49 ± 7.39	10.92 ± 0.88	2050 ± 91	0.98	45.2
2	52.62 ± 11.29	9.77 ± 0.39	57.25 ± 5.39	5.86 ± 0.50	2889 ± 130	0.98	45.7
3	42.67 ± 8.36	9.55 ± 0.43	57.30 ± 6.02	6.00 ± 0.57	2535 ± 121	0.98	44.9
4	97.93 ± 15.70	22.29 ± 0.87	207.30 ± 19.58	9.30 ± 0.80	2861 ± 96	0.99	54.3
5	132.52 ± 18.33	35.36 ± 1.31	99.36 ± 10.23	2.08 ± 0.20	5013 ± 150	0.98	24.7
6	110.39± 13.91	38.13 ± 1.65	194.46 ± 18.07	5.10 ± 0.41	5205 ± 109	0.98	31.5
7	105.03 ± 5.89	40.29 ± 0.93	576.77 ± 32.88	14.39 ± 0.75	6032 ± 154	0.99	49.3
8	142.84 ± 17.49	36.53 ± 1.14	578.27 ± 27.01	15.83 ± 0.55	4911 ± 100	0.99	48.3
9	107.56 ± 6.46	45.02 ± 1.23	612.27 ± 41.35	13.60 ± 0.84	5151 ± 130	0.98	58.3
10	5.41 ± 0.32	2.73 ± 0.08	35.92 ± 2.74	13.02 ± 0.81	614 ± 19	0.98	48.2
11	9.54 ± 1.21	3.00 ± 0.12	32.70 ± 1.35	10.90 ± 0.11	477 ± 16	0.98	32.6
12	4.48 ± 0.16	4.08 ± 0.13	34.90 ± 2.21	8.56 ± 0.47	1012 ± 66	0.98	33.5

phase. As expected part of the deformation generated by the loading phase was not recovered because of the viscoelastic character of the hydrogels.

5.4 Conclusions

In this study the rheological properties of hydrogel-based nanodispersions made of alginate and lemongrass essential oil were analyzed. Different alginate, essential oil and calcium concentrations were considered. The flow curves of the hydrogels revealed a shear thinning behavior with the presence of a Newtonian plateau at low shear rates in hydrogel formed at low and medium calcium concentrations in absence of oil, and which persisted in the presence of an oil phase only at low alginate concentrations. Strain sweep tests allowed determining the LVE region of the hydrogels and the evaluation of the gel strength. Frequency sweep tests confirmed that the characteristics of the hydrogels were mainly influenced by the alginate and calcium concentration. The thixotropic tests revealed that after the breakage of the hydrogel structure, the complete structure restoration is a slow process; finally, through the creep recovery experiments, the hydrogels were found to be fit with the Burger model. Among the hydrogel systems studied, the only one that appeared in some way to be influenced by the presence of oil was the one with low alginate concentration, which in creep-recovery experiments deformed differently with the oil concentration increase. In order to give more details on the structural differences, other studies should be carried out.

References

1. Ghica, M.V.; Hîrjău, M.; Lupuleasa, D.; Dinu-P rvu, C.-E. Flow and thixotropic parameters for rheological characterization of hydrogels. *Molecules* **2016**, 21, 786.

2. Ahmed, E.M. Hydrogel: Preparation, characterization, and applications: A review. *Journal of Advanced Research* **2015**, 6, 105-121, doi:https://doi.org/10.1016/j.jare.2013.07.006.

3. Tanaka, T. Gels. *Scientific American* **1981**, 244, 124-S-117.

4. Draget, K.I.; Skjåk Bræk, G.; Smidsrød, O. Alginic acid gels: the effect of alginate chemical compo-

sition and molecular weight. *Carbohydrate Polymers* **1994**, 25, 31-38, doi:https://doi.org/10.1016/0144-8617(94)90159-7.
5. Stokke, B.T.; Draget, K.I.; Smidsrød, O.; Yuguchi, Y.; Urakawa, H.; Kajiwara, K. Small-Angle X-ray Scattering and Rheological Characterization of Alginate Gels. 1. Ca-Alginate Gels. *Macromolecules* **2000**, 33, 1853-1863, doi:10.1021/ma991559q.
6. Liu, X.; Qian, L.; Shu, T.; Tong, Z. Rheology characterization of sol-gel transition in aqueous alginate solutions induced by calcium cations through in situ release. *Polymer* **2003**, 44, 407-412, doi:https://doi.org/10.1016/ S0032-3861(02)00771-1.
7. Josef, E.; Zilberman, M.; Bianco-Peled, H. Composite alginate hydrogels: an innovative approach for the controlled release of hydrophobic drugs. *Acta Biomaterialia* **2010**, 6, 4642-4649.
8. Arora, R.; Aggarwal, G.; Harikumar, S.L.; Kaur, K. Nanoemulsion based hydrogel for enhanced transdermal delivery of ketoprofen. *Advances in Pharmaceutics* **2014**, 2014.
9. Kaur, A.; Gupta, S.; Tyagi, A.; Sharma, R.K.; Ali, J.; Gabrani, R.; Dang, S. Development of Nanoemulsion Based Gel Loaded with Phytoconstituents for the Treatment of Urinary Tract Infection and in Vivo Biodistribution Studies. *Advanced pharmaceutical bulletin* **2017**, 7, 611.
10. Nakagawa, K.; Sowasod, N.; Tanthapanichakoon, W.; Charinpanitkul, T. Hydrogel based oil encapsulation for controlled release of curcumin by using a ternary system of chitosan, kappa-carrageenan, and carboxymethylcellulose sodium salt. *LWT-Food Science and Technology* **2013**, 54, 600-605.
11. Lei, L.; Zhang, Y.; He, L.; Wu, S.; Li, B.; Li, Y. Fabrication of nanoemulsion-filled alginate hydrogel to control the digestion behavior of hydrophobic nobiletin. *LWT-Food Science and Technology* **2017**, 82, 260-267.
12. Halla, N.; Fernandes, I.P.; Heleno, S.A.; Costa, P.; Boucherit-Otmani, Z.; Boucherit, K.; Rodrigues, A.E.; Ferreira, I.C.; Barreiro, M.F. Cosmetics preservation: a review on present strategies. *Molecules* **2018**, 23, 1571.
13. Maccioni, A.; Anchisi, C.; Sanna, A.; Sardu, C.; Dessi, S. Preservative systems containing essential oils in cosmetic products. *International journal of cosmetic science* **2002**, 24, 53-59.
14. Chen, J.; Jiang, Q.-D.; Wu, Y.-M.; Liu, P.; Yao, J.-H.; Lu, Q.; Zhang, H.; Duan, J.-A. Potential of essential oils as penetration enhancers for transdermal administration of ibuprofen to treat dysmenorrhoea. *Molecules* **2015**, 20, 18219-18236.
15. Liakos, I.; Rizzello, L.; Scurr, D.J.; Pompa, P.P.; Bayer, I.S.; Athanassiou, A. All-natural composite wound dressing films of essential oils encapsulated in sodium alginate with antimicrobial properties. *International journal of pharmaceutics* **2014**, 463, 137-145.
16. Salvia-Trujillo, L.; Rojas-Graü, M.A.; Soliva-Fortuny, R.; Martín-Belloso, O. Use of antimicrobial nanoemulsions as edible coatings: Impact on safety and quality attributes of fresh-cut Fuji apples. *Postharvest Biology and Technology* **2015**, 105, 8-16.
17. Cofelice, M.; Lopez, F.; Cuomo, F. Rheological Properties of Alginate-Essential Oil Nanodispersions.*Colloids and Interfaces* **2018**, 2, 48.
18. Sovrani, V.; de Jesus, L.I.; Simas-Tosin, F.F.; Smiderle, F.R.; Iacomini, M. Structural characterization and rheological properties of a gel-like β-d-glucan from Pholiota nameko. *Carbohydrate Polymers* **2017**, 169, 1-8, doi:https://doi.org/10.1016/j.carbpol.2017.03.093.
19. Patel, A.R.; Dumlu, P.; Vermeir, L.; Lewille, B.; Lesaffer, A.; Dewettinck, K. Rheological characterization of gel-in-oil-in-gel type structured emulsions. *Food Hydrocolloids* **2015**, 46, 84-92, doi:https://doi.org/10.1016 /j.food hyd.2014.12.029.
20. Mezger, T.G. *The rheology handbook: for users of rotational and oscillatory rheometers*; Vincentz Network GmbH & Co KG: **2006**.
21. Abdurrahmanoglu, S.; Okay, O. Rheological behavior of polymer-clay nanocomposite hydrogels: Effect of nanoscale interactions. *Journal of applied polymer science* **2010**, 116, 2328-2335.
22. Suriano, R.; Griffini, G.; Chiari, M.; Levi, M.; Turri, S. Rheological and mechanical behavior of polyacrylamide hydrogels chemically crosslinked with allyl agarose for two-dimensional gel electrophoresis. *Journal of the mechanical behavior of biomedical materials* **2014**, 30, 339-346.

6 Alginate films encapsulating lemongrass essential oil as affected by spray calcium application

«Nothing in life is to be feared, it is only to be understood»
M. Curie

Abstract

The necessity of producing innovative packaging systems has directed the attention of food industries towards the use of biodegradable polymers for developing new films able to protect foods and to extend their shelf-life, with lower environmental impact. In particular, edible films combining hydrophilic and hydrophobic ingredients could retard moisture loss, gas migration and ensure food integrity, reducing the necessity of using synthetic plastics. Alginate-based films obtained from emulsions of lemongrass essential oil (at 0.1% and 0.5%) in aqueous alginate solutions (1%), with Tween 80 as surfactant (0.3%), were obtained by casting and characterized as to microstructure and thermal behavior, as well as tensile, barrier and optical properties. Films were also crosslinked through spraying calcium chloride onto the film surface and the influence of oil emulsification and the crosslinking effect on the final film properties were evaluated. The film microstructure, analyzed through Field Emission Scanning Electron Microscopy (FESEM) revealed discontinuities in films containing essential oil associated with droplet flocculation and coalescence during drying, while calcium diffusion into the matrix was enhanced. The presence of essential oil reduced the film stiffness whereas calcium addition lowered the film's water solubility, increasing tensile strength and reducing the extensibility coherent with its crosslinking effect.

6.1 Introduction

Edible films and coatings are two forms of packaging assembled following different routes. The former are pre-formed wrapping layers that can be used to pack food products separately and the latter are thin layers tightly adhering to the food surface and generally formed on it [1]. Edible films, as well as the traditional films, have specific functions, such as retarding moisture loss and gas migration, ensuring food integrity or retaining flavor. Alginate, as other hydrocolloids, is a good candidate to participate to the composition of the edible films as the hydrophilic component responsible for the mechanical aspects. Essential oils (EO), on the other hand, can enrich the film composition with a hydrophobic contribution bringing also antioxidant and antimicrobial properties, that could replace chemical preservatives in foods [2]. Of the EOs, lemongrass essential oil (LEO) exhibited antimicrobial activity against *E. coli* and *S. aureus*, when encapsulated in nanocapsules of polylactic acid, and also against *Botritis cynerea* [3,4]. When incorporated in edible coating, LEO prolonged the shelf life of different fresh-cut fruits, such as pineapples and apples [5,6]. The aim of this study was to analyze the physicochemical behavior of alginate films formed from emulsions of LEO in alginate solutions, stabilized by nonionic surfactant Tween 80. The films were subjected, or not, to a crosslinking with calcium chloride applied through spray, in order to simulate an in-line process when the film-forming solutions are used as food coatings and calcium can be subsequently applied by spraying on the coated surface. In particular, four film-forming formulations have been used to evaluate how film properties are influenced by the presence of surfactant and LEO (at low and high concentrations) and the effect of the cross-linking agent in each case.

6.2 Materials and Methods

6.2.1 Materials

Food-grade sodium alginate was obtained from Farmalabor (Canosa di Puglia, Italy), Tween 80 (Polyoxyethylene (20) sorbitan monooleate), non-ionic surface active agent (T), and Lemongrass Essential Oil (LEO) were purchased from Sigma-Aldrich (Madrid, Spain). Calcium chloride, $Mg(NO_3)_2$ and P_2O_5 were supplied by Panreac Química, S.A. (Castellar del Vallés, Barcelona, Spain). For all the preparations ultra-pure water was used.

6.2.2 Emulsion preparation and characterization

Primary emulsions were obtained, according to previous studies [7,8], by mixing LEO (0.5-2.5% w/w) as lipidic phase and Tween 80 (1.5% w/w) as surface active agent in an aqueous suspension of sodium alginate (1% w/w) with a laboratory T25 digital Ultra-Turrax rotor-stator homogenizer (S25-N25 - IKA, Staufen, Germany) at 20000 rpm for 4 min. The obtained dispersions were then subjected to ultrasonic treatment (Vibra Cell, Sonics & Materials, Inc. USA) for 20 min at 40% amplitude with pulses of 1 s. A suspension containing only Tween 80 (1.5% w/w) and alginate (1% w/w) was prepared in order to evaluate the influence of the surfactant on the studied properties. Emulsions were characterized as to the particle size of the dispersed phase, the polydispersity index (PDI) and ζ-potential through a Zetasizer Nano instrument (Malvern Instruments Ltd., Worcestershire, UK) using a HeNe laser at 633 nm and a detector with scattering angle at 173°. Samples were first diluted with ultra-pure water to prevent multiple scattering effects. Particle size was determined at 25 °C after 120 s of equilibration time. The ζ-potential of samples was measured using a specific cuvette (DTS1070) and the Smoluchowski model was selected to analyze the recorded data.

6.2.3 Film preparation

Solutions of sodium alginate were obtained by dissolving the polymer (1% w/w) in hot water at 70 °C under continuous stirring. Film-forming dispersions (FFDs) with LEO were also prepared by mixing the primary emulsions or the surfactant dispersion into the alginate solution to obtain a final concentration of LEO of 0%, 0.1% (low content) and 0.5% (high content) w/w. In order to form polymer films, a known amount of each formulation was spread onto Teflon disks (diameter 15 cm) to have 1 g of polymer per plate. Films were left to dry at room temperature at a relative humidity (RH) of 45-50%. Prior to testing, films were equilibrated at 25 °C in desiccators containing a saturated solution of $Mg(NO_3)_2$ (53% RH). Film crosslinking was carried out by spraying the film surface with a solution of $CaCl_2$ 0.1 M. The solution was applied through an airbrush (model E4182, Elite pro) equipped with a 0.8 mm nozzle, onto the surface of the film for 1 minute considering a flow of about 6 mL/min. The plate was rotated 90° during the application of the calcium chloride solution to cover the film surface uniformly as shown in Fig. 6.1. The application of calcium was carried out when the FFDs were partially dried

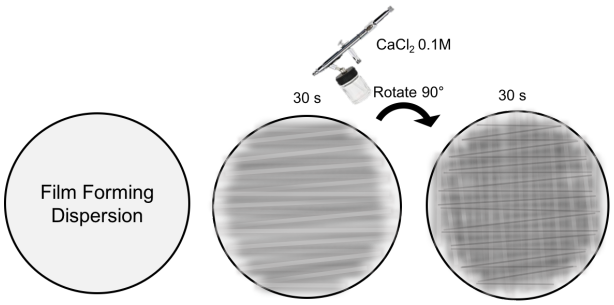

Figure 6.1: *Representation of the application of calcium chloride solution on films through spaying.*

(about 60% weight loss). Once sprayed, the films were left to complete the drying process in the same conditions as mentioned above, then peeled and equilibrated. All the sample codes and compositions are given in Table 6.1.

Table 6.1: Sample codes, composition and nominal mass fraction (X) of different components in the dried films.

Sample	Composition	X_A	X_T	$X_{\mathbf{CaCl_2}}$	X_{LEO}
A	Alginate	1.00			
A-Ca	Alginate + $CaCl_2$	0.92		0.081	
A-T	Alginate - Tween 80	0.77	0.23		
A-T-Ca	Alginate-Tween 80 + $CaCl_2$	0.72	0.23	0.063	
A-T-LEO L	Alginate - Tween 80 - LEO Low	0.71	0.21		0.072
A-T-LEO L-Ca	Alginate - Tween 80 - LEO Low + $CaCl_2$	0.67	0.20	0.059	0.067
A-T-LEO H	Alginate - Tween 80 - LEO High	0.55	0.17		0.279
A-T-LEO H-Ca	Alginate - Tween 80 - LEO High + $CaCl_2$	0.53	0.16	0.046	0.266

X_A fractional mass of alginate, X_{T80} fractional mass of Tween 80, X_{CaCl_2} fractional mass of calcium chloride incorporated by spraying, X_{LEO} fractional mass of Lemongrass Essential Oil.

6.2.4 Film characterization

Film microstructure

For the microstructural analysis, samples were conditioned in desiccators containing P_2O_5 in order to eliminate the water content. Then the films without calcium were immersed in liquid nitrogen to obtain cryofractured cross-sections [9] while the film treated with calcium were partially fractured with a scalpel to avoid the separation of the different lamina. After that, the samples were mounted on copper stubs and covered with platinum. Images were obtained by Field Emission Scanning Electron Microscopy (FESEM) (ZEISS®, model ULTRA 55, Germany), using an accelerating voltage of 1.5 and 2 kV.

Film thickness

The film thickness was measured using a digital electronic micrometer (Palmer, COMECTA, Barcelona, Spain) to the nearest 0.001 mm. Six measurements were taken on each tensile testing sample along the length of the strip, as well as six measurements for water vapor permeability samples. Means were used for the tensile strength (TS) and water vapor permeability (WVP) calculations, respectively.

Mechanical properties

A universal test Machine (TA.XT plus model, Stable Micro Systems, Haslemere, England) was used to determine the tensile properties of films using the ASTM standard method D882 [10]. Film samples (2.5 cm wide and 10 cm long), conditioned at 25 °C and 53% RH, were mounted in the film extension grips with an initial separation set at 50 mm and stretched at 0.83 mm $s^{-}1$ until breaking. At least six replicates were obtained for each sample. The force-distance data obtained were transformed into true stress-Hencky strain curves, from which elastic modulus (EM), tensile strength (TS) and percentage of elongation at break (%E) were obtained. In particular, TS and %E were calculated using the following Eqs.:

$$TS = \frac{F_{max}}{A} \tag{6.1}$$

where F_{max} is the maximum load (N) needed to break the sample and A is the initial cross-sectional area (m^2) of the sample.

$$\%E = (\frac{L}{L_0}) \cdot 100 \tag{6.2}$$

where L_0 is the original length of the film and L is the stretched length when the film breaks.

Water Vapor Permeability

The water vapor permeability (WVP) of the films was determined following a modification of the ASTM E96-95 gravimetric method [11] at 25 °C and a RH gradient of 53-100%. Payne permeability cups (3.5 cm diameter, Elcometer SPRL, Hermelle/s Argenteau, Belgium) were filled with 5 mL of distilled water (100% RH). Three circular samples of each formulation were prepared and secured to the cups with the side in contact with the Teflon plate during drying exposed to the 100% RH, attempting to simulate an application of the film on a wet surface (fresh cut fruit, vegetables). Cups were then placed in pre-equilibrated cabinets containing saturated solutions of $Mg(NO_3)_2$ to generate a RH of 53%. Each cabinet was equipped with a fan placed on the top of the cup to reduce the resistance to water vapor transport. Cups were weighed periodically at intervals of 1.5 h for 24 h after the steady state had been reached.

Eq.6.3, reporting the water vapor transmission rate (WVTR), was used to calculate the vapor pressure on the film's inner surface (p_2) according to McHugh et al. [12].

$$WVTR = \frac{P \cdot D \cdot ln[\frac{(p-p_2)}{(p-p_1)}]}{R \cdot T \cdot \Delta z} \tag{6.3}$$

where P, total pressure (atm); D, diffusivity of water through air at 25 °C (m^2s^{-1}); R, gas law constant ($82.057x10^{-3}m^3atmkmol^{-1}K^{-1}$); T, absolute temperature (K); Δz, mean stagnant air gap height (m), considering the initial and final z values; p_1, water vapor pressure on the solution's surface (atm). Finally, the WVP of films was obtained using Eq. 6.4, where p_3 is the pressure on the film's outer surface in the cabinet.

$$WVP = \frac{WVTR}{(p_2 - p_3)} \cdot thickness \tag{6.4}$$

Moisture Content and Solubility

The moisture content of the film samples was determined by means of the gravimetric method. Three samples per formulation were considered. The water was removed using a two-step method: desiccation at 60 °C for 24 h in a vacuum oven (Vacioterm-T, JP Selecta S.A., Barcelona, Spain) and storage in desiccators with P_2O_5 until constant weight was reached. The results were expressed as g of water per 100 g of dry film. Then the film solubility in water was determined. A known mass of dried films (m_0) was immersed in 15 mL of distilled water (m_w) and left for 24 h at 25 °C. Solutions were filtered and an aliquot of the filtrate was left to dry in an oven at 60 °C for 24h, then weighed to determine the mass ratio of soluble solids per g of water of the filtrate (m_{ss}). The solubility was calculated as the g of the soluble solid per g of the water of the filtrate (Eq.6.5).

$$\%S = \frac{m_{ss} \cdot m_w}{m_0} \cdot 100 \tag{6.5}$$

Thermal Analysis

To characterize the thermal stability of the films, a thermo-gravimetric analyzer (TGA/SDTA 851e, Mettler Toledo, Schwarzenbach, Switzerland) equipped with an ultra-micro-weighing scale ($\pm$ 0.1 μg) was used. The analysis was performed from 25 to 600 °C at a heating rate of 10°C/min under a nitrogen flow (10 mL/min). Approximately 3 mg of sample, previously conditioned in P_2O_5, were used in each test. Derivative thermo-gravimetric analysis (DTGA) curves were analyzed and the onset temperature (T_{onset}) and maximum degradation rate temperature were registered (T_{max}).

Optical properties

The optical properties of film specimens were determined using a spectrophotometer CM-5 (Minolta CO, Tokyo, Japan). The measurements were taken in triplicate and the opacity was determined by applying the Kubelka-Munk theory for multiple scattering [13]. The reflection spectra of samples were obtained from 400 to 700 nm on both black (R_0) and white (R) backgrounds as well as the spectra of the white background used (R_g). From these spectra, the R_∞ (the reflectance of an infinitely thick film) and T_i (internal transmittance, a transparency indicator) were calculated with the following Eqs:

$$R_\infty = a - b \tag{6.6}$$

$$a = \frac{1}{2}(R + \frac{R_0 - R + R_g}{R_0 R_g}) \tag{6.7}$$

$$b = \sqrt{a^2 - 1} \tag{6.8}$$

$$T_i = \sqrt{(a - R_0)^2 - b^2} \tag{6.9}$$

The CIE L* a* b* color coordinates were obtained from R_∞ spectra using illuminant D65 and observer 10° as reference. Chroma (C^*_{ab}) and hue (h^*_{ab}) were also determined, as well as the whiteness index (WI) and total color differences (ΔE), using Eqs 6.10-6.13:

$$C^*_{ab} = \sqrt{a^{*2} + b^{*2})} \tag{6.10}$$

$$h^*_{ab} = \arctan(\frac{b^*}{a^*}) \tag{6.11}$$

$$WI = 100 - \sqrt{(100 - L^*)^2 + (a^*)^2 + (b^*)^2} \tag{6.12}$$

$$\Delta E = \sqrt{(L^*_0 - L^*_s)^2 + (a^*_0 - a^*_s)^2 + (b^*_0 - b^*_s)^2} \tag{6.13}$$

where L^*_0, a^*_0 and b^*_0 are the values of alginate films, while L^*_s, a^*_s and b^*_s are the measured values of the other samples.

6.2.5 Statistical Analysis

An analysis of variance (ANOVA) of the obtained data was performed using Statgraphics Centurion XVI software (Manugistics Corp., Rockville, Md.). Fisher's least significant difference (LSD) procedure was used at the 95% confidence level.

6.3 Results and Discussion

6.3.1 Alginate emulsions

Alginate primary emulsions were obtained using a solution of sodium alginate as the continuous phase and two different concentrations of EO, while the amount of surfactant was fixed in order to obtain different ratios between Tween 80 and LEO and to study whether the properties of films were affected by the different size of the dispersed phase in the starting emulsions. The size distributions of the emulsions with high (2.5% w/w) and low (0.5% w/w) oil content are compared with a suspension made of alginate and Tween 80 in Fig. 6.2. As can be noted by the size distributions, formulations without LEO were characterized by a small peak around 12 nm, indicating the presence of surfactant micelles as expected, since the concentration of Tween 80 was higher than its critical micelle concentration [14], while the peak centered at 1µm was probably due to the presence of alginate aggregates (the same peak was observed for alginate suspensions-data not reported). Formulations obtained with the lower concentration of LEO were characterized by the same peak as in the absence of LEO, at 12 nm, indicating that the amount of surfactant used was enough to cover all the oil surface and to stabilize the emulsion. The (weight) ratio of surfactant to oil (SOR) is, in general, a key parameter for the production of emulsion of different sizes [15]. Specifically, the higher the SOR value, the smaller the size of the dispersed phase, and *vice versa*, the lower the SOR value, the greater the diameter of the dispersed phase. In this study, the emulsion with the lowest amount of LEO has a SOR of 3 and, accordingly, smaller oil droplets were observed compared to emulsions with a high oil content (2.5% LEO) and a lower SOR value, where the z-average was 158 nm. The presence of

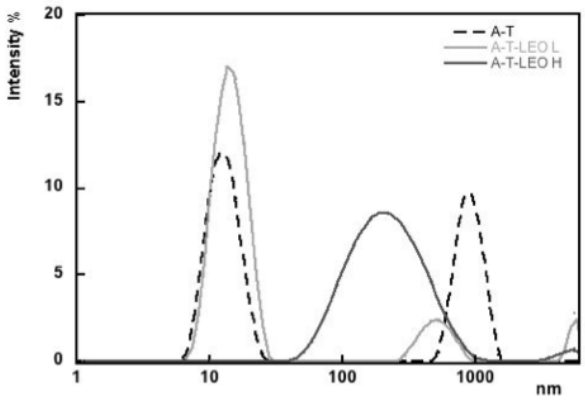

Figure 6.2: *Particle size distribution of a suspension of alginate and Tween 80 (dashed black line), of primary alginate/lemongrass essential oil (LEO) emulsions with low (solid grey line) and high (solid black line) oil content.*

smaller or bigger droplets also influenced the visual appearance of the emulsion. The dispersions made by pure surfactant or LEO at low concentrations were transparent, while those with higher amount of oil, characterized by droplets with a greater diameter, appeared opaque due to the different light-scattering behavior of the samples. To understand the stability of the emulsion, the ζ-potential was measured. This parameter is related to the electrokinetic potential of a particle and it is measured by evaluating its ability when interacting with a liquid surface. The determination of ζ-potential can be affected by the interaction between the particle surface and the dispersing medium by means of ionically charged functional groups present at the interface or through the adsorption of ionic species present in the medium. Values of ζ-potential higher than 30 mV (positive or negative) are usually indicators of a good system stability [16]. Primary emulsions presented values of ζ-potential that indicate stable systems, in particular it was of -53 $\pm$ 11 mV for A-T-LEO L and -24 $\pm$ 1 mV for A-T-LEO H. The negative electrical charge observed can be mainly attributed to the anionic residues of sodium alginate that characterize the continuous phase [16]. Both, the suspension with only alginate and with alginate plus Tween 80, showed a higher negative value of ζ-potential (-71 $\pm$ 5 mV and -45 $\pm$ 3 mV, respectively). This indicates that the surface electrical charge of the emulsion particles was affected by the partition of polymer chains between the continuous phase and the particle surface that are affected by the droplet size and volume fraction of dispersed phase determining the total interfacial area.

6.3.2 Film properties

Microstructure

Previously characterized emulsions were (after being diluted with alginate as the continuous phase) used to produce thin films. The microstructure of the films is the result of the structural arrangement of the different components that affect their physical and mechanical properties. The micrographs of the films' cross-sections obtained by means of FESEM are shown in Fig. 6.3. Film with alginate only (Fig. 6.3A) showed a homogeneous and compact cryofractured surface, which became thicker (from 50$\pm$4 to 62$\pm$7 μm) after the application of calcium chloride (Fig. 6.3B) that crosslinked the guluronic residues. It is also possible to notice a layer containing calcium on the top of the film that did not penetrate into the matrix, due to the high degree of cohesion of the polymer chain packing. The structure of films made of sodium alginate emulsions was completely different; the A-T film, in particular, presented a structure characterized by small particles embedded in the matrix that can be attributed to surfactant aggregates (Fig.

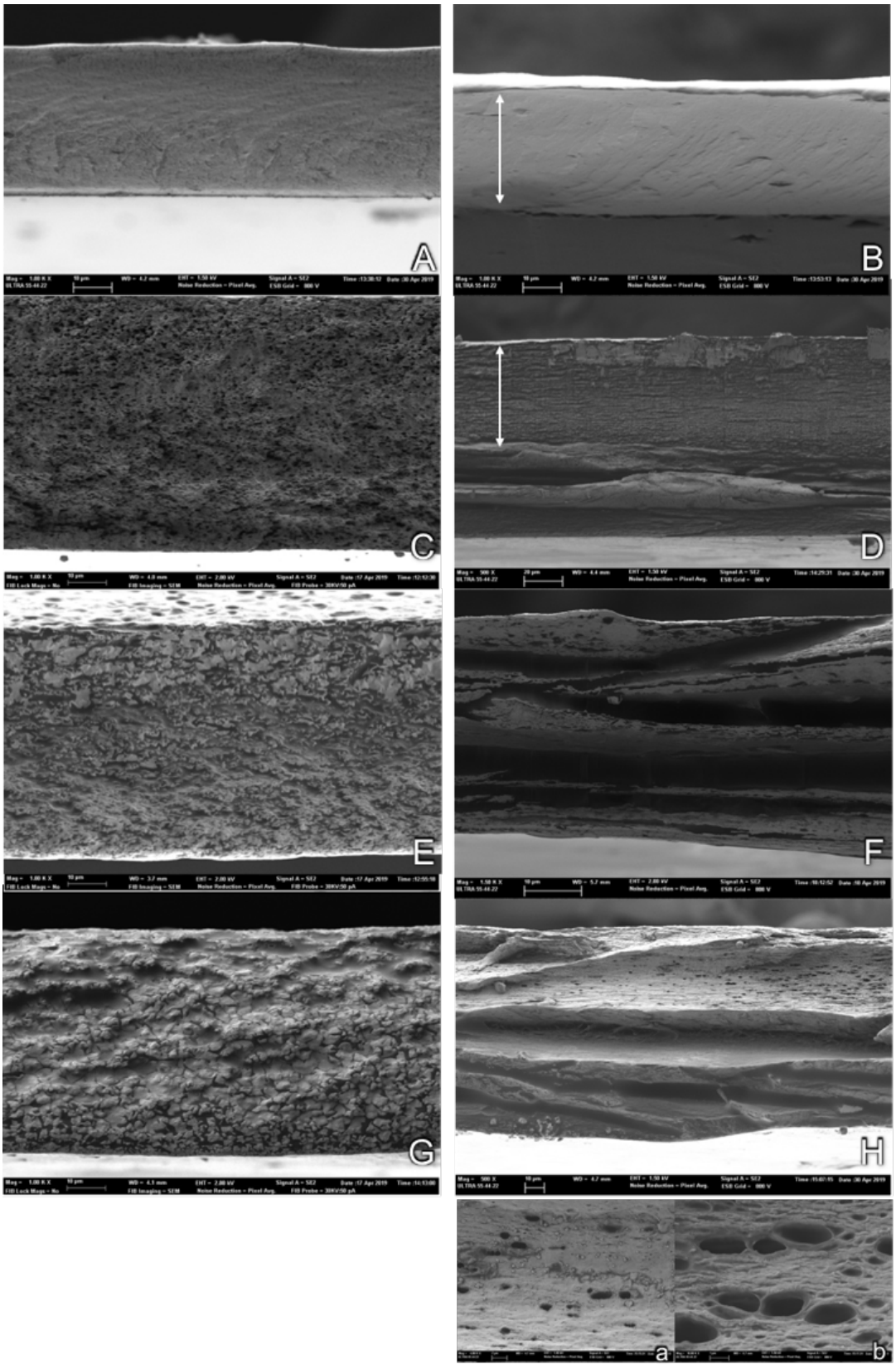

Figure 6.3: *Field Emission Scanning Electron Microscopy (FESEM) micrographs of the obtained films: (A) A, (B) A-Ca, (C) A-T, (D) A-T-Ca, (E) A-T-LEO L (F) A-T-LEO L-Ca (G) A-T-LEO H, and (H) A-T-LEO H-Ca; a, b-higher magnifications (4000x and 10,000 respectively) of A-T-LEO H-Ca. White arrows indicate the part of the film cut with a scalpel. All the other samples were cryofractured.*

6.3C); however, the structure changed when LEO was added (Fig. 6.3E,G). In presence of oil, indeed, the matrix lost its homogeneous structure with the formation of areas of differing densities, due to the destabilization phenomena that occurred during the film drying [17]. No oil droplets were visible, but the lipid entrapment inside the film network filled the porous structure generated inside the matrix. During the film drying step, droplet flocculation, coalescence and creaming occur, which can produce losses of the lipid compounds caused by the steam drag effect at the film surface in line with water evaporation [18]. For A-T based films treated with calcium (Fig. 6.3D), it was possible to notice the formation of a laminar structure, characterized by the assembly of parallel layers, probably separated by Tween 80, which reorganized during drying. Calcium-treated films containing essential oil (Fig. 6.3F,H), became thicker, especially samples with a higher amount of EO (91±16 μm), which had visible oil droplets trapped in the matrix (Fig. 6.3a, b). In both cases, the presence of oil gave rise to a laminar structure, which suggests a greater ability to promote calcium diffusion through the alginate matrix and a more extended crosslinking through the film. Nevertheless, the crosslinked layers were interrupted by the lipid lumps resulting from droplet flocculation and coalescence. The promoted calcium diffusion could be explained by a weakening effect that the lipid compounds exert on the chain attraction forces, allowing calcium mobility inside the polymer network. Further information about the physical properties of the obtained films concerned their thermal behavior. Through thermo-gravimetric analysis (TGA), it was possible to evaluate changes (losses of volatile compounds or polymer degradation) in the material associated to the temperature increasing at a constant heating rate. Mass sample changes are related to different events, such as desorption, absorption, sublimation, vaporization, oxidation, etc. Fig. 6.4 depicts the derivative curves (DTGA) obtained from TGA.

As can be seen from the figure, alginate as well as crosslinked films presented a first mass

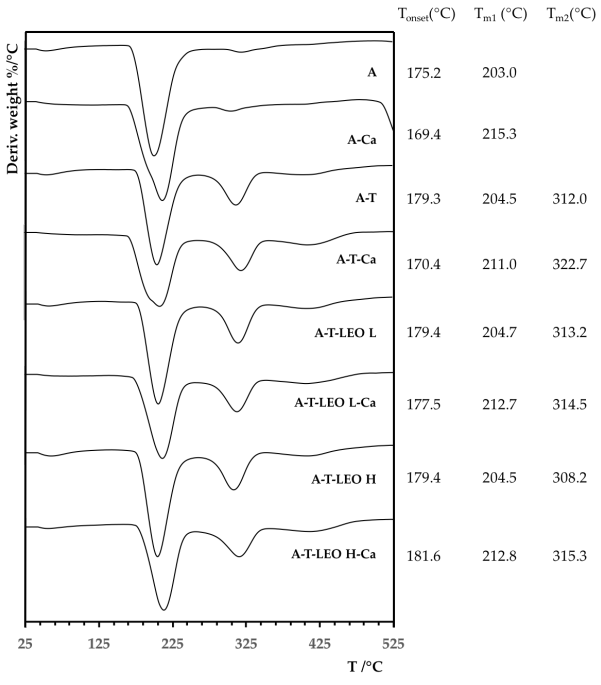

	T_{onset}(°C)	T_{m1} (°C)	T_{m2}(°C)
A	175.2	203.0	
A-Ca	169.4	215.3	
A-T	179.3	204.5	312.0
A-T-Ca	170.4	211.0	322.7
A-T-LEO L	179.4	204.7	313.2
A-T-LEO L-Ca	177.5	212.7	314.5
A-T-LEO H	179.4	204.5	308.2
A-T-LEO H-Ca	181.6	212.8	315.3

Figure 6.4: *Derivative thermo-gravimetric analysis (DTGA) curves of the obtained films. The embedded table gives the values of the onset and peak temperatures.*

reduction at around 200 °C, associated with the polymer degradation, with the consequent formation of carbonaceous residues and Na_2CO_3, according to Soares and co-workers [18]. Calcium incorporation provoked the shift of the degradation peak to a higher temperature, in agreement

with the formation of a more compact structure with greater cohesive forces. The DTGA curves of films made from emulsions showed two peaks, the first (T_{m1}) corresponding to the alginate degradation and a second peak (T_{m2}), also present in the A-T film, which could be associated with the surfactant degradation. As for the alginate film, when calcium was applied to films with LEO, it protected alginate and Tween from thermodegradation, with a shift toward higher values of the peaks corresponding to T_{m1} and T_{m2}.

Moisture Content and Solubility

To better understand the films' behavior and their ability to interact with water, the moisture content (MC) of samples conditioned at a RH of 53% and 25 °C was taken into consideration. Films obtained with only polymer showed MC values of between 10.7±11 g for 100 g of dry film (Table 6.2), regardless of whether calcium was applied or not. The MC values decreased when the films were obtained from emulsions, reaching the lowest value for sample A-T-LEO H, which can be associated with the presence of hydrophobic compounds or groups that prevented the water adsorption in the matrix [19,20]. Alginate is a biodegradable and hydrophilic polymer, and, in order to expand the possible application fields of its films, a reduction in the solubility is necessary. As expected, films made with pure polymer were totally water soluble and the incorporation of LEO did not significantly modify the film solubility. Other studies on hydrophilic films by Sapper et al. [21] also showed that when the essential oil was directly added to the polymer matrix, no changes in the film solubility occurred. However, all the films crosslinked with calcium were less soluble than their respective control. In particular, A-Ca and A-T-LEO L-Ca samples had the lowest values of solubility. In every case, the behavior was influenced by the presence of guluronic residues that, with carboxylic groups, can react with calcium ions (typical egg box), or water (like a competitive system).

Thickness

Film thickness is a crucial parameter for the determination of features, such as mechanical and barrier properties, and it is influenced by the preparation methods, the surface of the plate where the dispersion is cast, the drying time, the solid content and by the phenomena occurring during the drying of the film-forming dispersion. Samples had different thickness values; films obtained from emulsions, in particular, were thicker due to the higher solid content of the film-forming dispersions containing LEO and Tween 80 (Table 6.2). When calcium chloride was applied, an increase in this parameter was observed, in all likelihood due to the crosslinking effect and the formation of hydrogel during the drying process. During this process, a network starts to be formed as soon as calcium ions find guluronic residues to react with. Pavlath et al. [22] also found an increase in the thickness of alginate films obtained by immersion in solutions of multivalent ion salts and explained that two coupled processes occurred: dissolution of alginate in the solution and the crosslinking between divalent cations and carboxylic groups that made films thicker.

Mechanical properties

The presence of LEO and the application of calcium influenced the mechanical properties in different ways. This is due to the different microstructure formed, as mentioned above, that depended on both the composition of the film-forming dispersion and its stability during the drying process. Interactions between polymer, essential oil compounds, surface active agent and crosslinker influenced the structure of the film formed. The ratio of G and M residues in alginate also plays an important role in the mechanical and stability properties of alginate films. The values of different mechanical properties are summarized in Table 6.2 for every sample. Curves of

Table 6.2: Moisture content (MC as g/100 g dry film), water solubility (S, % soluble solids in the film), water vapor permeability (WVP) and tensile properties (EM, elastic modulus; TS, tensile strength; E, percentage elongation) of the films.

	MC (g/100g)	**S (%)**	**WVP · 10^{-9} (g/msPa)**	**EM (MPa)**	**TS (MPa)**	**E (%)**	**Thickness (um)**
A	$10.7(0.4)^{a,b}$	$99(0)^{c}$	$2.5(0.2)^{a}$	$3200(120)^{d}$	$80(5)^{a}$	$5(1)^{a}$	$50(4)^{a}$
A-Ca	$11.3(0.8)^{b}$	$58(3.7)^{a}$	$3.1(0.6)^{a,b}$	$3800(200)^{e}$	$133(16)^{b}$	$7(2)^{a,b}$	$62(7)^{b}$
A-T	$9.4(0.2)^{a,b}$	$95(2.7)^{c}$	$3.1(0.5)^{a}$	$2500(98)^{a,b,c}$	$82(5)^{a}$	$11(1)^{d}$	$61(4)^{b}$
A-T-Ca	$10.1(0.3)^{a,b}$	$76(0)^{a,b,c}$	$2.8(0.8)^{a}$	$2600(400)^{b,c}$	$77(27)^{a}$	$5(3)^{a,b}$	$89(16)^{c}$
A-T-LEO L	$9.6(1.1)^{a,b}$	$88(2.4)^{b,c}$	$2.9(0.6)^{a,b}$	$2000(150)^{a}$	$70(7)^{a}$	$9(3)^{b,c,d}$	$66(6)^{b}$
A-T-LEO L-Ca	$9.1(0.6)^{a,b}$	$65(7.3)^{a,b}$	$3.6(0.5)^{b}$	$2800(130)^{c,d}$	$122(18)^{b}$	$11(3)^{c,d}$	$83(12)^{c}$
A-T-LEO H	$8.9(1.0)^{a}$	$98(2.7)^{c}$	$2.9(0.4)^{a}$	$2400(90)^{a,b}$	$70(7)^{a}$	$7(2)^{a,b,c}$	$64(6)^{b}$
A-T-LEO H-Ca	$8.8(0.9)^{a}$	$75(11.4)^{a,b,c}$	$3.1(0.4)^{a,b}$	$2600(140)^{a,b,c}$	$72(16)^{a}$	$4(2)^{a}$	$91(16)^{c}$

Standard deviation is shown in brackets. Any means in the same column followed by different letters are significantly different ($p < 0.05$) for the Fisher's least significant difference (LSD) procedure.

force versus distance obtained in the test curves were transformed into stress (σ) versus Hencky strain (ϵ_H) and reported in Fig. 6.5. From the curves, it is possible to appreciate a first linear $\sigma - \epsilon_H$ relationship, associated with the elastic component and a second one indicative of the plastic behavior. Alginate films are hard and strong, with a high value of EM (Elastic Modulus), linked to the film's rigidity and tensile strength (TS) with a moderate value of elongation at break (%E). Different values of tensile properties were reported for alginate films; the TS ranged from 40 to 80 MPa, when conditioned at different %RH and with the presence of plasticizer [23]. The weaker films showed elongation at break from 3 to 5% [24]. When using crosslinking agents, TS values up to 134 MPa were observed for alginate mulching films [25]. Differences in the tensile properties are also related to the different sources of the polymer, the grade of purity or the extraction method.

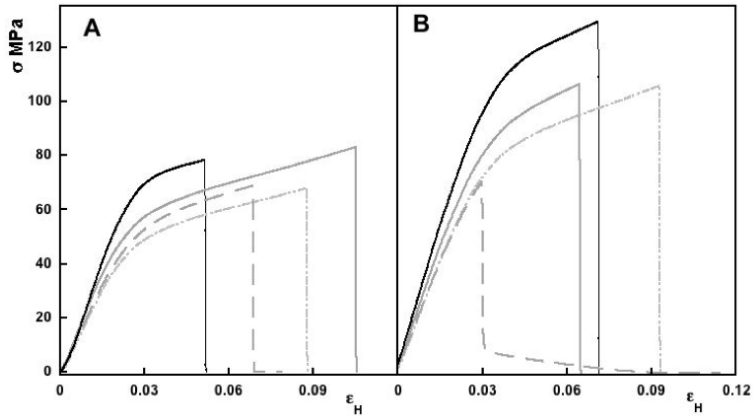

Figure 6.5: *Representative tensile stress (σ)-Hencky strain (ϵH) curves obtained for the different films: A (solid black line), A-T (solid grey line), A-T-LEO L (dashed and dotted grey line) and A-T-LEO H (dashed grey line) without (**A**) and with (**B**) $CaCl_2$.*

The outcomes of the mechanical properties revealed that films formed by emulsions or A-T films exhibited a more plastic behavior compared to films made only of alginate. The elastic modulus was indeed higher in the latter case. The rigidity was similar in A and A-T films and was reduced in films made from emulsions, while the films made from emulsions and by A-T suspensions were more resistant to elongation compared to films made of pure alginate. This can be attributed to the fact that all the added components increased the chain mobility

and reduced the inter-chain forces, thus enhancing the percentage of elongation at break. In particular, LEO compounds could favor the sliding of the chains during film stretching [26]. This behavior concurs with that observed by other authors [27-29]. When calcium was applied, a significant increase ($p < 0.05$) in the tensile strength was clearly observed for every crosslinked sample, as was a reduction in the elongation at the break. Costa el at. [30] also observed the same effect on A-Ca films. High values of TS are usually due to the presence of H bounds or crosslinking between the chain of the polymer as promoted by calcium application [25,31]. The application of calcium during the drying step produced films in which the final structure was a compromise between the instantaneous formation of an insoluble complex and the dissolution of alginate in the matrix. Therefore, regions with a high density of crosslinking and others with a low density could be expected. This would explain the observed variability in the mechanical properties.

Barrier properties

Water vapor permeability (WVP) is related to the diffusion and solubility of water molecules through the film section and high values of WVP are usually recorded for hydrophilic films. The water vapor transfer process is conditioned by the hydrophilic/hydrophobic ratio of the film components and, as previously mentioned, the film's microstructure also influenced the barrier properties. WVP values of every sample are shown in Table 6.2. In general, for the obtained films, WVP was scarcely affected by the film composition or calcium application. The incorporation of essential oil did not significantly modify the WVP of the films, while calcium application seemed to slightly promote WVP, although no significant differences were observed between the values of the calcium treated films and the corresponding control sample. This is because the formation of an emulsion as well as the application of calcium could change the matrix and create pores or other channels that allowed water molecules to pass through the polymer matrix [32]. However, some authors [23] reported how increasing the calcium concentration led to an enhancement in the water vapor barrier properties up to a maximum value, and higher amounts of calcium lead to poorer water vapor barrier properties. As concerns the effect of essential oils, some studies demonstrated that their addition improved film properties, such as moisture content and water vapor permeability [33,34], whereas others reported that these properties were negatively influenced by the different structural arrangement that creates channels or fractures leading to a worsening of the barrier properties [29,32].

Optical properties

The optical properties of the films affect the appearance and quality of the foodstuff on which they are applied, having a great impact on consumer acceptability [17]. Color changes could usually be a sign of lipid oxidation that affects the quality of foods. Although all of the films studied appeared transparent, especially that made with pure alginate, samples obtained from emulsions were slightly opalescent. The addition of LEO at higher concentrations provided the film with a yellowish color. Table 6.3 reports the L*, C^*_{ab}, h^*_{ab}, WI and ΔE values (lightness, chrome, hue, whiteness index and total color difference respectively) and internal transmittance values for every film.

The lightness value was higher for films made of pure alginate. These values tend to decrease when emulsions were used to produce films, in particular for the highest amount of LEO. Moreover, for a determined film composition, calcium application provoked a decrease in the L* value. Hue values were less affected than chrome values. C^*_{ab} increased in the films containing LEO due to the natural color of the oil, while the opposite behavior was observed for the whiteness index (WI), which decreased in samples containing LEO. Nevertheless, it is not affected by the application of calcium. The differences in color parameters for the films were also determined

Table 6.3: Lightness L*, chrome C^*_{ab}, hue h^*_{ab}, whiteness index (WI), total color difference (ΔE) values and internal transmittance (T_i) at 450 nm of developed films.

Sample	L*	C^*_{ab}	h^*_{ab}	Ti 450nm	WI	ΔE
A	$83.6(0.9)^{d}$	$9.0(0.6)^{a,b,c}$	$89.3(0.9)^{a,b}$	$0.842(0.003)^{f}$	$81(1)^{d}$	-
A-Ca	$80.0(1.6)^{b,c}$	$8.4(1.0)^{a,b}$	$89.8(1.8)^{a,b}$	$0.838(0.006)^{e,f}$	$78(1)^{b,c}$	$3.8(1,6)^{a}$
A-T	$82.0(1.3)^{c,d}$	$10.7(1.0)^{c}$	$89.3(0.8)^{a,b}$	$0.826(0.008)^{d,e}$	$79(1)^{c,d}$	$2.7(0.8)^{a}$
A-T-Ca	$77.6(2.1)^{a,b}$	$7.1(0.8)^{a}$	$94.5(2.3)^{c}$	$0.798(0.012)^{b,c}$	$76(2)^{b,c}$	$6.9(1.7)^{c}$
A-T-LEO L	$79.6(1.6)^{b,c}$	$12.9(0.7)^{d}$	$88.0(0.9)^{a}$	$0.811(0.007)^{c,d}$	$76(1)^{b}$	$5.8(0.8)^{b,c}$
A-T-LEO L-Ca	$78.7(4.1)^{a,b,c}$	$10.1(1.9)^{b,c}$	$91.0(2.1)^{b}$	$0.782(0.015)^{b}$	$76(3)^{b}$	$4.2(1.5)^{a,b}$
A-T-LEO H	$77.4(1.5)^{a,b}$	$17.1(1.6)^{e}$	$89.4(1.4)^{a.b}$	$0.810(0.007)^{c}, d$	$72(1)^{a}$	$10.5(0.9)^{d}$
A-T-LEO H-Ca	$75.3(2.0)^{a}$	$15.1(1.7)^{e}$	$90(1.6)^{a,b}$	$0.763(0.010)^{a}$	$71(1)^{a}$	$10.6(1.0)^{d}$

Standard deviation is shown in brackets. Any means in the same column followed by different letters are significantly different ($p < 0.05$) for the Fisher's least significant difference (LSD) procedure.

through the ΔE values (total color difference) calculated with respect to alginate films. As expected from the individual values of color parameters, the highest ΔE was obtained for film with the highest amount of essential oil. The spectral distribution of internal transmittance is shown in Fig. 6.6. Films with essential oil exhibit less internal transmittance at lower values of wavelength due to the selective light absorption of oil compounds. As also observed by Sanchez-Gonzalez et al. [35], the transparency of hydrophilic films with EO decreases due to the presence of a dispersed phase in the matrix, with different refractive index, which promotes light dispersion.

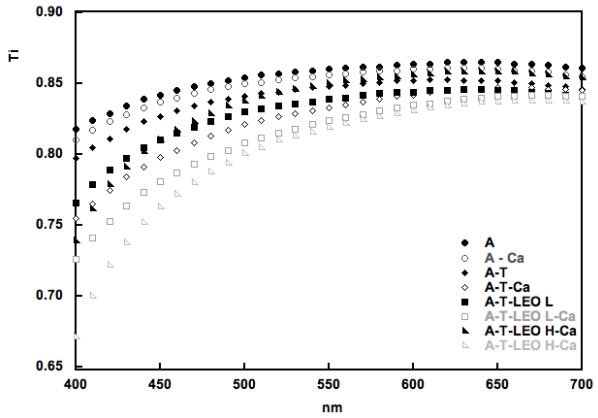

Figure 6.6: *Spectral distribution of internal transmittance (Ti) of films with and without calcium chloride.*

Likewise, compared to the respective control, the application of calcium gave rise to more opaque films. The opacity effect of calcium application was more intense in films containing surfactant and LEO, coherent with the greater penetration of the ion into the network and the progress of crosslinking in the internal part of the film, as deduced from the microstructural observations. The heterogeneous microstructure of the films crosslinked with calcium would provoke greater light dispersion and higher degree of opacity. Finally, considering all the outcomes of this study, some aspects can be highlighted. The decrease in the film's solubility caused by calcium is correlated with an increase in the tensile strength, underlying the fact that low values of solubility and greater resistance to an external stress are related to the formation of a crosslinked structure through the action of calcium in the guluronic cavities of the polymer network. A further correlation was recognized between the sample microstructure and the optical properties of the films. These become less transparent, darker and with a more saturated color

when they contained essential oil, while calcium application induced more opacity. However, the crosslinked structures did not exhibit an improved barrier capacity against water vapor.

6.4 Conclusions

Reinforced films of alginate, containing or not emulsified lemongrass essential oil, were obtained by spraying calcium chloride onto their surface. The film-forming emulsions were stabilized by Tween 80, exhibiting a particle size affected by the surfactant:oil ratio and negative ζ-potential values. Calcium diffusion through the film was favored in emulsified formulations, although the discontinuities introduced by the oil in the polymer network gave rise to weaker films, with lower elastic modulus and tensile strength at break. The crosslinking caused by calcium ions reduced the water solubility of the films, promoted the film's opacity and increased the temperature of the polymer thermal degradation. These effects were more pronounced in films containing essential oil, in line with the greater diffusion of the cation in the less compact, discontinuous oil-polymer matrix. Then, the proposed method of film production based on alginate emulsions and calcium spraying could be a suitable way to extend the field of application of polymeric edible films.

References

1. Embuscado, M.E.; Huber, K.C. *Edible films and coatings for food applications*; Springer: **2009**; Vol. 9.
2. Burt, S. Essential oils: their antibacterial properties and potential applications in foods-a review. *International journal of food microbiology* **2004**, 94, 223-253.
3. Liakos, I.; Grumezescu, A.; Holban, A.; Florin, I.; D'Autilia, F.; Carzino, R.; Bianchini, P.; Athanassiou, A. Polylactic acid-lemongrass essential oil nanocapsules with antimicrobial properties. *Pharmaceuticals* **2016**, 9, 42.
4. Mbili, N.C.; Opara, U.L.; Lennox, C.L.; Vries, F.A. Citrus and lemongrass essential oils inhibit *Botrytis cinerea* on 'Golden Delicious','Pink Lady' and 'Granny Smith' apples. *Journal of Plant Diseases and Protection* **2017**, 124, 499-511.
5. Azarakhsh, N.; Osman, A.; Ghazali, H.M.; Tan, C.P.; Adzahan, N.M. Lemongrass essential oil incorporated into alginate-based edible coating for shelf-life extension and quality retention of fresh-cut pineapple. *Postharvest Biology and Technology* **2014**, 88, 1-7.
6. Cofelice, M.; Lopez, F.; Cuomo, F. Quality Control of Fresh-Cut Apples after Coating Application. *Foods 2019*, 8, 189.
7. Cofelice, M.; Cuomo, F.; Lopez, F. Rheological Properties of Alginate-Essential Oil Nanodispersions. *Colloids and Interfaces* **2018**, 2, 48.
8. Cuomo, F.; Cofelice, M.; Lopez, F. Rheological Characterization of Hydrogels from Alginate-Based Nanodispersion. *Polymers* **2019**, 11, doi:doi:10.3390/polym11020259.
9. Valencia-Sullca, C.; Jiménez, M.; Jiménez, A.; Atarés, L.; Vargas, M.; Chiralt, A. Influence of liposome encapsulated essential oils on properties of chitosan films. *Polymer International* **2016**, 65, 979-987.
10. Astm. Standard test method for tensile properties of thin plastic sheeting. *Annual Book of American Standard Testing Methods* **2001**, 162-170.
11. Astm. Standard test methods for water vapour transmission of materials. *Annual Book of ASTM* **1995**, 406-413.
12. McHugh, T.H.; Avena-Bustillos, R.; Krochta, J. Hydrophilic edible films: modified procedure for water vapor permeability and explanation of thickness effects. *Journal of food science* **1993**, 58, 899-903.

13. Hutchings, J.B. Instrumental specification. In *Food colour and appearance*, Springer: **1999**; pp. 199-237.
14. Dawson, R.; Elliott, D.; Elliott, W. Jones KM: Data for Biochemical Research. Oxford: Clarendon Press: **1986**.
15. Rao, J.; McClements, D.J. Formation of flavor oil microemulsions, nanoemulsions and emulsions: influence of composition and preparation method. *Journal of agricultural and food chemistry* **2011**, 59, 5026-5035.
16. McClements, D.J. *Food emulsions: principles, practices, and techniques*; CRC press: **2015**.
17. Atarés, L.; Chiralt, A. Essential oils as additives in biodegradable films and coatings for active food packaging. *Trends in food science & technology* **2016**, 48, 51-62.
18. Soares, J.d.P.; Santos, J.; Chierice, G.O.; Cavalheiro, E. Thermal behavior of alginic acid and its sodium salt. *Ecl tica Qu mica* **2004**, 29, 57-64.
19. Hosseini, M.H.; Razavi, S.H.; Mousavi, S.M.A.; Yasaghi, S.A.S.; Hasansaraei, A.G. Improving antibacterial activity of edible films based on chitosan by incorporating thyme and clove essential oils and EDTA. *Journal of Applied Sciences* **2008**, 8, 2895-2900.
20. Riquelme, N.; Herrera, M.L.; Matiacevich, S. Active films based on alginate containing lemongrass essential oil encapsulated: Effect of process and storage conditions. *Food and bioproducts processing* **2017**, 104, 94-103.
21. Sapper, M.; Wilcaso, P.; Santamarina, M.P.; Rosell , J.; Chiralt, A. Antifungal and functional properties of starch-gellan films containing thyme (*Thymus zygis*) essential oil. *Food control* **2018**, 92, 505-515.
22. Pavlath, A.; Gossett, C.; Camirand, W.; Robertson, G. Ionomeric films of alginic acid. *Journal of Food Science* **1999**, 64, 61-63.
23. Olivas, G.I.; Barbosa-Cánovas, G.V. Alginate-calcium films: water vapor permeability and mechanical properties as affected by plasticizer and relative humidity. *LWT-Food science and technology* **2008**, 41, 359-366.
24. Siracusa, V.; Romani, S.; Gigli, M.; Mannozzi, C.; Cecchini, J.; Tylewicz, U.; Lotti, N. Characterization of Active Edible Films based on Citral Essential Oil, Alginate and Pectin. *Materials* **2018**, 11, 1980.
25. Liling, G.; Di, Z.; Jiachao, X.; Xin, G.; Xiaoting, F.; Qing, Z. Effects of ionic crosslinking on physical and mechanical properties of alginate mulching films. *Carbohydrate polymers* **2016**, 136, 259-265.
26. Bonilla, J.; Atarés, L.; Vargas, M.; Chiralt, A. Effect of essential oils and homogenization conditions on properties of chitosan-based films. *Food hydrocolloids* **2012**, 26, 9-16.
27. Atarés, L.; Pérez-Masiá, R.; Chiralt, A. The role of some antioxidants in the HPMC film properties and lipid protection in coated toasted almonds. *Journal of Food Engineering* **2011**, 104, 649-656.
28. Benavides, S.; Villalobos-Carvajal, R.; Reyes, J. Physical, mechanical and antibacterial properties of alginate film: Effect of the crosslinking degree and oregano essential oil concentration. *Journal of food engineering* **2012**, 110, 232-239.
29. Pranoto, Y.; Salokhe, V.M.; Rakshit, S.K. Physical and antibacte rial properties of alginate-based edible film incorporated with garlic oil. *Food research international 2005*, 38, 267-272.
30. Costa, M.J.; Marques, A.M.; Pastrana, L.M.; Teixeira, J.A.; Sillankorva, S.M.; Cerqueira, M.A. Physicochemical properties of alginate-based films: Effect of ionic crosslinking and mannuronic and guluronic acid ratio.*Food hydrocolloids* **2018**, 81, 442-448.
31. Rhim, J.-W. Physical and mechanical properties of water resistant sodium alginate films. *LWT-Food science and technology* **2004**, 37, 323-330.
32. Baek, S.-K.; Kim, S.; Song, K. Characterization of Ecklonia cava Alginate Films Containing Cinnamon Essential Oils. *International journal of molecular sciences* **2018**, 19, 3545.
33. Abdollahi, M.; Rezaei, M.; Farzi, G. A novel active bionanocomposite film incorporating rosemary essential oil and nanoclay into chitosan. *Journal of Food Engineering* **2012**, 111, 343-350.
34. Tongnuanchan, P.; Benjakul, S.; Prodpran, T. Properties and antioxidant activity of fish skin gelatin

film incorporated with citrus essential oils. *Food Chemistry* **2012**, 134, 1571-1579.
35. Sánchez-González, L.; González-Martínez, C.; Chiralt, A.; Cháfer, M. Physical and antimicrobial properties of chitosan-tea tree essential oil composite films. *Journal of Food Engineering* **2010**, 98, 443-452.

7 Quality control of fresh-cut apples after coating application

«Let the food be thy medicine and medicine be thy food»
Hippocrates

Abstract

The growing demand of ready-to-eat fresh fruits has led to set-up appropriate strategies for preserving fruit quality and freshness of such commodities. To slow down the deterioration events such as respiration, moisture loss and enzymatic activity, *ready-to-eat* products should be protected with an edible film. A suitable coating should combine hydrophilic and hydrophobic features to ensure good mechanical and gas barrier properties. Alginate/essential oil nanoformulations, one with low and the other with high oil content, here proposed to protect apple pieces during storage, were first characterized through dynamic light scattering and rheology. The effect of the application of the nanoformulations on the quality parameters of apples stored at 4 °C was considered by evaluating weight loss, pH and titratable acidity, total phenols content and the fruit appearance during storage. Mainly on the basis of pH and titratable acidity variation, the nanoformulation with low oil content resulted eligible for preserving the quality of fresh-cut apple pieces during storage.

7.1 Introduction

The high attention to healthy and nutritional food products enlarged the request of *ready-to-eat* products, like fresh-cut fruit. As already reported, the weakness of this kind of commodities is that they are perishable and difficult to preserve because they go through sensory deteriorations (browning, water loss, off-flavors production, loss of firmness) [1].
Edible coating can be recognized as a strategy for ensuring food protection, but in a broader view, the use of complex coatings is of interest for other biotechnological applications [2]. Thus emulsions and nanoemulsions represent a suitable method for producing coatings where more ingredients are used and, for their interesting characteristics, these colloidal systems have been proposed as functional tools for being enriched with bioactive compounds [3]. Thanks to their outstanding properties, essential oils (EO) represent a suitable ingredient for the formulation of nanoemulsions for food applications [4,5]. The principal complication hampering their wide use is the strong impact on organoleptic properties. Among EOs, lemongrass essential oil (LEO) has been found to be effective against several foodborne pathogens when it was incorporated in minimally processed fruit [6,7].
The enrichment of alginate-based coatings with EOs has been recently studied [8] for applications on fish and meat products and on fresh-cut fruit. Heydari et al. in 2015 [9] studied the combined effect of sodium alginate coating and horsemint EO on the quality of refrigerated bighead carp fillets and they observed reduced spoilage of the fillets and extended shelf-life. Successively, Raeisi and coworkers [10] studied the microbial quality of chicken meat fillets during storage time by using sodium alginate active coatings incorporated with different natural antimicrobials including nisin, cinnamon and rosemary EOs, added individually and in combination.
They demonstrated that all treatments significantly inhibited microbial growth when compared to the control. Along this line, Vital et al. [11] applied alginate-based edible coatings containing rosemary or oregano EOs as natural antioxidants for preserving beef steaks during 14 days. The coatings protected beef from color losses, water losses and had a positive effect on consumer acceptance. Raybaudi-Massilia et al., already in 2008, [12] incorporated malic acid and cinnamon, palmarosa and lemongrass EOs into an alginate-based edible coating to test their effects on the shelf-life of melon pieces. The coatings enriched with EOs protected the fresh-cut melon from the microbial proliferation but some fresh-cut melon characteristics were affected such as firmness and color, causing a reduction of physicochemical shelf-life. Lately, Azarakhsh and coworkers [13] investigated on how different LEO concentrations dispersed into an alginate-based edible coating influenced respiration rate, physicochemical properties, and microbiological and sensory quality of fresh-cut pineapple during 16 days of storage. The results indicated that an alginate-based edible coating formulation containing 0.3% LEO was suitable for extending the fresh-cut pineapple shelf-life. Higher concentrations of LEO, on the contrary, affected negatively the fruit quality.
The efficiency of emulsions or nanoemulsions made of alginate and LEO applied as coating on apples was studied in 2015 [14] against *Escherichia coli* proliferation during storage time. The study also focused on how the fruit respiration rate and ethylene production were influenced by LEO concentration. Here, to investigate on how some other physicochemical quality parameters are influenced by the application of edible coatings, two nanoformulations are used for protecting fresh-cut apples. The oil in water nanodispersions were made of sodium alginate suspension (1% w/w) and LEO at two different concentrations (0.1% and 1% w/w) stabilized by the non-ionic surfactant, Tween 80. The rheological behavior of the nanodispersions was determined with rotational and oscillatory tests and the edible coating was applied on apple slices by dipping method. The effectiveness of nanodispersions as edible coating was investigated on coated fruits stored at 4°C for 14 days while uncoated slices were used as control. Physicochemical parameters like pH, titratable acidity, weight loss and total phenolic content were analyzed during storage.

7.2 Materials and Methods

7.2.1 Materials

Food-grade sodium alginate was obtained from Farmalabor, non-ionic surface active agent polyoxyethylene (20) sorbitan monooleate (Tween 80), calcium chloride and citric acid were purchased from Sigma-Aldrich while Lemongrass (*Cymbopogon nardus*) Essential Oil (LEO) (Erbamea, San Giustino, Perugia, Italia) was purchased from a local shop. Fuji apples were purchased in a local supermarket. For all the preparations, ultra-pure water was used.

7.2.2 Preparation of coating nanoformulation

Sodium alginate (1% w/w) was dissolved in hot water at 70 °C under continuous stirring. Coarse primary dispersions were made by mixing aqueous sodium alginate suspension, LEO (0.5% - 5% w/w) as lipidic phase and Tween 80 (5% w/w) with a laboratory T25 digital Ultra-Turrax mixer (IKA, Staufen, Germany) with a S25N-8G probe, working at 24000 rpm for 4 min. These dispersions were then subjected to ultrasonic treatment (Ultrasonic Homogenizer Model 300 VT, BioLogics Inc., Manassas, VA, USA) for 1 min at 120 W with 50% pulsed frequency to achieve finely dispersed hydrophobic particles providing stable suspensions [15,16]. The so obtained nanodispersions were diluted with the 1% alginate suspension in order to have a final EO concentrations of 0.1 and 1% w/w and Tween 80 concentration of 1% w/w.

7.2.3 Nanoformulations characterization

The average size of the dispersed phase of both the nanodispersions was determined by means of dynamic light scattering (DLS) using a Malvern UK Zetasizer-Nano ZS 90 instrument operating with a 4mW He-Ne laser (633 nm). The average diameter was measured at fixed detector angle of 90° by cumulant analysis of the autocorrelation function using software provided by the manufacturer. Before analysis samples were diluted 1:10 with ultra-pure water to avoid multiple scattering effects according to previous studies [17,18]. Rheological measurements were carried out using a rotational rheometer (Haake MARS III - Thermo Scientific, Karlsruhe, Germany) equipped with a 60 mm parallel plate geometry probe (PP60). The instrument was equipped with a Peltier element combined with a Phoenix II digital system (Thermo Scientific, Karlsruhe, Germany) for the temperature control. Samples (2.9 mL) were poured on the surface of the lower plate and the upper plate was lowered to the gap distance of 1 mm. Samples were left equilibrating for 5 minutes before measurements. Steady-shear flow tests were performed in controlled shear rate (CR) in the range of 0.01 to 1000 s^{-1} reached in three steps. Oscillation strain sweep measurements were carried out for determining the linear viscoelastic range (LVE) at a fixed frequency of 1 Hz. Frequency sweep tests were performed using a fixed strain within the LVE and in a range of frequency from 0.1 to 100 Hz. The storage modulus (G') and loss modulus (G") were determinate as function of frequency. All measurements were performed at 25°C.

7.2.4 Coating application

Fuji apples were first sanitized by immersion in a sodium hypochlorite solution and then rinsed with tap water. 16 pieces were obtained using an apple-cutting tool. Peel and additional 2-3 mm of tissue from the core side of each piece were removed. Any small blemishes or bruises were cut away. Apple slices were dipped for 2 min into coating-forming nanoformulation and left to drip off the excess of coating for 1 minute. Successively, apple pieces were dipped in a solution of citric acid 1% (w/v) and calcium chloride 2% (w/v) for 2 min as represented in Fig.

7.1. Afterwards, samples were placed in polypropylene plastic trays (17 cm x 20 cm x 6.5 cm), covered with a lid, and stored at 4°C until analyses. Uncoated apple pieces were used as control. On days 0, 3, 7, 11 and 14, three samples per treatment were taken for quality evaluation.

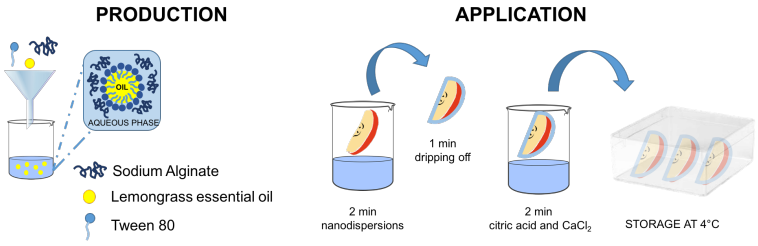

Figure 7.1: *Representation of oil in water nanodispersion production (left) and application on apple slices surface (right).*

7.2.5 Fresh-cut fruit evaluation

Weight loss

Apple pieces were weighed before being placed at 4 °C and at prefixed intervals (0, 3, 7, 11, 14 days). The difference between the initial and the weight during storage of the fruit was considered as weight loss and the results were expressed as the percentage loss of the initial weight.

Titratable acidity and pH

5 g of samples were taken in a beaker and homogenized with distilled water using Ultra-Turrax. The blended material was filtered and transferred in 50 mL volumetric flasks. pH of the solution was measured (pH meter). Titratable acidity (% T.A.) was determined through the titration of the apple juice with NaOH 0.1 M up to pH 8.2. % T.A. was calculated using the following formula:

$$\%T.A = \frac{V_{NaOH} \cdot M_{NaOH} \cdot E}{W \cdot 1000} \cdot 100 \tag{7.1}$$

where V is the volume of titrant (NaOH) used, M is the molarity of NaOH, E is the equivalent weight of malic acid and W is the weight of sample (in grams). In case of coated samples, a thin layer was removed before the material homogenization, in order to avoid overestimation of some parameters.

Total phenol content

Total phenolic content was determined according to Folin-Ciocalteu colorimetric method. 100 µL of apple juice, obtained as reported for the pH and titratable acidity, were added to 500 µL of Folin-Ciocalteu reagent and placed in the dark for 4 minutes. Successively, 400 µL of sodium carbonate 7.5% (w/v) were added and the cuvettes were allowed to stand in the dark at room temperature for 1 h before the detection of the absorbance at 760 nm. Caffeic acid was used as standard for calibration curve. Results are reported as ratio between the content of total phenols at certain time of storage (T_{Ph}) and their initial value (T_{Ph0}).

7.2.6 Statistical Analysis

SPSS software (version 23.0, IBM SPSS Statistics, Armonk, NY, USA) was used for all statistical analysis. Differences between treatments were tested with analysis of variance (ANOVA), followed by Tukey HSD multiple comparisons tests. Differences at $p<0.05$ were considered significant.

7.3 Results and Discussion

7.3.1 Characterization of coating formulations

With the aim of further expanding the exploration of the applicability of LEO/alginate-based nanodispersions in routine coating experiments, we considered two type of nanodispersion that differ with respect to LEO content [8]. The two nanoformulations were characterized through

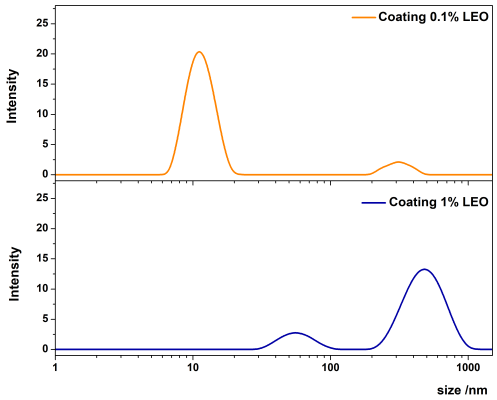

Figure 7.2: *Size distributions of alginate based nanoformulations containing 0.1% LEO (upper panel) or 1% LEO (lower panel).*

DLS and rheology before coating application. From the DLS investigation (Fig. 7.2) it was found that 0.1% LEO nanodispersions had a dispersed phase size of about 12 nm with a 0.5 value of polydispersity index (PDI). A lower homogeneity, instead, was found for the 1% LEO nanodispersion presenting two populations of aggregates around 60 and 600 nm respectively, and a higher PDI value of about 0.8. The rheological characterization of the nanodispersions was determined with rotational and oscillatory tests. In Fig. 7.3A, flow curves of both the nanoformulations showed that apparent viscosity decreased along with the shear rate, indicating a shear-thinning behavior, generally attributable to the alignment of the polymer molecules with the flow [19]. The difference in apparent viscosity that was higher at lower LEO content can be explained with a dilution effect of alginate in the continuous phase promoted by the increase of the oil concentration [20]. Fig. 7.3B illustrated the frequency sweep spectra carried out at a strain value extrapolated in the linear viscoelastic range (LVE) of the strain sweep (LVE range corresponds to the linear region of inset of Fig. 7.3B). Dynamic oscillatory mechanical spectra revealed that either at high or low frequency (on short and long term) the loss modulus, G", is higher than the storage modulus, G', and that the moduli are highly frequency dependent. This evidence indicated that both the nanoformulations had similar liquid-like behavior compatible with the application of the coating by dipping [21]. In the further step, after the gelation of the nanoformulation promoted by calcium ions (see Fig. 7.1), a change to a solid-like behavior is expected [22].

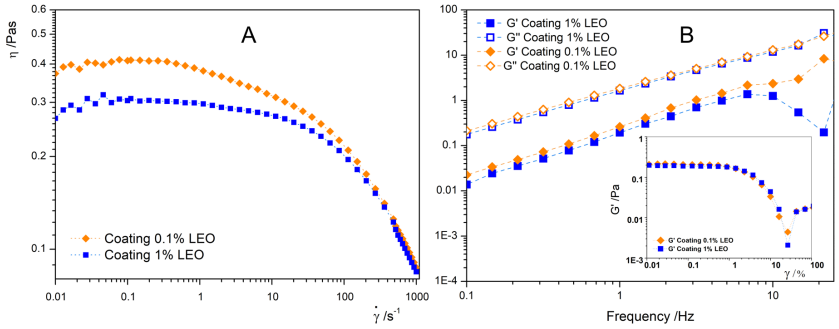

Figure 7.3: *(**A**) Apparent viscosity curves as function of the shear rate for alginate based nanoformulations containing 0.1% LEO or 1% LEO; (**B**) frequency sweep spectra of nanodispersions; storage moduli G' represented with full symbols and loss moduli, G", represented with empty symbols. Inset shows strain sweep of nanoformulations highlighting the linear viscoelasticity region. Nanoformulation containing 0.1% LEO is represented with orange diamonds, nanoformulation with 1% LEO is represented with blue squares.*

7.3.2 Fresh-cut fruit evaluation

Cutting and peeling of fruits like apples rapidly induces changes in color and appearance and over time, skinless fruit slices undergo moisture (and weight) loss. The occurrence of weight loss, an inevitable phenomenon when fruit surface is deprived of any protection, is an aspect that negatively influences the quality of the product. [23,24]. Through the application of a surface coating a reduction of moisture loss, is expected. The outcomes of the weight loss evaluation are reported in Fig. 7.4, where the moisture loss of coated apple slices is compared with uncoated pieces. As can be seen, within the first three days of storage, uncoated samples

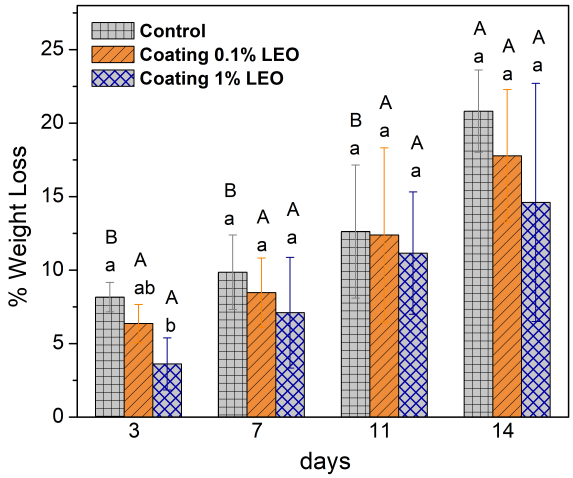

Figure 7.4: *Weight loss percentage of coated and uncoated (control) fresh-cut apples with different treatment during storage at 4°C. Means with the same letters (lowercase: amongst different treatments for the same time; uppercase: for the same treatment during different storage times) are not significantly different according to Tukey's test (p>0.05). Vertical bars indicate standard deviation.*

showed higher weight loss compared to coated apple pieces. The layer of coating seemed, indeed, effective in preventing water loss by producing high relative humidity at the surface of sliced apples [25]. Overall, the 1% LEO nanoformulation, in the whole storage period, reduced the

weight loss more due to the higher amount of lipid phase that enhanced the barrier effect against moisture loss. Other authors [26-28] observed that the coating ability in reducing fruit weight loss was influenced by different permeability to water vapor of the polysaccharides used in the formulation. The effect of coating application on pH and titratable acidity of the stored apples was also monitored. These two parameters are important to evaluate the fruit freshness and are strongly correlated because pH depends on the presence of acidic compounds. Acid content in fruits tends to decrease over time probably due to the organic acids oxidation which occurs with fruit ripening [29], as a consequence a pH increase is expected during the storage time. As can be observed from upper panels of Fig. 7.5, the presence of coating reduced the pH increase and in the case of alginate-based formulations with 0.1% LEO it was even reduced in particular after the seventh day of storage. This indication can be explained considering a precise stage of the coating application corresponding to the dipping of fruit pieces in the solution containing citric acid and calcium chloride. During that step citric acid penetrated through the coating film to the apple tissues with a larger extent in 0.1% LEO than in 1% LEO nanoformulations because the presence of a higher oil content reduced, in part, the permeability to citric acid. Moreover, the evidence that fruits coated with the 0.1% LEO nanoformulation had a pH stabilized around 3.7, represents an interesting aspect because at that pH value both the polyphenol oxidase (PPO, enzyme present in the apple tissue) and the microbial activities are slowed down [30]. On the other side, titratable acidity (TA) is an important parameter that accounts for all the acids present in the fruit pieces and is crucial to determine fruit ripening and flavor. Lower panels of Fig. 7.5 show the percentage of titratable acidity expressed as malic acid

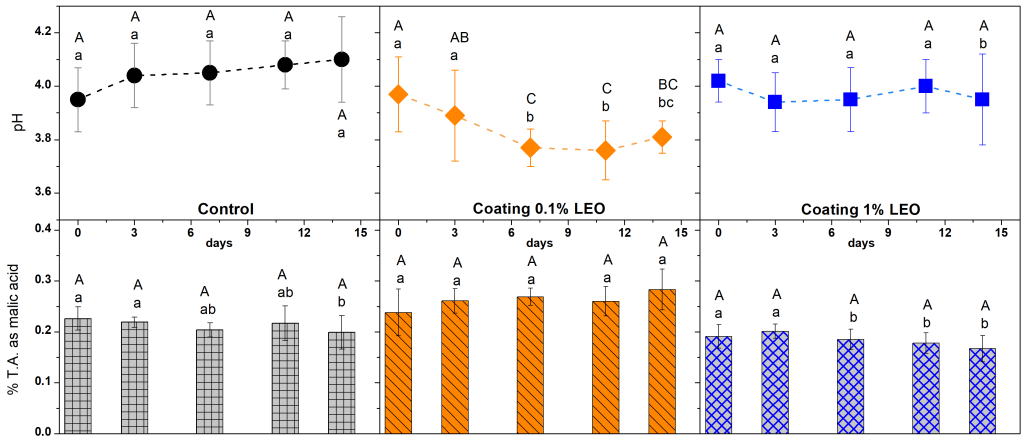

Figure 7.5: *pH (upper panels) and titratable acidity (lower panels) of fresh-cut apples with different treatment during storage at 4°C. Means with the same letters (lowercase: among different treatments for the same time; uppercase: for the same treatment during different storage times) are not significantly different according to Tukey's test (p>0.05). Vertical bars indicate standard deviation.*

during storage. According to the pH evolution that has a tendency towards higher values, the TA is expected to decrease within the storage timeframe because there is an intensification of the apple respiration rate as a result of peeling, cutting and other minimal processing activities [30]. As pointed out by Soares and Fonseca [31], factors such as treatment, variety and storage conditions are all important to determinate the degree of change in acidity. Organic acids might be used as an alternative respiratory substrate during storage, leading to reduced TA levels. The latter had a specular trend compared to the pH evolution as observed by other authors [32] and apple pieces coated with the nanoformulation containing LEO at 0.1% had higher values of TA that could be associated either to the deceleration of the respiration rate or to the presence of the citric acid that contribute to preserve the fruit freshness. The higher

presence of LEO in the 1% oil alginate based formulation gave TA values almost constant within the considered time interval. Compared to other studies, the results on pH and tritatable acidity achieved with the application of the nanodispersion containing 0.1% LEO represented a positive outcome. Olivas et al. [25] that covered apples slices with alginate based coatings, enriched or not with a lipophilic phase, obtained decreasing values of titratable acidity regardless the type of coating applied. Zambrano-Zaragoza et al. [33] that applied a coating based on nanodispersion of capsules loaded with α-tocopherol also detected a decrease in titratable acidity during storage time coupled with pH increase and Salvia-Trujillo et al. [14] that used alginate-LEO emulsions and nanoemulsions as apple coating did not evaluated these parameters. Apples, as well as many other vegetable products, represent a source of healthy compounds, such as phenols, molecules associated with antioxidant activity [34]. Chlorogenic, p-coumaric and caffeic acid, as well as quercetin, epicatechin, catechin, rutin, phlorizin are among the main phenolic compounds present in apples [35]. The quantity of phenolic compounds is highly variable, and gradients of concentration can also be found within the single fruit. Even considering the time evolution of the phenolic concentration there are no general rules for predicting accumulation or degradation because the total phenols amount depends on several aspects. An increase is, indeed, a consequence of the minimal process operations such as cutting and peeling that trigger activity of PAL (phenylalanine ammonia lyase), an enzyme that promotes the synthesis of phenols [26]. On the other hand, a decrease in phenols is due to the activity of PPO. These processes can be slowed down or inhibited by the presence of edible coatings or by the use of antioxidants. The time evolution of the phenolic compounds measured in the present study are illustrated in Fig. 7.6 in terms of relative phenols values ratio. The variations observed were similar even for

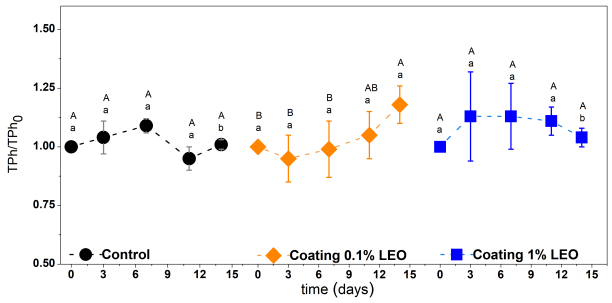

Figure 7.6: *Total phenols ratio of fresh-cut apples with different treatment during storage at 4°C. Means with the same letters (lowercase: amongst different treatments for the same time; uppercase: for the same treatment during different storage times) are not significantly different according to Tukey's test (p>0.05). Vertical bars indicate standard deviation.*

coated apple pieces. An increase of total phenols ratio in the storage time is detected for fruit pieces covered with the 0.1% LEO nanoformulations, while at higher LEO content (1%) after an initial increase, that could be due to the essential oil migration inside the fruit tissues, constant values of total phenols were detected. Finally, Fig. 7.7 illustrates the changes in fresh cut-apple pieces within 7 days of storage. As expected apple tissues underwent surface browning during storage due to the PPO, bringing to the formation of dark colored pigments [30]. Browning occurrence is a critical aspect that makes the produce less desirable to consumers. As can be observed from Fig. 7.7 apple pieces coated with nanoformulation containing 0.1% LEO and 1% LEO during storage are less browned. The first row of Fig. 7.7 shows apple pieces as soon as cut and coated, when all the samples share a good appearance. The aspect of the coated pieces was still agreeable and, in particular, apple pieces covered with 1% LEO nanoformulation seemed clearer than the others, maybe because the larger oil droplets, with their light scattering contribution added a whitening effect to the fruit pieces. During the storage period, after 3 and

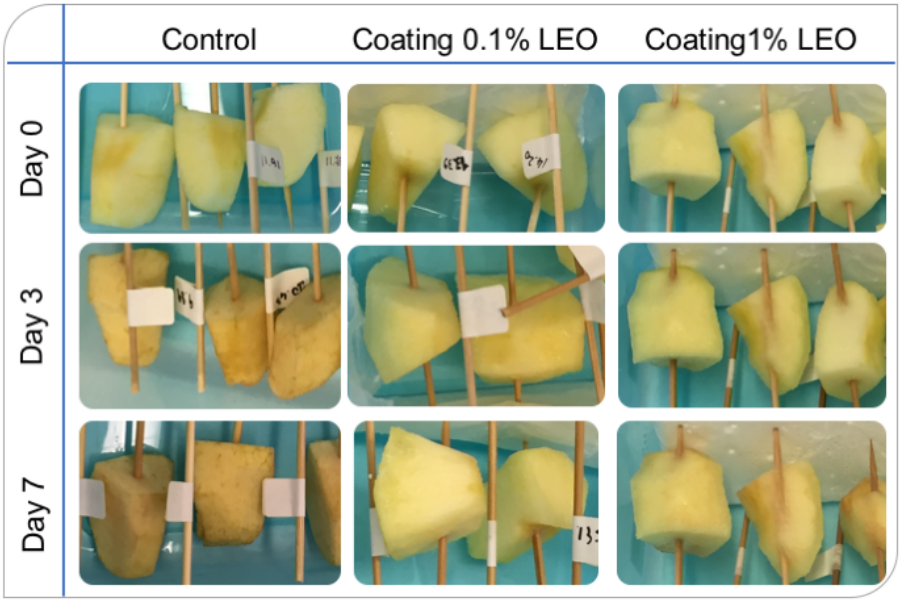

Figure 7.7: *Appearance of the fresh-cut apples subjected to different treatments during storage at 4°C.*

7 days (second and third rows of Fig. 7.7, respectively) the apple pieces coated with the 0.1% LEO nanoformulation were the least browned. On the whole, as well as illustrated in Fig. 7.7, the presence of a surface coating helps preserving the aspect of the fruit during storage. As next step, it would be useful to determine the browning index during storage according to the methodology recently assessed by other authors [36,37].

7.4 Conclusions

On balance, the present study was focused on the determination of some physicochemical fruit quality characteristics after the application of an edible coating on fresh-cut apple pieces. The coatings were realized starting from alginate-based nanoformulations containing high (1%) or low (0.1%) amount of LEO and their effects on fruit were compared with uncoated apple pieces. Both the nanoformulations had suitable rheological characteristics for being applied on fruit by dipping method, but their oil content influenced differently the fruit quality during storage. Considering the quality parameters analyzed such as the weight loss, the appearance and the positive effects detected on pH and titratable acidity, the nanoformulation with the low essential oil content (0.1% LEO) seemed more promising and appropriate than the nanoformulation with high oil content (1% LEO) for being applied on *ready-to-eat* fresh products. Nevertheless, the outcomes of this study, based on the application of surface coating on fresh-cut pieces of Fuji apples, have to be considered as encouraging preliminary results to be used as starting point to further extend the application of the here proposed coating to other cultivars and to other kinds of fruit.

References

1. Yildiz, F.; Wiley, R.C. *Minimally processed refrigerated fruits and vegetables;* Springer: **2017**.
2. Raudino, M.; Selvolini, G.; Montis, C.; Baglioni, M.; Bonini, M.; Berti, D.; Baglioni, P. Polymer films removed from solid surfaces by nanostructured fluids: Microscopic mechanism and implications for the conservation of cultural heritage. *ACS applied materials & interfaces* **2015**, 7, 6244-6253.
3. Salvia-Trujillo, L.; Soliva-Fortuny, R.; Rojas-Graü, M.A.; McClements, D.J.; Martín-Belloso, O. Edible nanoemulsions as carriers of active ingredients: a review. *Annual review of food science and technology* **2017**, 8, 439-466.
4. Burt, S. Essential oils: their antibacterial properties and potential applications in foods-a review. *International journal of food microbiology* **2004**, 94, 223-253.
5. Rojas-Graü, M.A.; Soliva-Fortuny, R.; Martín-Belloso, O. Edible coatings to incorporate active ingredients to fresh-cut fruits: a review. *Trends in food science & technology* **2009**, 20, 438-447.
6. Raybaudi-Massilia, R.M.; Rojas-Graü, M.A.; Mosqueda-Melgar, J.; Martín-Belloso, O. Comparative study on essential oils incorporated into an alginate-based edible coating to assure the safety and quality of fresh-cut Fuji apples. *Journal of Food Protection* **2008**, 71, 1150-1161.
7. Rojas-Graü, M.A.; Raybaudi-Massilia, R.M.; Soliva-Fortuny, R.C.; Avena-Bustillos, R.J.; McHugh, T.H.; Martín-Belloso, O. Apple puree-alginate edible coating as carrier of antimicrobial agents to prolong shelf-life of fresh-cut apples. *Postharvest biology and Technology* **2007**, 45, 254-264.
8. Cofelice, M.; Lopez, F.; Cuomo, F. Rheological Properties of Alginate-Essential Oil Nanodispersions *Colloids Interfaces* **2018**, 2, 48.
9. Heydari, R.; Bavandi, S.; Javadian, S.R. Effect of sodium alginate coating enriched with horsemint (*Mentha longifolia*) essential oil on the quality of bighead carp fillets during storage at 4° C. *Food science & nutrition* **2015**, 3, 188-194.
10. Raeisi, M.; Tabaraei, A.; Hashemi, M.; Behnampour, N. Effect of sodium alginate coating incorporated with nisin, *Cinnamomum zeylanicum*, and rosemary essential oils on microbial quality of chicken meat and fate of *Listeria monocytogenes* during refrigeration. *International journal of food microbiology* **2016**, 238, 139-145.
11. Vital, A.C.P.; Guerrero, A.; de Oliveira Monteschio, J.; Valero, M.V.; Carvalho, C.B.; de Abreu Filho, B.A.; Madrona, G.S.; do Prado, I.N. Effect of edible and active coating (with rosemary and oregano essential oils) on beef characteristics and consumer acceptability. *PloS one* **2016**, 11, e0160535.
12. Raybaudi-Massilia, R.M.; Mosqueda-Melgar, J.; Martín-Belloso, O. Edible alginate-based coating as carrier of antimicrobials to improve shelf-life and safety of fresh-cut melon. *International journal of food microbiology* **2008**, 121, 313-327.
13. Azarakhsh, N.; Osman, A.; Ghazali, H.M.; Tan, C.P.; Adzahan, N.M. Lemongrass essential oil incorporated into alginate-based edible coating for shelf-life extension and quality retention of fresh-cut pineapple. *Postharvest Biology and Technology* **2014**, 88, 1-7.
14. Salvia-Trujillo, L.; Rojas-Graü, M.A.; Soliva-Fortuny, R.; Martín-Belloso, O. Use of antimicrobial nanoemulsions as edible coatings: Impact on safety and quality attributes of fresh-cut Fuji apples. *Postharvest Biology and Technology* **2015**, 105, 8-16.
15. Salvia-Trujillo, L.; Rojas-Graü, A.; Soliva-Fortuny, R.; Martín-Belloso, O. Physicochemical characterization of lemongrass essential oil-alginate nanoemulsions: effect of ultrasound processing parameters. *Food and Bioprocess Technology* **2013**, 6, 2439-2446.
16. Sánchez-Ortega, I.; García-Almendárez, B.E.; Santos-López, E.M.; Reyes-González, L.R.; Regalado, C. Characterization and antimicrobial effect of starch-based edible coating suspensions. *Food Hydrocolloids* **2016**, 52, 906-913.
17. Guttoff, M.; Saberi, A.H.; McClements, D.J. Formation of vitamin D nanoemulsion-based delivery systems by spontaneous emulsification: Factors affecting particle size and stability. *Food Chemistry* **2015**, 171, 117-122, doi:https://doi.org/10.1016/j.foodchem.2014.08.087.
18. Perugini, L.; Cinelli, G.; Cofelice, M.; Ceglie, A.; Lopez, F.; Cuomo, F. Effect of the coexistence of sodium caseinate and Tween 20 as stabilizers of food emulsions at acidic pH. *Colloids and Surfaces B:*

Biointerfaces **2018**, 168, 163-168, doi:https://doi.org/10.1016/j.colsurfb.2018.02.003.
19. Michel-Sanchez, E. Impact of particle morphology on the rheology of PCC-based coatings. Georgia Institute of Technology, **2005**.
20. Bonilla, J.; Atarés, L.; Vargas, M.; Chiralt, A. Effect of essential oils and homogenization conditions on properties of chitosan-based films. *Food hydrocolloids* **2012**, 26, 9-16.
21. Ferreira, M.S.L.; Fai, A.E.C.; Andrade, C.T.; Picciani, P.H.; Azero, E.G.; Gonçalves, É.C.B.A. Edible films and coatings based on biodegradable residues applied to acerolas (*Malpighia punicifolia* L.). *Journal of the Science of Food and Agriculture* **2016**, 96, 1634-1642.
22. Liu, X.; Qian, L.; Shu, T.; Tong, Z. Rheology characterization of sol-gel transition in aqueous alginate solutions induced by calcium cations through in situ release. *Polymer* **2003**, 44, 407-412.
23. Liu, X.; Ren, J.; Zhu, Y.; Han, W.; Xuan, H.; Ge, L. The preservation effect of ascorbic acid and calcium chloride modified chitosan coating on fresh-cut apples at room temperature. *Colloids and Surfaces A: Physicochemical and Engineering Aspects 2016*, 502, 102-106.
24. Olivas, G.I.; Barbosa-Cánovas, G.V. Edible coatings for fresh-cut fruits. *Critical reviews in food science and nutrition* **2005**, 45, 657-670.
25. Olivas, G.I.; Mattinson, D.S.; Barbosa-Cánovas, G.V. Alginate coatings for preservation of minimally processed ´Gala´ apples. *Postharvest biology and Technology* **2007**, 45, 89-96.
26. Guerreiro, A.C.; Gago, C.M.L.; Faleiro, M.L.; Miguel, M.G.C.; Antunes, M.D.C. The effect of edible coatings on the nutritional quality of ´Bravo de Esmolfe´ fresh-cut apple through shelf-life. *LWT-Food Science and Technology* **2017**, 75, 210-219.
27. Serrano, M.; Martínez-Romero, D.; Guillén, F.; Valverde, J.M.; Zapata, P.J.; Castillo, S.; Valero, D. The addition of essential oils to MAP as a tool to maintain the overall quality of fruits. *Trends in Food Science & Technology* **2008**, 19, 464-471.
28. Vargas, M.; Pastor, C.; Chiralt, A.; McClements, D.J.; González-Mart nez, C. Recent advances in edible coatings for fresh and minimally processed fruits. *Critical Reviews in Food Science and Nutrition* **2008**, 48, 496-511.
29. Islam, M.; Khan, M.Z.H.; Sarkar, M.A.R.; Absar, N.; Sarkar, S.K. Changes in acidity, TSS, and sugar content at different storage periods of the postharvest mango (Mangifera indica L.) influenced by Bavistin DF. *International journal of food science* **2013**, 2013.
30. Rocha, A.; Morais, A. Shelf life of minimally processed apple (cv. Jonagored) determined by colour changes. *Food control* **2003**, 14, 13-20.
31. Soares, J.M.; Fonseca, G.G. Effect of L-ascorbic acid and sodium metabisulfite in the inhibition of the enzymatic browning of minimally processed apple. *Int. J. Agric. Res* **2008**, 3, 196-201.
32. Song, H.Y.; Jo, W.S.; Song, N.B.; Min, S.C.; Song, K.B. Quality change of apple slices coated with Aloe vera gel during storage. *Journal of food science* **2013**, 78, C817-C822.
33. Zambrano-Zaragoza, M.L.; Mercado-Silva, E.; Del Real L, A.; Gutiérrez-Cortez, E.; Cornejo-Villegas, M.A.; Quintanar-Guerrero, D. The effect of nano-coatings with α-tocopherol and xanthan gum on shelf-life and browning index of fresh-cut ´Red Delicious´ apples. *Innovative Food Science & Emerging Technologies* **2014**, 22, 188-196, doi:https://doi.org/10.1016/j.ifset.2013.09.008.
34. Soares, M.C.; Taciana Ribeiro, É.; Kuskoski, E.M.; Valdemiro Gonzaga, L.; Lima, A.; Mancini Filho, J.; Fett, R. Composition of phenolic acids content in apple (Malus sp) pomace. *Semina: Ciências Agrárias* **2008**, 29.
35. Heras-Ramírez, M.E.; Quintero-Ramos, A.; Camacho-Dávila, A.A.; Barnard, J.; Talamás-Abbud, R.; Torres-Muñoz, J.V.; Salas-Muñoz, E. Effect of blanching and drying temperature on polyphenolic compound stability and antioxidant capacity of apple pomace. *Food and Bioprocess Technology* **2012**, 5, 2201-2210.
36. Arias, E.; Oria, R.; López-Buesa, P. Determination of acceptability and shelf life of fresh-cut pear by digital image analysis. *Journal of Food Measurement and Characterization* **2018**, 12, 2916-2926.
37. Rana, S.S.; Pradhan, R.C.; Mishra, S. Image analysis to quantify the browning in fresh cut tender jackfruit slices. *Food chemistry* **2019**, 278, 185-189.

Concluding remarks

Nanodispersions, in this work of thesis, have been used as the starting material to produce edible layers for food packaging. The coatings and films realized were composite packaging materials made by mixtures of a hydrophilic structural matrix and a hydrophobic compound. This formulation has been designed to provide better moisture barrier properties than pure hydrocolloid films. In particular, the hydrophilic structural matrix was realized through the use of alginate, an anionic polyelectrolyte, and the lemongrass essential oil (LEO) was the hydrophilic compound we chose to work with for its antioxidant and antimicrobial properties. The hydrophilic and the hydrophobic phases were held together by a nonionic surfactant (Tween 80). Generally, edible coatings and films used on fresh fruits must be transparent, contain food-grade substances and their cost of technology production, as well as the cost of the raw materials, has to be relatively low. For these reasons, in the first stage of the study, the optimization of the nanodispersions production based on a biodegradable, non-toxic and inexpensive polymer was carried out. As resulted by the rheological investigation, alginate-based nanodispersions containing essential oil can be handled like the alginate suspensions (without LEO), with the added value of the benefits offered by the properties of the oil. In fact, the rheological behavior was only slightly affected by the presence of LEO, that in turn inhibited the growth of fungus mycotoxin like *P.expansum* and *A.niger* as well as moulds such as *Rhizopus oligosporus* (Chapter 4). Successively, Ca^{2+} cross-linking of alginate has been exploited to obtain hydrogel-based nanodispersions, through the method of inner gelation (Chapter 5). The process of gelation was studied since it is on the basis of the formation of coating and films from alginate. The hydrogels' rheological properties resulted, also in this case, not depending on the presence of LEO but on the amount of calcium and polymer. For the production of edible films calcium chloride was sprayed on the surface of the film layer (Chapter 6) and the obtained films were characterized for their microstructure and for the mechanical and thermal properties. It resulted that the presence of essential oil reduced the film stiffness whereas calcium addition lowered the film's water solubility, increased the tensile strength and reduced the extensibility. The principal aim of edible films as well as edible coatings is to improve the quality and extend the shelf life of minimally processed fruit by acting as a barrier to water loss, creating a micro modified atmosphere around the product. Therefore, the alginate/LEO nanodispersions have been finally used as an edible coating on fresh-cut apples (Chapter 7) allowing to prolong the shelf-life of such commodities reducing weight loss and other negative phenomena thanks to the incorporation of natural compounds that can help in reducing enzymatic browning and controlling microbial growth of fresh-cut products.

List of Papers regarding the Thesis

- Cofelice M., Cuomo F., Chiralt A. *Alginate Films Encapsulating Lemongrass Essential Oil As Affected By Spray Calcium Application*, Colloids and Interfaces 3(3) 58 (2019). https://doi.org/10.3390/colloids3030058;
- Cofelice M., Lopez F., Cuomo F. *Quality control of fresh-cut apples after coating application*, Foods 8(6) 189 (2019). https://doi.org/10.3390/foods8060189;
- Cuomo F., Cofelice M., Lopez F. *Rheological characterization of hydrogel from alginate based nanodsipersion*, Polymers 11(2) 259 (2019). https://doi.org/10.3390/polym11020259;
- Cofelice M., Cuomo F., Lopez F. *Rheological properties of alginate-essential oil nanodispersions.* Colloids and Interfaces. 2(4) 48 (2018). https://doi.org/10.3390/colloids2040048.

Other Papers

- Perugini L., Cinelli G., Cofelice M., Ceglie A., Lopez F., Cuomo F. *Effect of the coexistence of sodium caseinate and Tween 20 as stabilizers of food emulsions at acidic pH.* Colloids and Surfaces B: Biointerfaces (168), 163-168 (2018); https://doi.org/10.1016/j.colsurfb.2018.02.003.
- Cuomo F., Cofelice M., Venditti F., Ceglie A., Miguel M.G., Lindman B., Lopez F. *In-vitro digestion of Curcumin loaded chitosan-coated liposomes.* Colloids and Surfaces B: Biointerfaces (168) 29-34 (2018). https://doi.org/10.1016/j.colsurfb.2017.11.047.

Ringraziamenti

Al termine di questo percorso di dottorato è doveroso ringraziare coloro che mi hanno seguita, dandomi la possibilità di apprendere, crescere e formarmi da un punto di vista scientifico e personale. È grazie alla vostra dedizione per questo bellissimo lavoro che è la ricerca che ho imparato tante cose.
Ringrazio quindi il prof. Francesco Lopez, per questa opportunità, per i suoi discorsi, suggerimenti e le sue parole sempre mirate. Un ringraziamento speciale va alla dottoressa Francesca Cuomo, alla pazienza, alla passione che mette nella ricerca e ai suoi insegnamenti e consigli, scientifici e di vita. Ringrazio tutti coloro che fanno e hanno fatto parte del laboratorio di Chimica Fisica, in particolare il dott. Giuseppe Cinelli.
La bellezza di questo lavoro credo stia nella possibilità di imparare, confrontarsi e condividere. Per questo mi sento di ringraziare la prof.ssa Amparo Chiralt, alla sua disponibilità e professionalità. Grazie per avermi accolta nel suo laboratorio dove, oltre ad apprendere nuove tecniche, ho conosciuto persone splendide. Grazie chic@s per avermi fatto sentire parte del vostro gruppo e per avermi aiutata nei momenti difficili. Grazie a Carolina e Eva, a Emma travolgente e positiva, Alina donna, mamma, ricercatrice dall´estro creativo, Mayra e Sofia, due ragazze forti, così diverse, così uguali, così speciali. Un grazie particolare a due persone che spero resteranno nella mia vita nonostante il tempo e le distanze...
grazie a Johana y Ramon, ai momenti condivisi fuori e dentro il laboratorio e ai nostri *dialogues de doctorandos*...conversazioni senza fine!
Grazie a quelle persone che hanno incrociato la strada della mia vita...grazie a chi è stato solo di passaggio, a chi è lontano, ma sempre vicino, grazie a chi c'è da sempre e grazie a chi è arrivato all'improvviso...ognuno di voi mi ha insegnato qualcosa che porterò sempre con me.
Grazie a Luana e Angela, alla nostra amicizia e alla passione che mettete in ciò che fate che mi rende fiera di voi, stimolandomi a fare sempre di più.
Grazie a Pallino, sei l'amico un po' matto di cui tutti hanno bisogno. Grazie a Nicoletta...come si dice, non è il tempo a dimostrare la forza di un'amicizia...e le parole non sarebbero abbastanza per descriverla.
Un grazie alla mia famiglia. A mio padre, instancabile lavoratore, e a mia madre e alla sua creatività. Grazie a mio fratello, nonostante la lontananza sei sempre presente e so che credi in me più di ogni altra persona.
Grazie a chi ha condiviso questo percorso con me ... Ad Maiora semper...